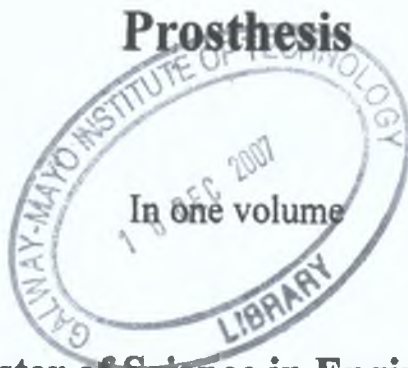




# **Optimising the Design and Manufacture of a Customised, Prescription Fit, Maxillo-facial**

## **Prosthesis**



## **Master of Science in Engineering**

**Supervisors:**

**Gerard O'Donnell  
Gabriel Costello**

**Author:**

**Paul McGarry**

Submitted to the Higher Education and Training Awards Council.

September 2007.



**Original Prosthesis**



**Optimised Prosthesis**

I hereby declare that the work presented in this thesis is my own, and that it has not been used to obtain a degree in this institute or elsewhere

---

Paul McGarry

## ACKNOWLEDGMENT

I would like to thank my main thesis supervisor Gerard O'Donnell for all his help and advice on this project, and for giving me the opportunity to work in research for the past two years. Gerard spent many hours from beginning to end, guiding me through this project and discussing the different topics. I would also like to thank my second thesis supervisor Gabriel Costello for his background information on the CNC milling machine, and his help and guidance through the machining phase of the project.

Aside from my supervisors there were a number of people who helped and encouraged me over the past two years, among them I want to thank, John Noone for his advice on the workshop machine set up's. Dr. Liam Morris for his help with the rapid prototyping machine. John Robinson from Advanced Titanium Metals Ltd, for supplying all the titanium free of charge. John Prior, and all the staff at Prior Tool and Die, for machining the prosthetic and doing all the CMM work, free of charge. Dr. Carine Gauchon for her help with the tensile testing machine. Ronan Carroll for helping with the animation software program. Finally, my research colleagues Mike, Damien, Kevin, Carmen, and the two Niall's, good luck with your respective Masters or Ph D's.

Thanks very much to each one of them.

## Funding

This research was funded by the Galway-Mayo Institute of Technology  
Internal Research Development Programme. (IRDP).



## **Published Work Associated with this Thesis**

McGarry, P. "*Creating a helical path*" [http://ansys.net/ansys/tips/Helical\\_Path.pdf](http://ansys.net/ansys/tips/Helical_Path.pdf)  
Published in Ansys net (2 October 2006)

## Abstract

**Paul McGarry: Optimising the Design and Manufacture of a Customised, Prescription Fit, Maxillo-facial Prosthesis.**

This Thesis is a continuation of the Enterprise-Ireland Research Innovation Fund (RIF) Project entitled "Design and Manufacturing of Customised Maxillo-Facial Prostheses" The primary objective of this Internal Research Development Program (IRDP) project was to investigate two fundamental design changes

- 1 To incorporate the over-denture abutments directly into the implant
- 2 To remove the restraining wings by the addition of screws, which affix the implant to the dense material of the jawbone.

The prosthetic was redesigned using the ANSYS Finite Element Analysis software program and analysed to:

- Reduce the internal von Mises stress distribution The new prosthetic had a -63.63 % lower von Mises stress distribution when compared with the original prosthetic.
- Examine the screw preload effects. A maximum relative displacement of  $22.6 \cdot 10^{-6}$  mm between the bone and screw was determined, which is well below the critical threshold of micromotion which prevents osseointegration
- Investigate the prosthetic-bone contact interface. Three models of the screw, prosthesis, and bone, were studied. (Axisymmetric, quarter volume, and full volume), a recommended preload torque of 0.32 Nm was applied to the prosthetic and a maximum von Mises stress of 1.988 MPa was predicted
- Study the overdenture removal forces. This analysis could not be completed because the correct plastic multilinear properties of the denture material could not be established

The redesigned prosthetic was successfully manufactured on a 3-axis milling machine with an indexing system The prosthetic was examined for dimensional quality and strength The research established the feasibility of the new design and associated manufacturing method.

## TABLE OF CONTENTS

<b>ACKNOWLEDGEMENT</b> .....	I
<b>FUNDING</b> . . . . .	II
<b>PUBLISHED WORK ASSOCIATED WITH THIS THESIS</b> .....	III
<b>ABSTRACT</b> ... . . . .	IV
<b>TABLE OF CONTENTS</b> .....	V
<b>LIST OF FIGURES</b> . . . . .	XI
<b>LIST OF TABLES</b> .....	XVI
<b>Chapter 1. INTRODUCTION</b> .....	1
1 1 Background to the Study . . . . .	1
1 2 Objectives of the Thesis	2
1.2.1 Specific Technical Objectives.....	3
1 3 Thesis Structure . . . . .	4
<b>CHAPTER 2. CURRENT STATE OF RESEARCH IN</b>	
<b>MAXILLO-FACIAL SURGERY</b> . . . . .	5
2 1 History of Maxillo-Facial Surgery	5
2 1 1 Suitability of Titanium for Implant Purposes	6
2 1 2 Titanium Performance in Medical Applications	8
2 2 Osseointegration . . . . .	9
2 3 Contact Analysis . . . . .	10
2.4 Machining Titanium . . . . .	11



2 4 1	Cubic Boron Nitride Cutting Tools . . . . .	11
2 5	Reverse Engineering . . . . .	13
2.6.	Rapid Prototyping Vs CNC Milling.....	14
2 6.1	Rapid Prototyping . . . . .	14
2.6.2	Computer Numerically Controlled (CNC) Milling... . . . . .	14
<b>CHAPTER 3. FINITE ELEMENT ANALYSIS.....</b>		<b>17</b>
3.1.	Introduction. . . . .	17
3.2.	Redesign of the Customised Maxillo-Facial Prosthesis. . . . .	18
3 3	First Modification	19
3.3.1	Design Criteria.....	19
3 3 2	Original Prosthesis Analysis	20
3.3.2.1	Mesh.....	20
3 3 2 2	Material Properties. . . . .	21
3 3 2 3	Boundary Conditions	23
3.3.2.4	Load Step Options. ....	24
3 3 3	New Prosthesis Analysis ... ..	25
3 3 3 1	Mesh	25
3 3 3.2	Material Properties.....	25
3 3 3 3	Boundary Conditions . . . . .	26
3 3 3 4	Load Step Options . . . . .	27
3 4	Prosthesis, Screw, and Bone Contact Analysis	28
3 4 1	Two Dimensional Model (Axisymmetric).....	28
3 4 2	Three Dimensional Model (Quarter Volume)	33

3 4 3	Three Dimensional Model (Full Volume)	37
3 5.	Screw Preload Analysis.	43
3.6.	Second Modification.....	49
3 6 1	Design Criteria	49
3 6 2	Abutment Design	49
3.6.2 1	Mesh.....	51
3.6.2 2	Material Properties	51
3 6 2 3	Boundary Conditions .. .	52
3 6 2 4	Load Step Options	53
3 7	Final Design	57
3 8	Discussion	58
<b>CHAPTER 4. MACHINING.....</b>		<b>60</b>
4 1	Introduction	60
4.2.	CAD/CAM Software.....	61
4 3	CNC Machining Centre	62
4 4	GMIT Machining Strategy	64
4.4 1	First Operation.....	66
4 4 2	Second, Third, Fourth, and Fifth Operations .	69
4 4 3	Sixth Operation	72
4 4 4	Seventh Operation . .	74
4 4 5	Eight Operation . . .	76
4 5	Outsourced Vendors	77
4 6	Pallet Indexing System	78



6.3	Titanium FEA Analysis	100
6.5.1	Mesh	100
6.5.2	Material Properties.....	100
6.5.3	Boundary Conditions	101
6.5.4	Load Step Options	101
6.6	Conclusions	102
<b>CHAPTER 7. ANIMATION.....</b>		<b>105</b>
7.1	Introduction	105
7.2	Sectioning the Prosthetic	106
7.3	The Prosthetic Moving Into Position	110
7.4	The Screws Moving Into Position	111
7.5	Presentation.....	115
<b>CHAPTER 8. DISCUSSION AND CONCLUSIONS.....</b>		<b>114</b>
8.1	Main Findings of the Research..	114
8.1.1	Finite Element Analysis	115
8.1.2	Machining	115
8.1.3	Coordinate Measuring Machine	116
8.1.4	Physical Testing	116
8.1.5	Animation	116
8.1.6	Limitations.....	118
8.2	Conclusions	118
8.3	Recommendations for Future Study	119

---

<b>REFERENCES</b> .....	122
<b>APPENDIX A</b> Helical Path GUI Method. ....	126
<b>APPENDIX B</b> Hexagonal Abutment Part Drawing . . . . .	129
<b>APPENDIX C</b> Round Abutment Part Drawing ..... ..	130
<b>APPENDIX D</b> Proposed Prosthesis... . . . .	131
<b>APPENDIX E</b> CMM Report ..... ..	132

## LIST OF FIGURES

Figure 2.1	Commercially Pure Solid Titanium Screw Implant.....	7
Figure 2.2	Titanium Screw Implant with a Hydroxylapatite (HA) Coating.....	9
Figure 2.3	Human Mandible Force and Moment Directions.....	10
Figure 2.4	Half-Skull Model Created By CNC Milling Showing a Large Cranial Defect.....	15
Figure 3.1	Original Customised Maxillo-Facial Prosthesis.....	18
Figure 3.2	Finite Element Prosthesis with Restraining Wings.....	20
Figure 3.3	Areas Used to Create the Prosthesis and Maxilla Bone Volumes...	21
Figure 3.4	Titanium Stress Strain Curve.....	22
Figure 3.5	Loads and Degree of Freedom Constraints on the Prosthesis with Wings.....	23
Figure 3.6	von Misses Stress State of Original Prosthesis (MPa).....	24
Figure 3.7	Prosthesis Hole Alignments with the Maxilla Bone.....	25
Figure 3.8	Degree of Freedom Constraints on Holes and Forces of the New Prosthesis.....	26
Figure 3.9	von Mises Plot of the New Prosthesis Design (MPa).....	27
Figure 3.10	Screw, Prosthesis and Bone Areas.....	28
Figure 3.11	Loads and Constraints Applied to the Axisymmetric Model.....	30
Figure 3.12	von Mises Stress for the Axisymmetric Contact Model (MPa).....	31
Figure 3.13	von Mises Plot of Contact at the Thread Areas (MPa).....	31
Figure 3.14	Contact Pressure at the Thread Area of the Axisymmetric Model (Pa).....	32

---

Figure 3 15	Finite Element Tetrahedral and Hexahedral Element Shapes Examples	33
Figure 3 16	von Mises Plot of the Quarter Volume Prosthesis, Screw and Bone Area (MPa)	35
Figure 3 17	von Mises Plot of the Thread Area (MPa)	36
Figure 3 18	Contact Pressure Plot on Quarter Volume Screw and Bone Area (Pa)	37
Figure 3 19	Full Volume Bone, Screw and Prosthetic with a Hole at the Centre of the Screw	38
Figure 3 20	Finite Element Volume Mesh at the Centre of the Screw	39
Figure 3 21	Full Volume Contact Elements	39
Figure 3 22	von Mises Stress Plot of the Screw-Bone-Prosthesis Connection (MPa)	40
Figure 3 23	von Mises Plot of Full Volume Threaded Area (MPa)	41
Figure 3 24	Maximum Displacement of the Bone Area (mm)	42
Figure 3 25	Screw-Prosthesis-Bone Volumes for Preload Analysis	43
Figure 3 26	Finite Element Volume Mesh	44
Figure 3 27	Preload Elements on the Screw	44
Figure 3 28	Preload Constraints	45
Figure 3 29	Full Model von Mises Plot of the Preload	46
Figure 3 30	von Mises Plot of the Screw Preload	47
Figure 3 31	von Mises Plot of the Preload on the Bone Area (MPa)	48
Figure 3 32	Examples of Abutment Design From Lifecore Biomedical	49
Figure 3 33	Hexagonal Abutment	50
Figure 3 34	Round Abutment and Over Denture Material Quartered Volume	51
Figure 3 35	Denture Material Stress Strain Curve	52

Figure 3 36	Boundary Conditions of the Abutment and Denture Material	53
Figure 3 37	Total Reaction Forces for the Quarter Volume Abutments with Different Clearances	55
Figure 3 38	Total Reaction Forces for the -0.03 mm Interference Fit Abutment with Increasing Coefficients of Friction	56
Figure 3 39	Final Prosthesis Design and Overdenture	57
Figure 4 1	Prosthetic Model with Hole Drill Paths	61
Figure 4 2	Prosthetic Surrounded By Work Piece Model	62
Figure 4 3	Bridgeport Interact 412 Vertical Machining Centre	62
Figure 4 4	Face Mill Sequence 1 (A) ProEngineer Tool Path (B) Machined Work Piece	66
Figure 4 5	Volume Mill Sequence 1 (A) ProEngineer Tool Path (B) Machined Work Piece	66
Figure 4 6	Volume Mill Sequence 2 (A) ProEngineer Tool Path (B) Machined Work Piece	67
Figure 4 7	Profile Mill Sequence 1 (A) ProEngineer Tool Path (B) Machined Work Piece	68
Figure 4 8	Abutment Trajectory Mill ProEngineer Tool Path	68
Figure 4 9	Milling Fixtures with Planes Normal to the Axes Holes	69
Figure 4 10	Work Piece Attached to Fixture	69
Figure 4 11	Counterbore Sequence ProEngineer Tool Path	70
Figure 4 12	Centredrill Sequence (A) ProEngineer Tool Path (B) Machined Work Piece	71
Figure 4 13	Drill Sequence ProEngineer Tool Path	71
Figure 4 14	Face Mill Sequence 2 ProEngineer Tool Path	72



Figure 4.15	Volume Mill Sequence 3. (A) ProEngineer Tool Path.	
	(B) Machined Work Piece.....	73
Figure 4.16	Profile Mill Sequence 2. (A) ProEngineer Tool Path.	
	(B) NC Tool Path.....	73
Figure 4.17	Surface Mill Sequence ProEngineer Tool Path.....	74
Figure 4.18	Face Mill Sequence 3. ProEngineer Tool Path.....	75
Figure 4.19	Profile Mill Sequence 3. (A) NC Tool Path.	
	(B) Machined Work Piece.....	75
Figure 4.20	Profile Mill Sequence 4. (A) ProEngineer Tool Path.	
	(B) Machined Work Piece.....	76
Figure 4.21	Erowa Swiss Palletising and Indexing Machine.....	78
Figure 4.22	(A) Work Piece Drilled and Tapped.	
	(B) Work Piece Fixed to the Pallet by Screws.....	78
Figure 4.23	Horizontal and Vertical Portable Chuck.....	79
Figure 4.24	First Operation Completed. (A) Unigraphics Tool Path Model.	
	(B) Machined Work Piece.....	80
Figure 4.25	Standard 3 Axis Milling Machine.....	81
Figure 4.26	Fixture Used to Locate the Prosthetic for the Manual Machining Centre.....	81
Figure 4.27	Lever Type Dial Indicator.....	82
Figure 4.28	(A)(B)(C)(D) Profiling Operation.....	83
Figure 4.29	Prosthetic Secured to a Fixture.....	84
Figure 4.30	Unigraphics Tool Path Model Profile Milling the top Surface.....	84
Figure 5.1	Mitutoyo Euro-M544. CMM.....	88
Figure 5.2	CMM Touch Probe.....	88

Figure 5 3	Operation of a 3-D Scanning Probe	89
Figure 5 4	Measurements Taken From Points on the Prosthetic Hole Areas	90
Figure 5 5	Measurements Taken From Points on the Prosthetic Surface Areas	91
Figure 5 6	Total Orthogonal Deviation of Each Measurement Point	92
Figure 6 1	Instron Tensile Testing Machine	95
Figure 6 2	FEA Tensile Test Model	96
Figure 6 3	Loads and Degree of Freedom Constraints on the Prosthesis and Brackets	98
Figure 6 4	Aluminium Physical Testing and FEA Analysis	99
Figure 6 5	Titanium Physical Testing and FEA Analysis	102
Figure 6 6	Aluminium and Titanium Multilinear Properties	103
Figure 6 7	Revised Titanium Multilinear Properties	103
Figure 6 8	Aluminium, Proposed Titanium, and RIF Titanium Material Properties	104
Figure 7 1	First Rendered Animation Sequence Sectioning the Skull	106
Figure 7 2	Zero Keyframe Location	107
Figure 7 3	Second Keyframe Location	107
Figure 7 4	Third Keyframe Location	108
Figure 7 5	Fourth Keyframe Location	109
Figure 7 6	Fifth Keyframe Location	109
Figure 7 7	Second Animation Sequence Locating the Prosthetic	110
Figure 7 8	Third Animation Sequence Locating the Screws	111
Figure 7 9	Third Animation Zero Keyframe	112
Figure 8 1	Flow Chart of the Prosthesis Manufacturing Process	117

## LIST OF TABLES

Table 2 1	Mechanical Properties of BCBN and CBN	12
Table 3 1	Titanium Isotropic Multilinear Plastic Values	22
Table 3 2	Results of the Prosthesis Analyses	27
Table 3 3	Summary of Maximum von Mises Stress Analysis Results	41
Table 3 4	Dental Material Multilinear Plastic Values	52
Table 3 5	Abutment Total Reaction Forces	54
Table 3 6	Total Reaction Forces for Different Quarter Abutment Models	54
Table 3 7	Total Reaction Forces with Different Coefficients of Friction	56
Table 4 1	GMIT Tools and Offsets	63
Table 4.2	GMIT Production Process Plan	65
Table 4.3	Milling Tools, Offsets, Feeds, and Speeds	77
Table 6 1	Aluminium Physical Testing Results	96
Table 6 2	Aluminium Isotropic Multilinear Plastic Values	97
Table 6 3	Aluminium FEA Analysis	98
Table 6 4	Titanium Physical Testing Results	99
Table 6 5	Titanium Isotropic Multilinear Plastic Values	100
Table 6 6	Titanium FEA Analysis	101

---

# Chapter 1

## Introduction

- 1.1. Background to the Study
- 1.2. Objectives of the Thesis
  - 1.2.1 Specific Technical Objectives
- 1.3 Thesis Structure

### **1.1. Background to the Study.**

In recent years, there has been a wide diffusion of Computer Assisted Surgery (CAS) techniques in clinical practice, to provide surgeons with new tools that can improve surgical accuracy and reliability, decrease surgical risks and achieve individualised planning to obtain shorter operating times and improved outcomes. Computer Assisted Surgery embraces the use of Computed Tomography (CT), Magnetic Resonance Imaging (MRI), Scan Conversion (SC), rapid prototyping (RP), three-dimensional Computer Aided Design (CAD), Robotics, Rapid Manufacturing, Reverse Engineering and Finite Element Analysis (FEA) to create and position customised implants for the purpose of improving surgical procedures [19]

Maxillo-facial surgery is required to address defects, deformities, or trauma in the jaws or facial bones. This can result from oral cancer, rare diseases, car accidents, assault, etc. Computer assisted surgical techniques permit high accuracy and facilitate the transfer of the surgical plan into the patient by creating customised implants that are positioned accurately using customised cutting and positioning jigs across a wide range of clinical situations from treatment of facial deformity to facial pain.

An Enterprise Ireland funded CORD feasibility study carried out on this research topic has revealed that Mr. Ninian Peckitt<sup>1</sup> is the only person performing customised Maxillo-facial surgery using large titanium implants. Peckitt has the only US patent on large customised implants used in maxillo-facial surgery (US Patent 6,254,639 Prosthetic Implants). The only European patent involving the use of rapid prototyping, CNC, customised tools, and implants in maxillo-facial surgery, Patent # GB2138058 "Three-dimensional modelling of maxillo-facial implants", also belongs to Mr. Peckitt [19].

The large customised titanium implants, as a facsimile of the resected bone, used by Peckitt, has used many techniques of computer assisted surgery to address surgical reconstruction, and evidence based results have indicated savings in time, cost, intensive care unit time, ambulation, morbidity and mortality. Furthermore, in some cases it became possible to perform the procedures on patients with compromised medical conditions or elderly people [19].

A Research Innovation Fund (RIF) Project entitled: "Design and Manufacture of Customised Maxillo-Facial Prostheses", which preceded this current project, developed a process where Medical Imaging by using CT/MRI scans, FEA, CAD, and RP, were presented as an integrated approach that could be used for the realistic modelling and simulation of damaged bone and the design of the implant. In comparison to Peckitt's method, the RIF project was more efficient, streamlined, dimensionally accurate, and even more cost effective. The RIF project produced an implant that was stronger, lighter, and easier to position surgically [19].

## 1.2 Objectives of the Thesis.

The primary objective of the present GMIT, Internal Research Development Program (IRDP) project was to investigate two possible design improvements to the RIF implant detailed in the first bullet point in section 1.2.1 below. These improvements also created the possibility of using CNC machining techniques to manufacture the implant, rather than investment casting or selective laser sintering of titanium powder. It is clear from the RIF project, that the work carried out in this project was highly novel, technically challenging and has not been achieved before [18].

---

<sup>1</sup> **Ninian Peckitt**, BDS MB ChB LRCP MRCS(Eng) FRCS FFD RCS FDS RCS, Consultant Cosmetic Maxillofacial Surgeon, Director ComputerGen Implants Ltd, UK

### 1.2.1 Specific Technical Objectives.

The specific technical objectives of this research were to

- Improve the design of the current maxillo-facial implant, by removing the restraining wings by the addition of screws, which affix the implant to the dense material of the cheekbone, and incorporate the over-denture abutments directly into the implant.
- Develop a computer based finite element modelling methodology for design and optimisation of the new implant and an understanding of the stress and force interaction between the screws and hard tissue anchorage points.
- Create a high quality titanium prototype by CNC machining techniques, which can be measured and tested in order to prove its effectiveness
- Perfect reverse engineering and quality metrics with equipment such as a Coordinate Measuring Machine (CMM), which can be applied to the manufactured implant
- Perform tensile mechanical tests on the manufactured implant to characterise the properties of the titanium implant produced using the CNC machining, for comparison with the values obtained in the finite element analysis
- Develop 3D animated video streams, which will assist the clinician in preparation for surgery. The animation will virtually remove the tumoured portion of the maxilla, animate the insertion path of the implant, and visualise the placement and tightening of the restraining screws

The methodology used for these objectives were to optimise the RIF design using the FEA software. Once the new design had been identified and perfected, a titanium prototype was manufactured using a CNC milling machine. This prototype was analysed with CMM techniques to determine its dimensional accuracy, and then a tensile test was performed on it to compare the findings with the FEA results. Finally, specialised software was used to create an animation of the surgical procedure.

### 1.3. Thesis Structure.

The thesis consists of eight chapters Chapter 3 to Chapter 8 detail a specific area from the objectives of the project. A brief overview of each Chapter is discussed below

- **Chapter 1** - Introduces the research topic, and details the associated objectives of the study
- **Chapter 2** – Gives the history, and a description of the current state of knowledge in maxillo-facial surgery It discusses the suitability of different types of titanium for implant purposes, the problems encountered when machining titanium and the most suitable cutting tools for milling titanium An overview of the reverse engineering techniques used in this project is given. In addition the benefits of titanium CNC milling as opposed to RP techniques is examined
- **Chapter 3** – Presents an FEA comparison study of the RIF implant with wings, to the new implant without wings, under typical human bite force conditions, with a view to developing a design that will have an optimised internal stress distribution, and a minimum weight. It also details and compares an axisymmetric, quarter volume, and full volume contact analysis of the bone-screw-implant interface In addition, an analysis of the literature recommended, screw preload is studied Finally, the reaction forces involved in pulling out and pushing in the abutments to and from the over denture are analysed.
- **Chapter 4** – Is a detailed study of two machining strategies used to mill the prosthetic It also looks at the costing of the preferred manufacturing method
- **Chapter 5** – Details the dimensional/tolerance checking of the prosthesis using the Coordinate Measuring Machine (CMM)
- **Chapter 6** – Examines the physical tests performed on the prosthesis, and compares them to the equivalent FEA analysis, with the aim of proving the validity of all the FEA analyses
- **Chapter 7** – Presents an account of the 3D animated video streams, which assist the clinician in preparation for surgery.
- **Chapter 8** – Contains the main findings and conclusions of the research.

---

## Chapter 2

### Current State of Research in Maxillo-facial Surgery

- 2.1 History of Maxillo-facial Surgery
  - 2.1.1 Suitability of Titanium for Implant Purposes
  - 2.1.2 Titanium Performance in Medical Applications
- 2.2 Osseointegration
- 2.3 Contact Analysis
- 2.4 Machining Titanium
  - 2.4.1 Cubic Boron Nitride Cutting
- 2.5 Reverse Engineering
- 2.6 Rapid Prototyping Vs CNC Milling
  - 2.6.1 Rapid Prototyping
  - 2.6.2 Computer Numerically Controlled (CNC) Milling

#### 2.1 History of Maxillo-facial Surgery

Maxillo-facial surgery is a relatively new speciality of medicine; it was not established as an organized specialty until the second half of the 20th century [1]

In the early 20th century, maxillo-facial surgery was characterized by a high intra- and postoperative death rate. After the Second World War with the application of endotracheal<sup>2</sup> anaesthesia [45], improvements in antibiotics, blood transfusion, and intensive care, major operations in the entire maxillo-facial region became more successful.

In the past 25 years many new surgical techniques have been developed, important technical progress has been made, and new scientific information has been gained, only to be outdated by more developments and even better techniques.

---

<sup>2</sup> **Endotracheal** Within or passing through the trachea



---

Today's routine use of anaesthesia and intensive care has made possible operations lasting for hours without endangering the patient

Modern technology in the form of imaging techniques such as CT and MRI scans have also played an important role in the development of maxillo-facial surgery [1,22,23,24], they have contributed to a rapid progress in diagnostic and therapeutical techniques. With these techniques it is now possible to make specific diagnoses and to plan operations with a high degree of accuracy

Ideally, the Surgeon would use the patient's own tissues for transplants, but this kind of surgery cannot always obtain the desired results. Artificial parts may be required to restore the ability to speak or eat as well as for cosmetic appearance

Osseointegrated<sup>3</sup> titanium implants meeting all the requirements of biocompatibility<sup>4</sup> and strength have made possible advances in surgery for the successful treatment of patients with large defects [25,26]. The high strength, low weight, low density [27], outstanding corrosion resistance [28], and low cost [29] possessed by titanium and titanium alloys, have led to a wide and range of successful applications in surgery and medicine, which demands the highest levels of reliable performance

### 2.1.1 Suitability of Titanium for Implant Purposes.

More than 1000 tonnes of titanium devices of every description and function are implanted in patients worldwide every year [6]. Requirements for joint replacement continues to grow as people live longer, damage themselves more through contact sports, or are seriously injured in accidents. Light, strong and biocompatible, titanium is one of the few materials that naturally match the requirements for implantation in the human body

Medical grade titanium alloys have a significantly higher strength to weight ratio than competing stainless steels [6]. The range of available titanium alloys enables designers to select materials and forms closely tailored to the needs of the application. The full range of alloys reaches from high ductility commercially pure titanium used where extreme formability is essential, to fully heat treatable alloys

---

<sup>3</sup> **Osseointegrated**: A direct structural and functional connection between living bone and the surface of a load carrying titanium implant

<sup>4</sup> **Biocompatibility**: The quality of compatibility in a living environment in spite of adverse or unwanted side effects

Commercially Pure (CP) is titanium in its purest form, unalloyed with any other elements. Successful clinical performance of machined/turned CP titanium implants has resulted in wide spread usage, for example the screw in Figure 2.1. However, in bone of poor quality and quantity, the results have been very poor [36].



Figure 2.1. Commercially Pure Solid Titanium Screw Implant.

The Ti-6Al-4V alloy is increasing in use as an implant material. One of the problems with the alloy is that Aluminium (Al) and Vanadium (V) are not biocompatible. The relationship between polarization resistance,<sup>5</sup> and the type of tissue reaction for various pure metals and alloys defines the biocompatibility grouping for elements [31]. Aluminium is classified in a capsule (scar tissue) group; Vanadium is classified in a sterile abscess (toxic) biocompatible group, while titanium with its excellent biocompatibility belongs to the loose connective vascularised (vital) group in tissue reaction [31]. A new Ti-15Zr-4Nb-4Ta alloy with its excellent mechanical properties, corrosion resistance and corrosion fatigue properties and biocompatibility can be expected to become a new alloy for medical applications in the future. Titanium (Ti), Zirconium (Zr), Niobium (Nb), and Tantalum (Ta) exhibit excellent biocompatibility [3].

Titanium foams made from a new powder metallurgical process have bimodal pore distribution architecture (macropores and micropores) mimicking natural bone [7]. The open porosity level of these foams is calculated as the difference between the total and closed porosity [32]. The open porosity ratio can be defined as the ratio of open porosity to total porosity [33]. This open porosity ratio can be manipulated to vary from 0.2-0.3 to replace cancellous<sup>6</sup> bone or 0.5-0.65 for cortical<sup>7</sup> bone. This

<sup>5</sup>**Polarization Resistance:** The method of measuring corrosion rates

<sup>6</sup>**Cancellous:** Also called trabecular bone; an inner spongy structure that resembles a honeycomb. The inner bone cavities contain bone marrow where red blood cells are produced.

<sup>7</sup>**Cortical:** The dense bone that forms the outer surface of bone

---

titanium has a good ability to form an apatite layer<sup>8</sup> throughout the foam. The porous scaffolds that mimic the bone are exploited to allow a steady blood supply and nutrient transport, therefore they can support bone regeneration throughout the foam.

The titanium foam is anticipated to be a promising implant material for bone tissue engineering applications in the future due to its excellent biomechanical properties and bioactivity, but further research into the area is needed [7,35].

### 2.1.2 Titanium Performance in Medical Applications.

‘Fit and forget’, is an essential requirement where equipment in critical applications, once installed, cannot readily be maintained or replaced. The effectiveness and reliability of implants, is an essential factor in saving lives and in the long-term relief of suffering and pain.

Implantation represents a potential assault on the chemical, physiological, and mechanical structure of the human body. There is nothing comparable to a metallic implant in living tissue. Corrosion of implanted metal by body fluids, results in the release of unwanted metallic ions, with a likely interference in the processes of life. Even in very small concentrations from a minimum level of corrosion, these may initiate rejection reactions. Titanium is judged completely inert and immune to corrosion by all body fluids and tissue, and is thus bio-compatible [6].

The natural selection of titanium for implantation is determined by a combination of its most favourable characteristics including immunity to corrosion, biocompatibility, strength, low modulus, density, and osseointegration [30,32,33,34,35].

The mechanical and physical properties of titanium alloys combine to provide implants that are highly damage tolerant. The lower modulus of titanium alloys compared to steel is a positive factor in reducing bone resorption<sup>9</sup>. Another parameter that defines the usefulness of the implantable alloy is the resistance to crack propagation, or fracture toughness [6].

---

<sup>8</sup> **Apatite:** Chief constituent of phosphate rock and of bones and teeth

<sup>9</sup> **Bone Resorption:** The process by which old bone tissue is broken down and removed by special cells called osteoclasts. Bone resorption is very fast and any one spot takes only about three weeks. Bone resorption is normally in balance with bone formation.

## 2.2 Osseointegration

The local mechanical and chemical environment around bone-interfacing implants determines successful bone formation, which leads to functional osseointegration [37,39].

Less stiff implants yield better osseointegration. A low-stiffness implant results in a more homogeneous stress distribution and less micro motion because it has similar strains with the adjacent bone tissue [40].

A reduction of screw stability after surgical insertion is a common problem encountered in fracture fixation or other instrumentation procedures, and a higher screw osseointegration appears to be an ideal way to improve the screw fixation. One approach to increase the likelihood of osseointegration has been to coat implant surfaces with a bioactive ceramic [36] for example a plasma-sprayed hydroxyapatite<sup>10</sup> (HA) coating [38].



Figure 2.2 Titanium Screw Implant with a Hydroxylapatite (HA) Coating.

Beyond an increase in surface area as compared to smooth surface implants, as seen in Figure 2.1, this HA surface has an accelerated initial integration, which makes it ideal for quick initial post-surgical stabilization in weak bone [37].

During the coating process the crystalline structure of the HA decreases and is chemically transformed to tricalcium phosphate, resulting in changes of crystal structure and specific surface area. These changes in turn affect the stability or dissolution behaviour of the ceramic coating layer [38].

The mechanical stability of the fixation during the initial postoperative phase depends on the interaction between the injured bony tissue and the surface of the implant. The fixation of uncoated implants to bone must rely heavily on mechanical

<sup>10</sup> **Hydroxyapatite:** The major component of tooth enamel, and a large component of bone material.

retention rather than chemical bonding. On the other hand, in the case of coated screws, chemical bonding is more important for osseointegration than mechanical bonding. At the bone–implant interface when the entire coating disappears, it is most likely that there will be no problem if the bioactive ceramic coating gradually disappears, because new bone will be laid in its place [37].

These osteoconductive bioactive ceramic coatings can reduce complications caused by early fixation weakness of standard screws, and thus allow early motion exercises and weight bearing [38]. They might also enable the reduction of implant size or number of implanted screws, resulting in improved clinical results [37].

### 2.3 Contact Analysis

A screw in a maxillo-facial prosthesis will only loosen if the loosening force is greater than the clamping force; the clamping force is the result of the preload. The preload should be within the elastic limit of the screw to prevent plastic deformation. The preload must be greater than the maximum biting force to prevent loosening [8]. The recommended torque for titanium screws is 32 N·cm.

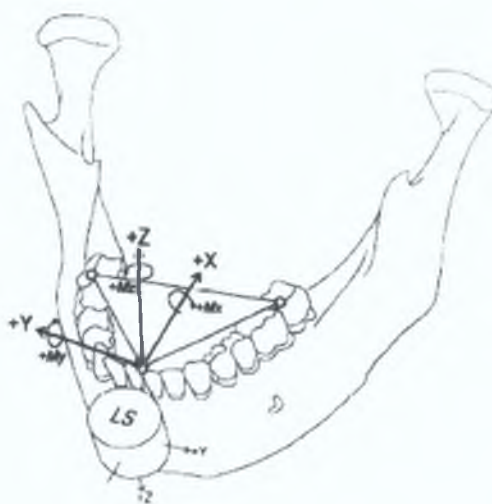


Figure 2.3. Human Mandible Force and Moment Directions.

Korioth et al [9] have shown that the highest resultant forces from biting occur in the positive Z direction, as seen in Figure 2.3, in the range of 24.5 to 28.4 N, and the largest moments are in the  $M_y$  (back and down) direction in the range of 8.9-17 N·cm. However, indications are that for dentate humans, the maximum biting force varies between individuals and different regions of the dental arch. Maximum bite forces depend on the capacity of supporting tissues to tolerate force during



---

measurements [10,11]. The greatest maximum biting force reported to date is 443 N. [12]. Dentate patients have 5–6 times higher bite force than complete denture wearers. [13]. Haraldson and Carlsson [14] measured an average of 15.7 N for gentle biting, 50.1 N for biting when chewing, and 144.4 N for maximal biting for 19 patients who had been treated with implants for 3.5 years. In another study, Carr and Laney [15] reported maximum bite forces between 4.5 and 25.3 N before and 10.2–57.5 N after three months of treatment with implant-supported prosthesis, and emphasized that, the amount of increase was dependent on the duration of being edentulous.

Mericske-Stern and Zarb [16] investigated occlusal forces<sup>11</sup> in a group of partially edentulous patients restored with implants supporting fixed partial prostheses.

They measured an average value of maximum occlusal force lower than 200 N for first premolars and molars, and 300 N in second premolars. This data suggest that implants placed in the posterior region of the mouth are at greater risk for overloading. Therefore, the use of wider and longer implants may be needed for implant treatment in the rear of the mouth.

## 2.4 Machining Titanium

### 2.4.1 Cubic Boron Nitride Cutting Tools.

The titanium chosen for this project is the widely used Ti-6Al-4V alloy[17,31]. When machining Ti-6Al-4V, conventional tools wear rapidly, because the poor thermal conductivity of the alloy results in a higher temperature closer to the cutting edge during machining, and there exists strong adhesion between the tool and workpiece material. In addition, titanium alloys are generally difficult to machine at cutting speeds of over 30m/min with high-speed steel (HSS) tools, and over 60m/min with cemented tungsten carbide (WC) tools, resulting in very low productivity [2,4,5,17].

A number of new cutting tool materials, such as cubic boron nitride (CBN), and polycrystalline diamond, have a good potential for use in high-speed milling, both are currently very expensive, in addition, they are highly reactive with titanium

---

<sup>11</sup> **Occlusal force:** The force produced between the teeth during mastication.

alloys at high temperatures, and consequently are not suitable for machining these alloys

CBN has a high hardness, second only to diamond, while its chemical and thermal stability is superior to diamond. Conventional CBN sintered tools are composed of CBN powder and metal or ceramics binder materials, which determine the bonding strength of the CBN particles. Therefore, the mechanical and thermal properties of these conventional CBN tools strongly depend on the type and quantity of these binder materials. Some single-phase CBN sintered tools without any binder materials are available, these binderless CBN (BCBN) tools are used for the high-speed milling of Ti-6Al-4V, BCBN tools have a far longer life than conventional CBN tools [2,17]

BCBN tools exhibit excellent mechanical properties and superior thermal stability because the sintered body consists of extremely fine CBN particles. Therefore, tools of this type show great promise for high-speed milling of difficult-to-cut materials.

	BCBN	CBN
CBN contents (volume%)	>99.9	85-90
CBN grain size (micron)	<0.5	1-3
Other constituents	-(Comp. hBN)	Binder (Co etc.)
Process	Direct comp	CBN + Binder
Hardness (GPa)	50-55	35-40
TRS <sup>c</sup> (GPa)	1.35	1.4
Thermal conductivity (W/m.K)	360-400	100-130
Thermal stability	1620	1270

Table 2.1 Mechanical Properties of BCBN and CBN

Table 2.1 details how BCBN tools have a higher hardness and thermal conductivity than CBN tools. Hardness and thermal conductivity are closely related to the resistance to wear and chipping of the cutting tool. For this reason BCBN tools are the most suitable cutting tools for high-speed milling of titanium alloys both economically and functionally [2,17]

---

## 2.5 Reverse Engineering.

There are two types of engineering forward and reverse Forward engineering is the traditional process of moving from high-level abstractions and logical designs to the physical implementation of a system Reverse engineering is the process of capturing the geometry of existing physical objects and then using the data obtained as a foundation for designing something new The new design can be a duplicate of the original or an entirely new adaptation [20]

Reverse Engineering is concerned with obtaining a 3D solid model from a component by using CMM techniques It can be viewed as the process of analysing a system to

- 1 Identify the system's components and their interrelationships
- 2 Create representations of the system in another form or a higher level of abstraction
- 3 Create the physical representation of that system

In some situations, designers give a shape to their ideas by using clay, plaster, wood, or foam rubber, but a CAD model is needed to enable the manufacture of the part As products become more complex in shape, designing in CAD may become challenging or impossible There is no guarantee that the CAD model will be acceptably close to the sculpted model Reverse engineering provides a solution to this problem because the physical model is the source of information for the CAD model This is also referred to as the part-to-CAD process

In maxillo-facial surgery, the reverse engineering technique can be used as a means of accurately specifying a computer model for subsequent finite element analysis, failure determination, or for checking if the accuracy of the manufactured prosthetic corresponds closely to the 3D CAD model

The solution to the reverse engineering problem requires application of the following techniques at successive stages of the process

- 1 Coordinate measurements—for the object identification,
- 2 Surface approximation—for geometrical modelling of the object,
- 3 CAD/CAM systems—to provide technical documentation and NC part programming,



---

## 4 CNC milling machine—for the part manufacturing

Proper information flow between these stages ensures quick and effective performance of the reverse engineering process. For this, the measurement results should be written in a format recognisable to the software used for surface approximation. The results of approximation, in turn, should be written in the form applicable to the CAD/CAM systems. The NC part program should be compatible with the control system of the CNC milling machine. Compatibility of data formats raises the automation level and speeds up the process [41].

### 2.6 Rapid Prototyping Vs CNC Milling.

#### 2.6.1 Rapid prototyping.

Rapid Prototyping (RP) refers to a class of technologies that can automatically construct physical models from CAD files. RP machines are essentially "three dimensional printers", that allow designers to create tangible prototypes of their designs.

Although several rapid prototyping techniques exist, all employ the same basic five-step process. The steps are [21,42]

- 1 Create a CAD model of the design
- 2 Convert the CAD model to an STL file format
- 3 Slice the STL file into thin cross-sectional layers
- 4 Construct the model one layer on top of another
- 5 Clean and finish the model

#### 2.6.2 Computer Numerically Controlled (CNC) milling.

Titanium rapid prototyping is an emerging technology that does not have a great deal of expertise yet, and the fact that proEngineer is so compatible with CNC milling i.e. there is no need to convert the files to STL format. 3-axis CNC machining would seem the natural choice for a solid model of simple geometry. If however, the model required has any internal features or complex surfaces facing a number of directions, then CNC milling would not be suitable [21,43].

CNC milling uses a cutting tool, which traverses a block of material, removing it on a layer-by-layer basis. Figure 2.4 shows a model of a skull defect (only half the skull has been created).

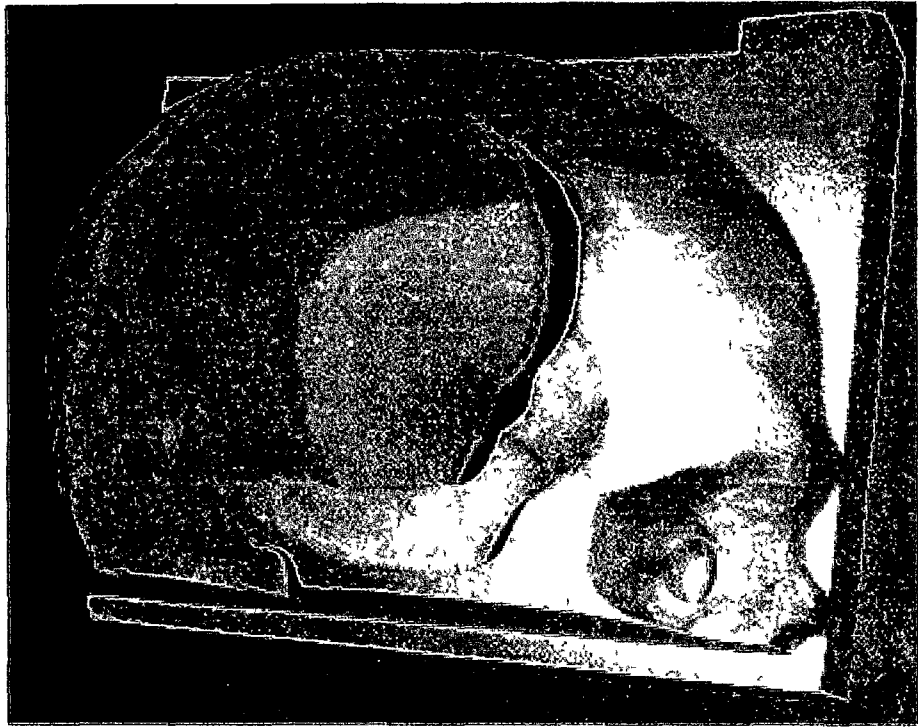


Figure 2 4 Half-Skull Model Created by CNC Milling Showing a Large Cranial Defect

Some of the advantages of using CNC milling over Rapid prototyping are [44]

- **Price of the system.**

Prices of high-end Layered Manufacturing Technology (LMT) machines like the StereoLithography Apparatus used to rapid prototype the prosthesis in the RIF project start at €100,000 (the total investment being higher because of the training needed) Concept Modellers are cheaper, however they still cost a minimum of least €50,000 In contrast, a complete CNC system (software and machine) is available for under €10,000 Most design offices can afford a light CNC milling machine, however, in-house RP machines are not always affordable This not only saves time, it also improves the design quality, as the designers will use a local machine more easily than an external service

- **Trouble-free operation.**

The process of removing material in CNC milling is not complicated, the chances of failure are low This is in contrast to the RP processes, where small variations in operating temperature and humidity may lead to unusable results

- **Capable of handling incorrect STL files.**

RP systems need correct STL files, containing correct normal vectors for each triangle and describing a solid geometry without cracks, gaps, orphan surfaces etc whereas CNC systems can still operate even with these small inconsistencies,

- **Large prototypes.**

CNC machines can handle models far greater in size to RP machines

- **Free choice of accuracy.**

RP systems operate using an almost constant layer thickness. When using CNC milling the distance between the tool paths can be freely chosen, from 0.001 mm (which will result in a very long machining time) to 10 mm or larger. This free choice in accuracy means a choice in building speed as well, opening the possibility to create 'quick and dirty' Concept Models.

## Chapter 3

### Finite Element Analysis

- 3.1 Introduction.
- 3.2 Redesign of the Customised Maxillofacial Prosthesis.
- 3.3 First Modification.
  - 3.3.1 Design Criteria.
  - 3.3.2 Original Prosthesis Analysis.
    - 3.3.2.1 Mesh.
    - 3.3.2.2 Material Properties.
    - 3.3.2.3 Boundary Conditions.
    - 3.3.2.4 Load Step Options.
  - 3.3.3 New Prosthesis Analysis.
    - 3.3.3.1 Mesh.
    - 3.3.3.2 Material Properties.
    - 3.3.3.3 Boundary Conditions.
    - 3.3.3.4 Load Step Options.
- 3.4 Prosthesis, Screw, and Bone Contact Analysis.
  - 3.4.1 Two Dimensional Model (Axisymmetric).
  - 3.4.2 Three Dimensional Model (Quarter Volume).
  - 3.4.3 Three Dimensional Model (Full Volume).
- 3.5 Screw Preload Analysis.
- 3.6 Second Modification.
  - 3.6.1 Design Criteria.
  - 3.6.2 Abutment Design.
    - 3.6.2.1 Mesh.
    - 3.6.2.2 Material Properties.
    - 3.6.2.3 Boundary Conditions.
    - 3.6.2.4 Load Step Options.
- 3.7 Final Design.
- 3.8 Discussion.

#### 3.1 Introduction

Finite Element Analysis (FEA) is a computer-based numerical technique for calculating the strength and behaviour of engineering structures [19,48,49]. It can be used to calculate deflection, stress, vibration, buckling behaviour and many other phenomena. Structures can be analysed for small deflection and elastic material properties (linear analysis), small deflection and plastic material properties (material non-linearity), large deflection and elastic material properties (geometric non-linearity), and for simultaneous large deflection and plastic material properties.

In the finite element method, a structure is broken down into several, sometimes thousands of small elements. The behaviour of an individual element can be described with a relatively simple set of equations. The equations describing the behaviours of the individual elements are assembled into a large set of equations that describe the behaviour of the whole structure. From the solution, the software package extracts the displacement of the individual nodes; it then obtains the strains and finally the stresses of all the parts of the structure. Typically, the user then analyses the results, to see if the structure will be suitable for its particular design. Finite Element Analysis makes it possible to perform detailed and complex analyses on the structural design.

### 3.2 Redesign of the Customised Maxillofacial Prosthesis

The main technical objective of this thesis was to create a new high quality titanium prototype by CNC machining techniques. To accomplish this aim the prosthesis had to be redesigned. The redesign of the prosthesis consisted of two modifications identified in the thesis proposal for this project [18].

The first modification was to remove the restraining wings, shown in Figure 3.1, which would be too difficult to machine using standard CNC machining techniques, and replace them with holes through which relatively long anchoring screws would connect the prosthesis to the high-density upper cheekbone. The surgeon would use these holes in the prosthesis as a jig to locate and orientate the fixing screws. The location and orientation of these holes was obtained from analysing the CT scans of the subject's skull to insure that they penetrated the high-density upper cheekbone, and would ensure the screws that protrude into the bone have the best chance of supporting the resulting biting force loads.

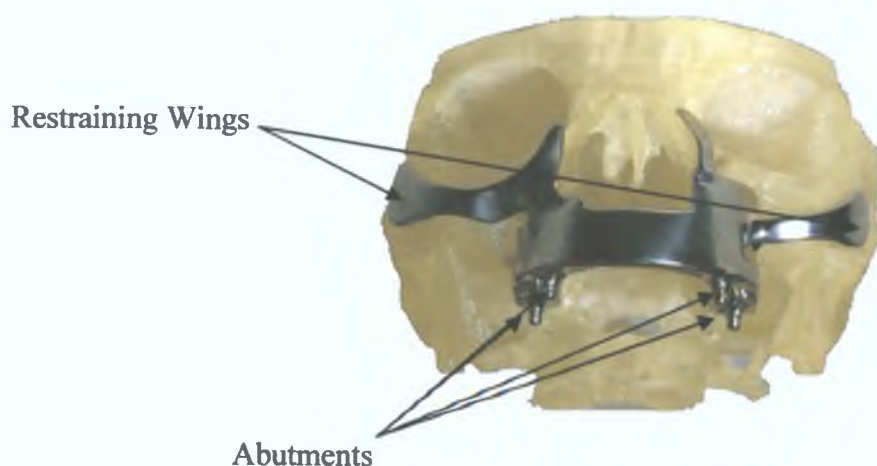


Figure 3.1 Original Customised Maxillofacial Prosthesis.

As shown in Figure 3 1, the original design included four short abutments, which anchored the over-denture to the prosthesis. These abutments were relatively expensive (Stg £ 100 each) and required four holes to be drilled and tapped in the prosthesis [18]. Thus adding to the overall fabrication costs.

The second modification was to include abutments as an integral part of the prosthesis. This change would reduce costs, and decrease the likelihood of infection, by removing four possible incubation sites for bacteria, i.e. the threaded holes [18].

### **3.3 First Modification.**

As a preface to the discussion on 3D modelling, the reader should know that this work was performed using the ANSYS 7.0 University-High license, as such, the maximum model size was restricted to 32,000 nodes [47].

The first modification in the new design was to remove the restraining wings in Figure 3 1 and replace them with four holes through which titanium screws connected the prosthesis to the maxilla bone structure.

The objectives of the analyses in the first modification were to

1. Compare the von Mises stresses of the prosthesis with, and without wings, subjected to the average bite force, determined from literature to be a force of 144 N [19].
2. Study the three-dimensional modelling of the contact stresses between the titanium prosthesis, screw and the maxilla bone.
3. Quantify what effect the application of a preload on the screw has on the prosthesis and maxilla bone behaviour response.

#### **3.3.1 Design Criteria.**

The design criteria for the first modification were

1. The four wings were to be removed, and replaced with four holes in the main body of the prosthesis, which would be used to affix the implant to the maxilla bone by four screws.
2. The surgeon should not have to mutilate the face to gain access to the four holes in the prosthesis.
3. The holes should be aligned with the densest part of the maxilla bone to allow the best chance for osseointegration.

4. The holes should be as large as the prosthesis will allow, providing as much surface area as possible on the screw thread-maxilla bone interface.
5. The geometry should be as simple as possible to reduce manufacturing set up lead times.

### 3.3.2 Original Prosthesis Analysis

The purpose of this analysis was to investigate the stress distribution of the original prosthesis design under occlusal forces. The results obtained from this analysis will be compared with those generated with the new design.

The model shown in Figure 3.2 was a result of the RIF project, and was imported into the FEA package (ANSYS version 7.0 university edition.) as an IGES file.



Figure 3.2 Finite Element Prosthesis with Restraining Wings.

#### 3.3.2.1 Mesh

No volumes were recognised in the model but it did list a total of 3385 areas. These areas were meshed with 8 noded shell elements giving one element to each area. In this model shell elements are only appropriate for the wings as they should only be used for thin sheets of material that are subjected to out of plane loading. The base of the prosthesis is solid with a thick wall and as such, it is more appropriate to mesh it with solid elements. The reason why the prosthesis was meshed with 8 noded shell elements in the first place was that originally it was hoped to hollow out the base to produce thin walls, which would dramatically reduce the weight of the prosthesis. This idea was abandoned because of the difficulty involved in milling such a complex geometry.



To mesh the prosthesis, the most appropriate solid elements were the 3-D ten node tetrahedral structural solid elements. To use solid elements, a volume or volumes, needed to be created. To create a single volume the areas in the wings were extruded 1.4mm in the positive Y direction, which represents the thickness given in the original shell elements. These extrusions created two new volumes. To create a volume from the main body of the prosthesis, strategic areas were created which retained the shape of the prosthesis. The new areas detailed in Figure 3.3 were used to create the main body volume. This volume was then added to the two extrusions on the wings to create one single volume.

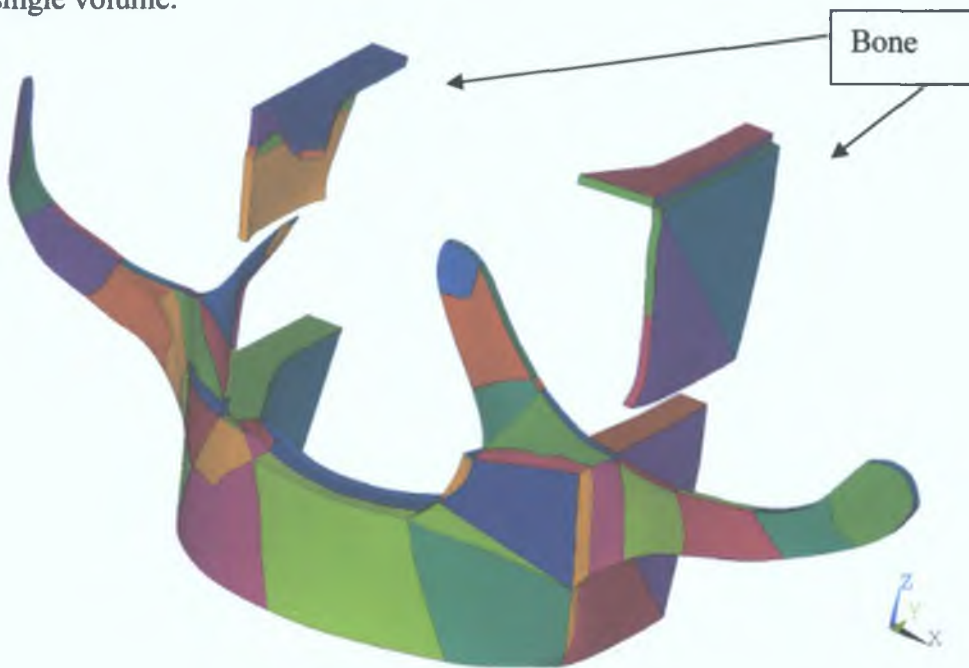


Figure 3.3 Areas Used to Create the Prosthesis and Maxilla Bone Volumes.

The reason these new areas were created was to reduce the number of nodes to within the 32,000-node limit of the ANSYS 7.0 University-High license used for these analyses. The overall accuracy of the results was necessarily reduced but this action was unavoidable. A distinct advantage of having fewer nodes was that the computational time for the analysis was greatly reduced.

### 3.3.2.2 Material Properties.

The material of the prosthetic was titanium with an elastic modulus of 114,000 MPa and a Poisson's ratio of 0.3 [8,19,72]. The isotropic hardening option was selected to represent the material behaviour. To allow for the plastic properties of the titanium, structural plastic multilinear properties were used. There was no information on the multilinear plastic properties of titanium in the literature, so the author had to



make an educated guess as to what they might be. These suggested values listed below are based on the titanium elastic modulus of 114,000 MPa, and what the author thought the stress strain curve should look like.

Strain (mm)	Stress (MPa)
0.001	114
0.002	225
0.003	337
0.004	360
0.005	375
0.025	450
0.06	532
0.1	585
0.15	630
0.2	652
0.25	673
0.275	675

Table 3.1 Titanium Isotropic Multilinear Plastic Values.

These values produce the following stress strain plot.

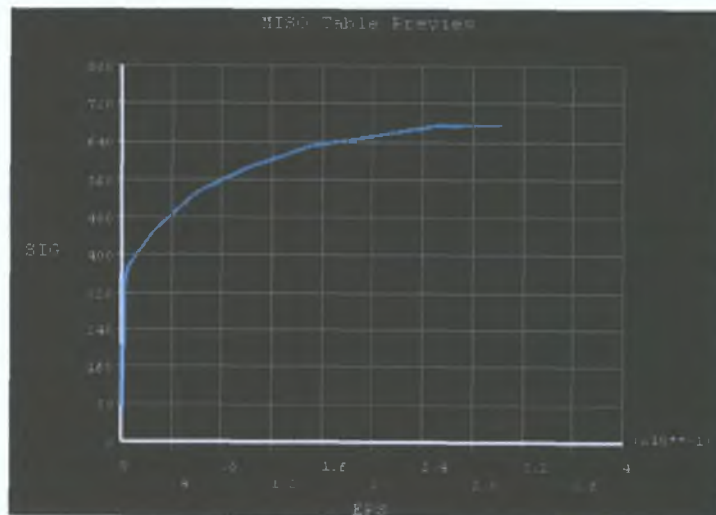


Figure 3.4 Titanium Stress Strain Curve.

The structural properties of cortical bone vary for different anatomical regions depending upon the bone density and orientation. Gordon [51] gives the elastic modulus a value of between 12,000 MPa and 17,000 MPa. While Lutfi Koca et al [52] give it a value of 13,400 MPa, and Polgar et al [53] determined that it is 15,000 MPa. Clearly no definitive value of the elastic modulus of the maxilla bone can be used, and a large

number of analyses within the range of 12,000 to 17,000 MPa would have been prohibitive, so the author decided to use the 13,400MPa value given by Lutfi Koca et al as the selected value, with a Poisson's ratio of 0.3. What degree of inaccuracy in results has been caused by these assumptions, if any remains uncertain [53].

### 3.3.2.3 Boundary Conditions

The prosthesis was constrained by fixing displacements in all degrees of freedom on the wings at several different node locations, which models the effect of the titanium screws fixing the prosthesis to the maxilla bone.

It was also constrained with no displacements in all degrees of freedom at the top flat surfaces, and the left and right outside areas of the bone volumes, which replicated where the maxilla bone structure would not allow the prosthesis to move. The average bite force determined from literature, a force of 144N [19] was then applied to the bottom of the prosthesis distributed over four locations and 16 nodes (with each node having a 9N force in the positive Z direction) to represent where the abutments were to be attached. See Figure 3.5.

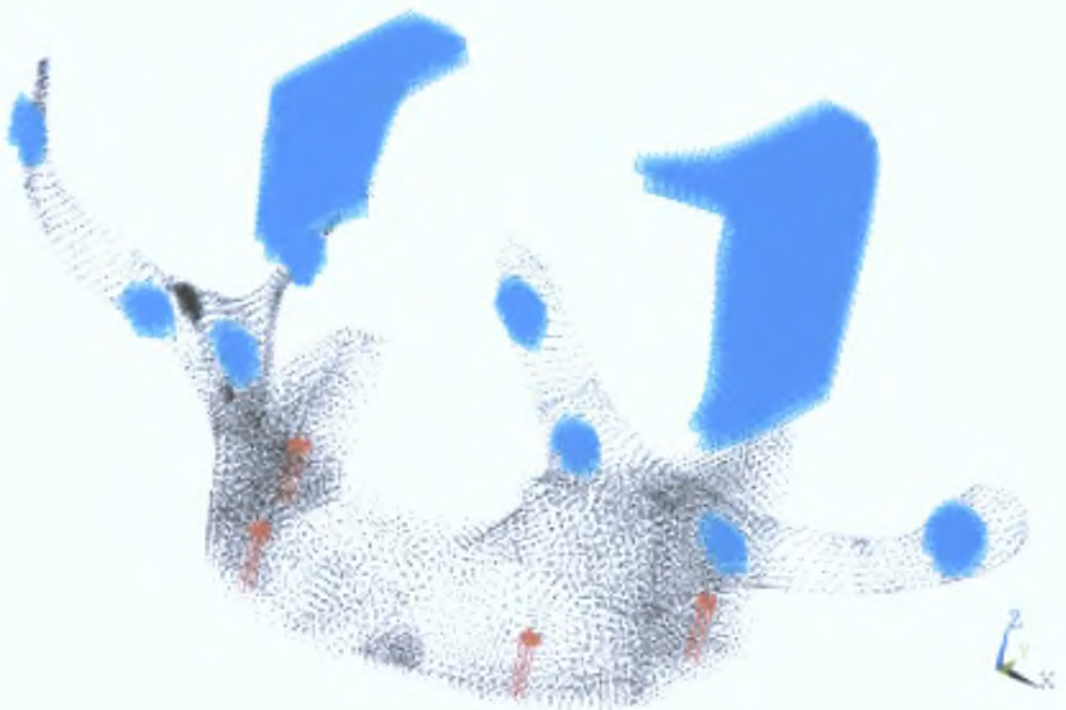


Figure 3.5 Loads and Degree of Freedom Constraints on the Prosthesis with Wings.

### 3.3.2.4 Load step options

A fixed loadstep was applied using the non-linear solution algorithm with a maximum of 10 and a minimum of 1 substeps. The stability of the three dimensional stress state was evaluated according to the von Mises hypothesis. Von Mises stresses summarise the overall stress state at any point. It is considered that if the maximum stress for the structure is exceeded, it may fail in service. A colour scale with 9 stress values served to evaluate quantitatively the stress distribution in the model [19]. The plot of the von Mises stress gradient can be seen in Figure 3.6 where a maximum stress level of 46.619 MPa was obtained. Because the static analysis results were so low an infinite life is suggested therefore a fatigue analysis was deemed unnecessary.

```
NODAL SOLUTION
STEP=1
SUB =6
TIME=100
SEQV (AVG)
TOP
DMX =.03971
SMX =46.619
```

**ANSYS**  
PLOT NO. 1

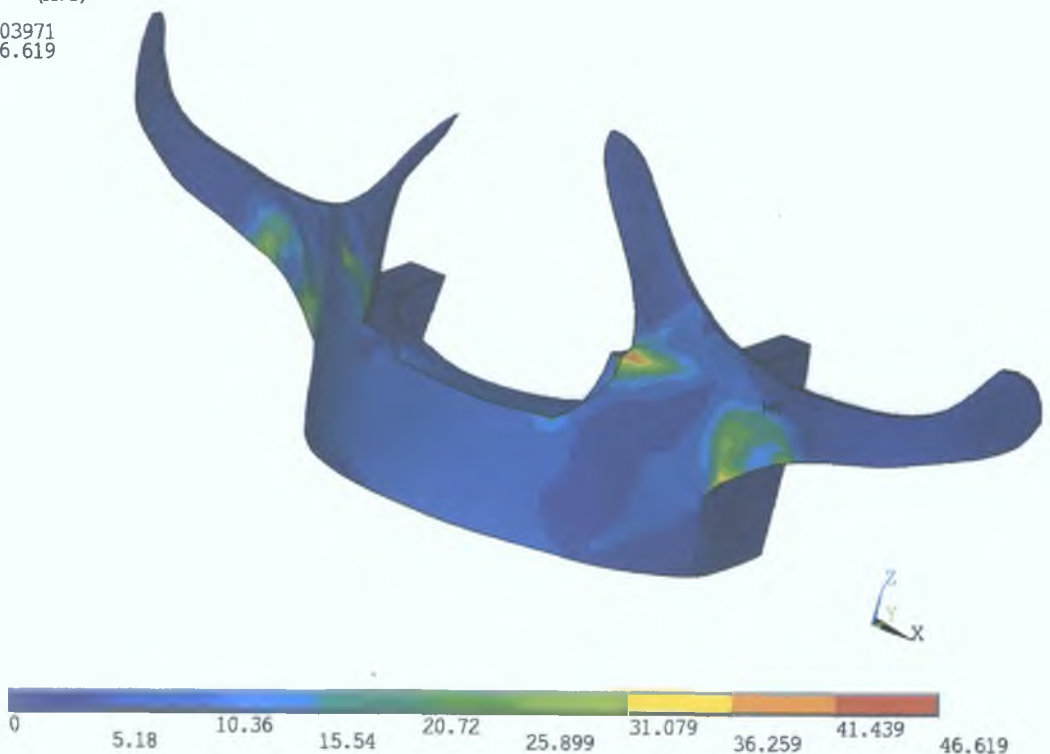


Figure 3.6 von Mises Stress State of Original Prosthesis (MPa).

The stress distribution on the prosthesis indicates that it would not fail in service. However, the high stress spots at some of the hole areas on the wings and the irregular stress gradient, could hinder the osseointegration of the screws to the maxilla bone and lead to inflammation, or hyperplasia<sup>12</sup> formation at the bone, and eventual failure of the prosthetic due to preload loosening [15,55,56].

<sup>12</sup> **Hyperplasia:** is an increase in the number of the cells of an organ or tissue causing it to increase in size.

### 3.3.3 New Prosthesis Analysis

For the new design, the wings were removed and four holes were added that would connect the prosthesis to the maxilla bone, which was obtained from the patients CT scan. The four holes were located by aligning 3mm diameter cylindrical volumes with the volume of the maxilla bone that would give the most contact between the bone and the screws, and so allow for the best chance for osseointegration, as shown in Figure 3.7

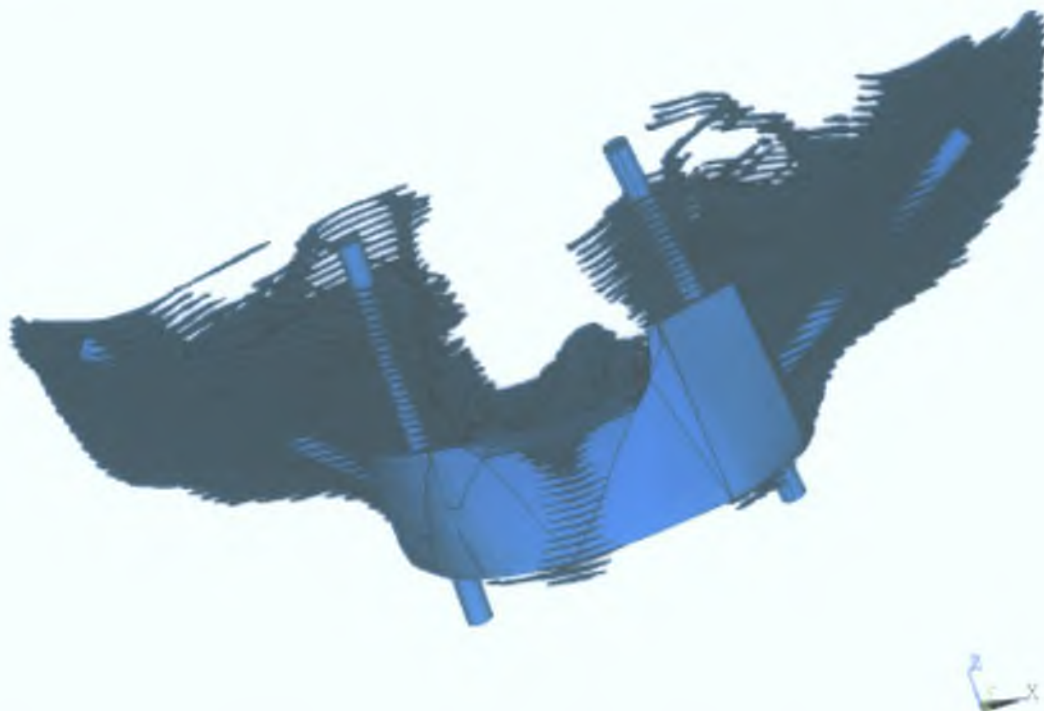


Figure 3.7 Cylindrical Volumes Where the Prosthesis Hole Alignments Will Be.

Once the alignments were made, the cylindrical volumes were subtracted from the prosthesis revealing the holes for the screws.

#### 3.3.3.1 Mesh

Like the original prosthesis, the new prosthesis was meshed with ten node tetrahedral elements with an element edge length of 2.5mm.

#### 3.3.3.2 Material Properties

The same titanium alloy as the original prosthesis was used with an elastic modulus of 114,000 MPa and a Poisson's ratio of 0.3 [8,19,72], and the same multilinear plastic properties from the original prosthesis were used.

For the maxilla bone, again the same elastic modulus of 13,400MPa value given by Lutfi Koca et al [52] was used with a Poisson's ratio of 0.3.



### 3.3.3.3 Boundary Conditions.

The prosthesis was constrained with no displacements in all degrees of freedom on the areas of the four hole locations, which models the effect of the titanium screws fixing the prosthesis to the maxilla bone. It was also constrained with no displacements in all degrees of freedom at the top flat surfaces, and the left and right outside areas of the bone volumes, which modelled where the maxilla bone structure would not allow the prosthesis to move. The same 144N forces [19] were applied as on the original prosthesis, as shown in Figure 3.8.

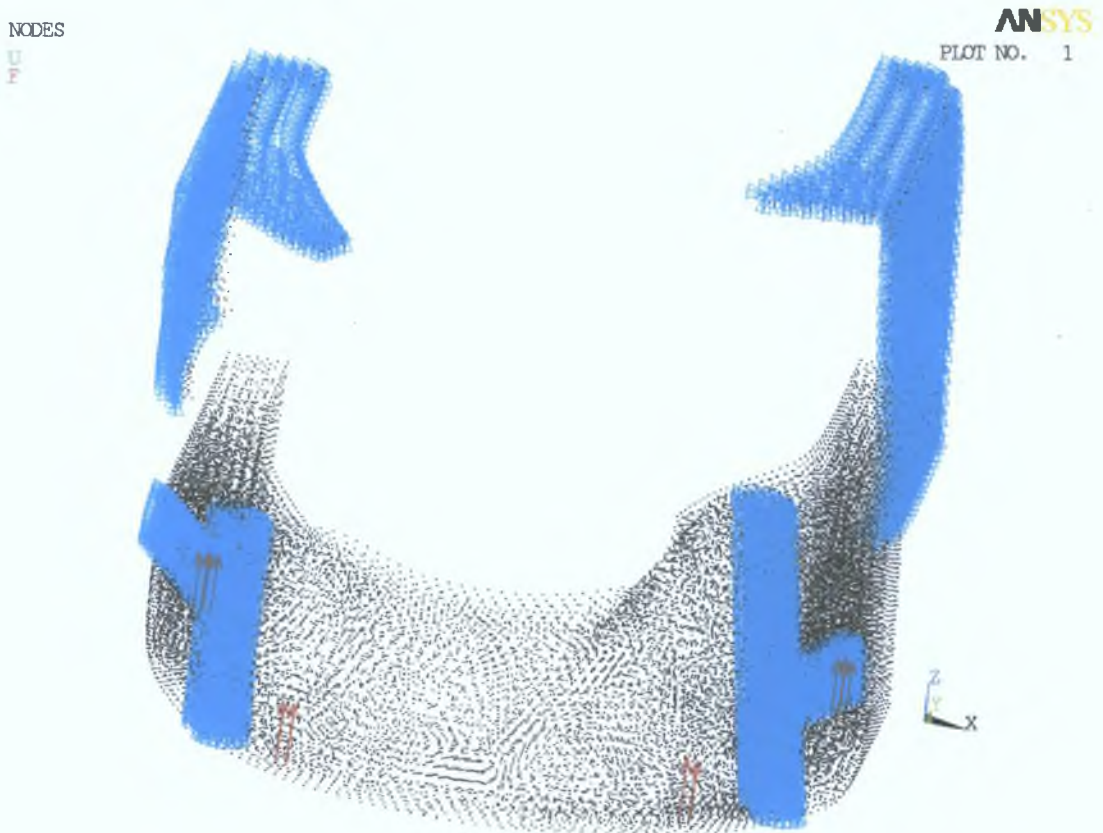


Figure 3.8 Degree of Freedom Constraints on Holes and Forces of the New Prosthesis.

### 3.3.3.4 Load Step Options.

A fixed loadstep was applied using 10 substeps and the non-linear solution algorithm. The stability of the three dimensional stress state was evaluated according to the von Mises hypothesis.

A plot of the von Mises stress is shown in Figure 3.9. Where a maximum stress level of 16.954 MPa was obtained.

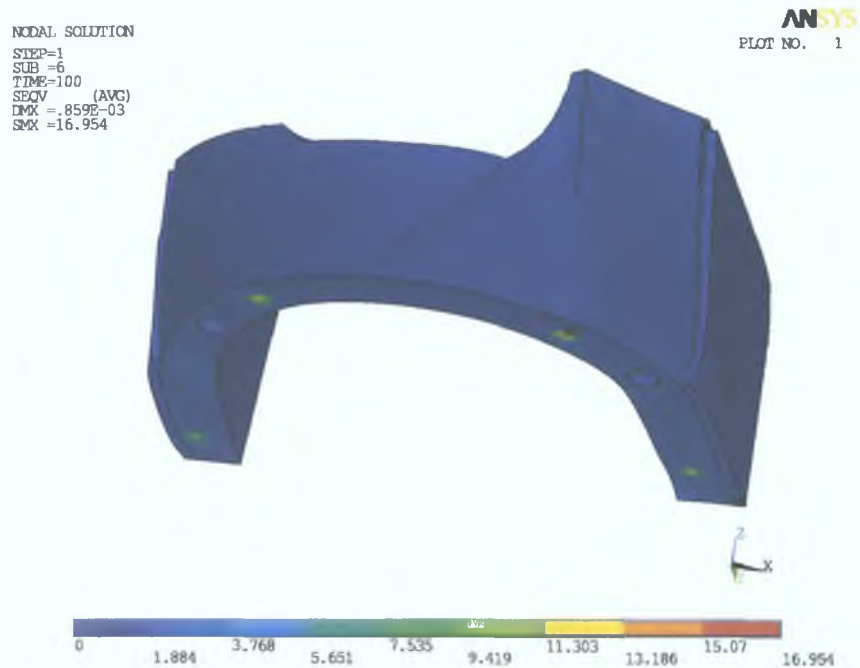


Figure 3.9 von Mises Plot of the New Prosthesis Design (MPa).

The new prosthesis compared to the stresses in Figure 3.6 shows a more homogeneous stress distribution. The reduced von Mises stress suggests that the chance of osseointegration with the new prosthesis was greatly improved.

The results of the prosthesis analysis are summarised below.

	Original Design	New Design	% Difference
Maximum Stress (MPa)	46.619	16.954	-63.63 %
Maximum Deflection (mm)	0.03971	0.000859	-99.914 %

Table 3.2 Results of the Prosthesis Analyses.

### 3.4 Prosthesis, Screw, and Bone Contact Analysis.

There are several theories about what happens when a threaded connection is loaded axially. The most widely accepted theory suggests that the first engaged thread tends to take more than its share of the load. The load then tapers off over the next few threads. This theory is generally accepted and is supported in previous FEA simulations [46,47].

This analysis assumes that the prosthesis has been fixed to the maxilla bone for a number of months and that a high degree of osseointegration has taken place, resulting in perfect contact between the bone and screw.

#### 3.4.1 Two Dimensional Model (Axisymmetric).

The first step of the contact analysis was to create a profile of the 3mm diameter, 0.6mm pitch threaded screw, prosthesis, and bone as a 2D axisymmetric model in the XY plane. Represented in Figure 3.10.

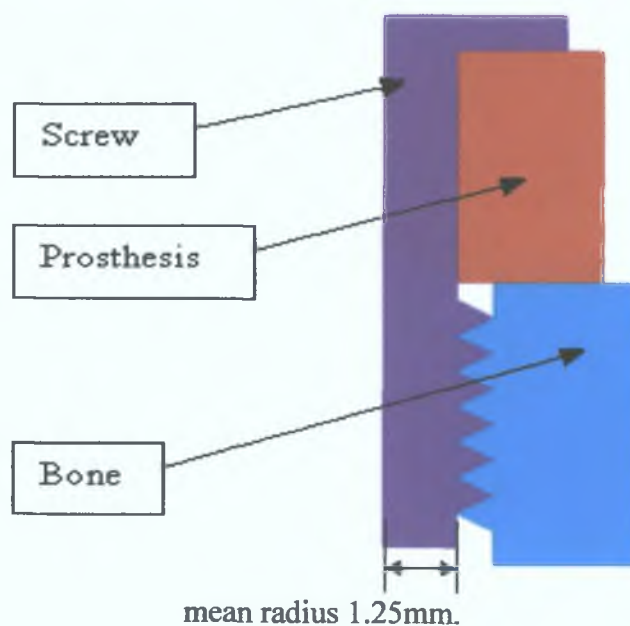


Figure 3.10 Screw, Prosthesis and Bone Areas.

The model was meshed with plane quadrilateral elements using the axisymmetric behaviour option. At the interface between the screw and the bone, and the bone and the prosthesis, contact elements were included to allow sliding and opening of the interfaces. Flexible line-to-line contact element pairs were used, and included a coefficient of friction of 0.2. The material of the screw and the prosthesis was titanium with an elastic modulus of 114,000 MPa and a Poisson's ratio of 0.3 [8,19,72]. The isotropic hardening option was selected to represent the material

behaviour; and the same structural multilinear plastic properties from the first prosthesis analysis were included. For the maxilla bone the same elastic modulus of 13,400MPa value given by Lutfi Koca et al [52] was used with a Poisson's ratio of 0.3.

Zero degree of freedom constraints were applied to the outside of the bone area in all degrees of freedom. The torque applied to the abutments is 0.32 Nm. This level of torque generates the recommended preload in the abutments [8, 54, 55, 56]. However torque cannot be applied as a load in an axisymmetric FEA analysis, so an equivalent force equal to the preload had to be applied to the top of the prosthesis in the positive Y direction to put the screw under a tensile stress shown in Figure 3.11. The mean diameter 2.5mm was taken from doubling the mean radius 1.25mm in Figure 3.10. The equivalent force was applied as a pressure over the surface of the prosthesis. The pressure was derived by applying the following formulae [59]

$$T = K F_1 d \quad (1)$$

T = Torque (Nm)

K = Torque coefficient ( $\cong 0.2$ )

$F_1$  = Preload (kN)

d = Mean diameter (2.5 mm)

A = Cross-sectional area ( $\text{mm}^2$ )

p = Pressure (kPa)

$$F_1 = \frac{T}{(0.2 \times 2.5)} = \frac{0.32}{0.5} = 0.64 \text{ kN} \quad (2)$$

$$A = \frac{\pi d^2}{4} = \frac{\pi 2.5^2}{4} = 4.91 \text{ mm}^2 \quad (3)$$

$$p = \frac{F_1}{A} = \frac{0.64}{4.91} = 0.13 \text{ kPa} = 130 \text{ Pa} \quad (4)$$

This pressure of 130 Pa was applied to the top of the prosthesis in the negative Y direction as seen in Figure 3.11.





Figure 3.11 Loads and Constraints Applied to the Axisymmetric Model.

The model was solved in a non-linear static analysis. There were two stages in this analysis; the first stage had only the zero constraints applied and was to allow the contact and target elements to obtain an equilibrium position. The second loadstep had the 130 Pa pressure applied to the top of the prosthesis in the negative Y direction. The axial load was incremented linearly over 15 substeps. No solution convergence problems were encountered.

A plot of the von Mises stress at the final load step is illustrated in Figure 3.12.

NODAL SOLUTION  
 STEP=2  
 SUB =15  
 TIME=200  
 SEQV (AVG)  
 DMX =.120E-03  
 SMN =.004876  
 SMX =4.145

ANSYS  
 PLOT NO. 1

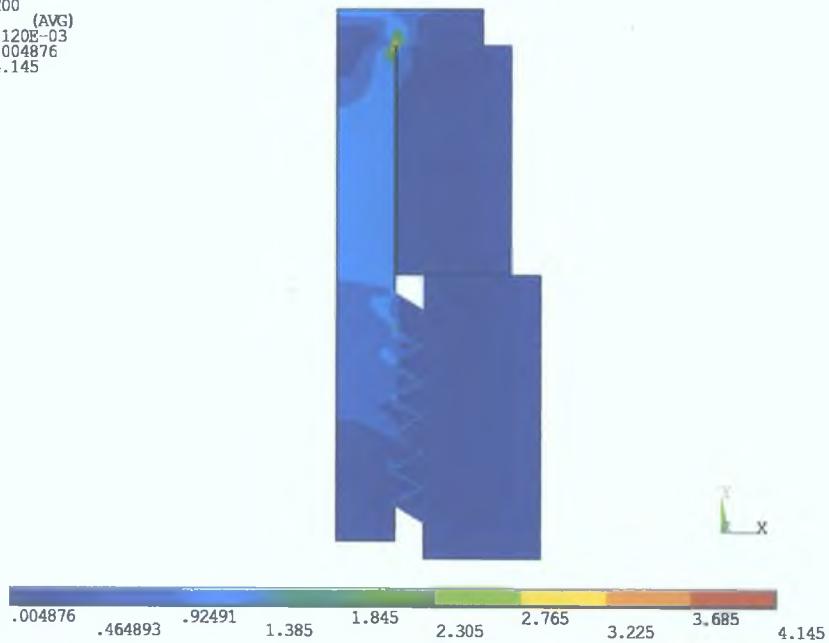


Figure 3.12 von Mises Stress for the Axisymmetric Contact Model (MPa).

The plot shows a high stress spot at the bone-prosthesis interface, caused by the fact that there was no fillet between the screw and the prosthesis. The author was only interested in the interface between the bone and the screw so a second von Mises Plot was made of this area, referred to in Figure 3.13.

NODAL SOLUTION  
 STEP=2  
 SUB =15  
 TIME=200  
 SEQV (AVG)  
 DMX =.110E-03  
 SMN =.010968  
 SMX =1.593

ANSYS  
 PLOT NO. 1

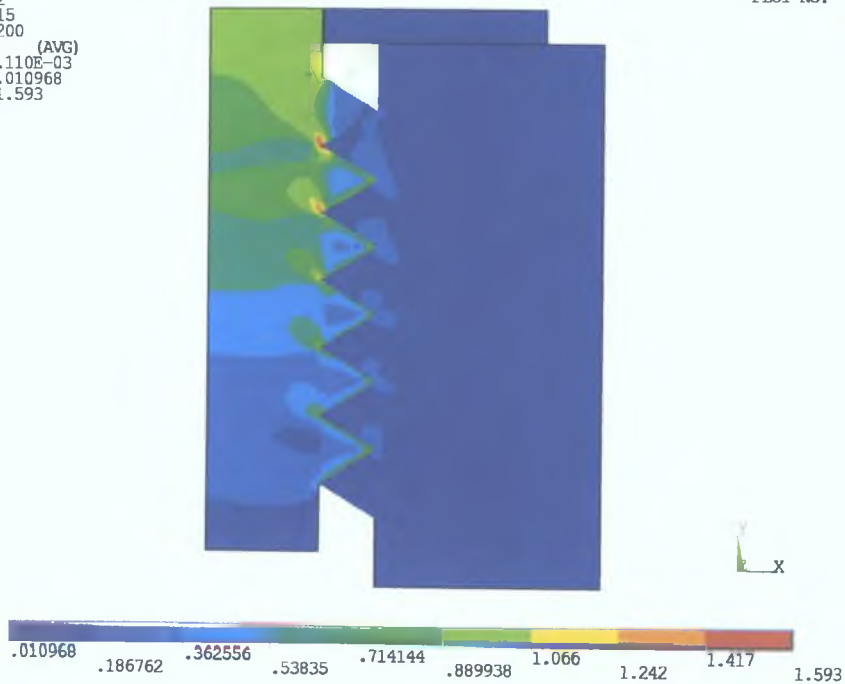


Figure 3.13 von Mises Plot of Contact at the Thread Areas (MPa).

The Maximum von Mises Stress was 1.593 MPa, as expected, the von Mises stress plot showed a high level of stress around the first engaged thread then tapering off on the remaining threads.

Figure 3.14 shows this phenomenon clearly with the highest contact pressure at the first engaged thread and the pressure decreasing in the remaining engaged threads.

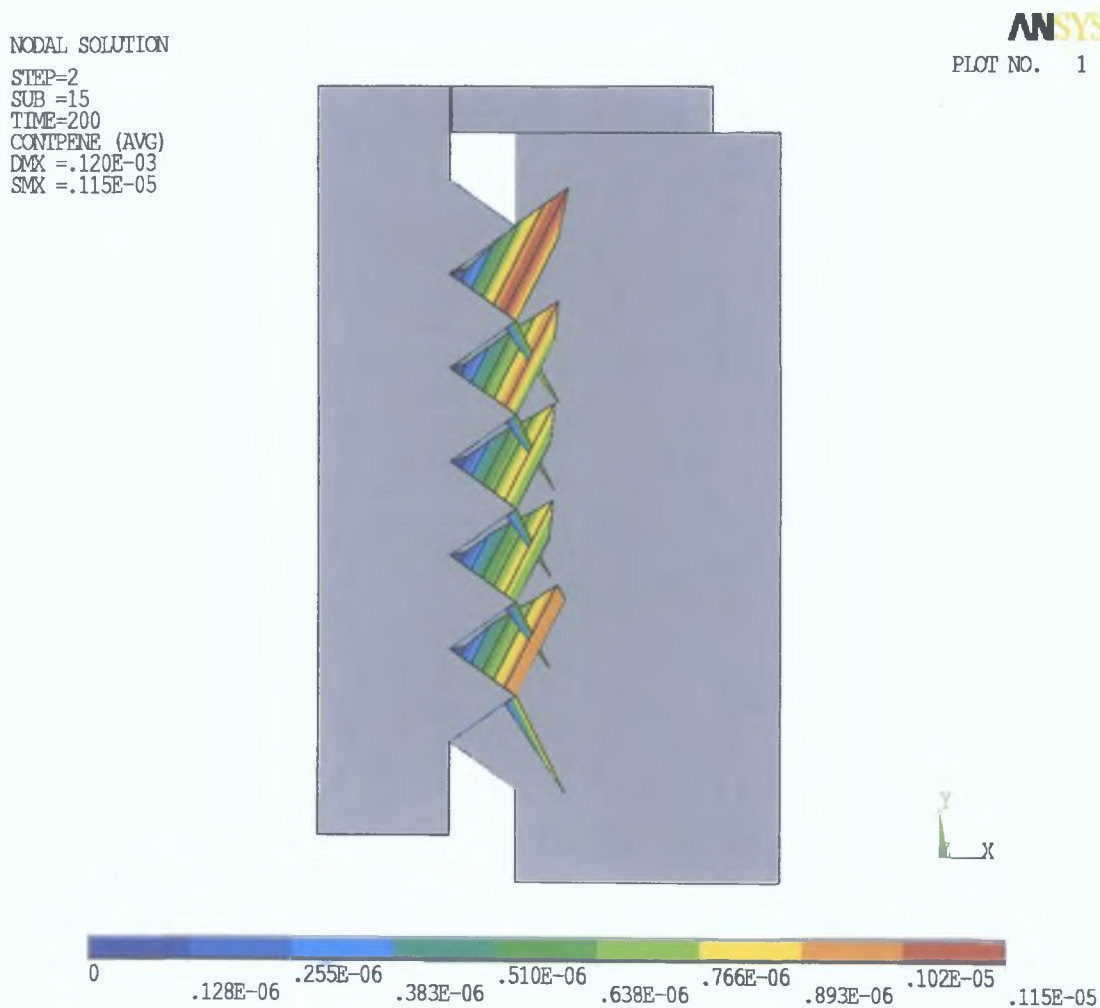


Figure 3.14 Contact Pressure at the Thread Area of the Axisymmetric Model (Pa).

The two-dimensional model shows the typical information used to evaluate the interaction between the prosthesis, the threads of the screw and the bone. However, the two-dimensional model did not consider the helical shape of the thread flank. To accommodate this feature and to measure the validity of the two dimensional approximation, a three-dimensional model was needed [46].

### 3.4.2 Three Dimensional Model (Quarter Volume).

The modelling of a three-dimensional threaded connection proved very difficult and required several attempts in order to achieve a reliable model, which delivered accurate results. This second step was to create a quarter volume from the previous 2D model.

The plane and contact elements from the 2D model were deleted, and a 0.25mm slice was removed from the profile at the centre of the axisymmetric screw to allow a sweep along a helical path to take place. This path was generated using the graphic user interface method detailed in Appendix A, This method left a gap at the centre of the screw; a volume was created to fill this gap and glued to the screw.

The model was meshed with solid 20 node brick elements which as indicated by Johnson et al [46], [60,61], and Benzley [62], are the most appropriate type of element for this analysis, as they lead to more accurate results for a given mesh density.

Three-dimensional solid elements come in two basic shapes: (tetrahedrons) and (hexahedrons) represented in Figure 3.15. FEA programs typically use a select set of elements chosen for their versatility, robustness, and their overall contribution to product ease of use. If the software program cannot sweep elements along a solid model geometry it will default to high-order 10 node tetrahedral elements, if on the other hand the geometry can be swept, high-order 20 node hexahedral elements are employed [60].

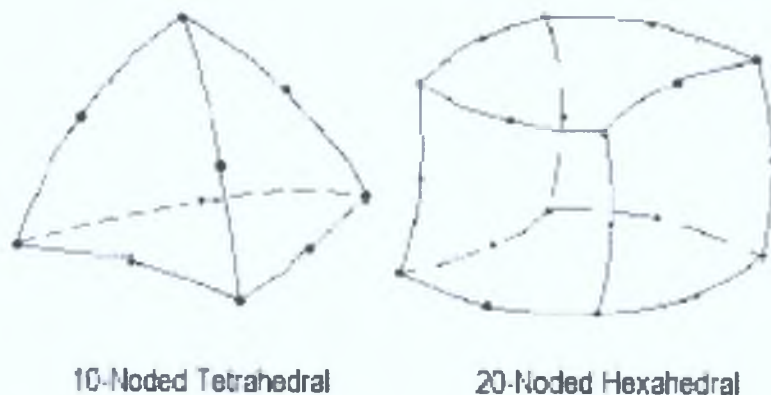


Figure 3.15. Finite Element Tetrahedral and Hexahedral Element Shapes Examples.

At the present moment most automatic mesh generators are incapable of meshing arbitrarily shaped volumes with the more accurate brick elements. However, tet elements can be meshed into any shaped volume.

The stiffness matrix eigenvalues for linear tetrahedrons are generally larger than those for linear hexahedrons. This fact demonstrates that hexahedrons can generally



deform in a lower strain energy state, thus making them more accurate than tetrahedrons [62].

The most compelling reason to use tetrahedral over hexahedral elements is for the improved ability to vary the node spacing within the domain. The structured nature of hexahedral meshes inhibits adjusting local element sizes independently of the surrounding elements, while the unstructured nature of the tetrahedral mesh density allows for adjusting of the local node spacing with minimal effects on the surrounding elements. A second advantage involves the coupling among the degrees of freedom. A linear hexahedral element in a uniform grid shares nodes with 26 other elements. With three translational degrees of freedom per node and all degrees of freedom coupled within an element, each degree of freedom is typically coupled to 81 degrees of freedom. In a mesh of approximately uniformly sized tetrahedral elements, each degree of freedom is typically coupled to only 40 degrees of freedom. This means that the stiffness matrix for a tetrahedral mesh requires roughly half the memory as that for a hexahedral mesh with the same number of nodes [61]. Since accuracy rather than the computational time of this analysis was more important the author decided to use the more accurate hexahedral elements.

Hexahedral elements could not mesh the volume if the top and bottom surfaces of the volumes were flat. As a result of this meshing failure a modelling sacrifice had to be made, which was to leave the top and bottom surfaces of the volumes on the same helical path as the screw threads. Since the author was only interested in the stresses at the threaded area, this sacrifice was considered to be an acceptable compromise.

The material of the screw and prosthesis was titanium with an elastic modulus of 114,000 MPa, and a Poisson's ratio of 0.3 [8,19]. The bone was given an elastic modulus value of 13,400 MPa with a Poisson's ratio of 0.3 [52]. The same structural multilinear plastic properties from the original prosthesis analysis were included. After the model was meshed successfully, contact elements pairs were included to allow sliding and opening of the interfaces, the contact elements included a coefficient of friction of 0.2. Zero displacement constraints were applied to the bone area in all degrees of freedom, and symmetry constraints were applied to the sliced section of the volumes. Again a pressure of 130 Pa was applied to the top of the prosthesis in the negative Y direction to put the screw under a tensile stress. This analysis would serve to make a direct comparison with the axisymmetric model.

The model was solved in a non-linear static analysis. The same two loadsteps as in the axisymmetric analysis were used again here. No solution convergence problems were encountered.

A plot of the von Mises Stress at the final load step is shown in Figure 3.16.

```
NODAL SOLUTION
STEP=2
SUB =15
TIME=200
SEQV (AVG)
DMX =.147E-03
SMN =.007358
SMX =4.457
```

ANSYS  
PLOT NO. 1

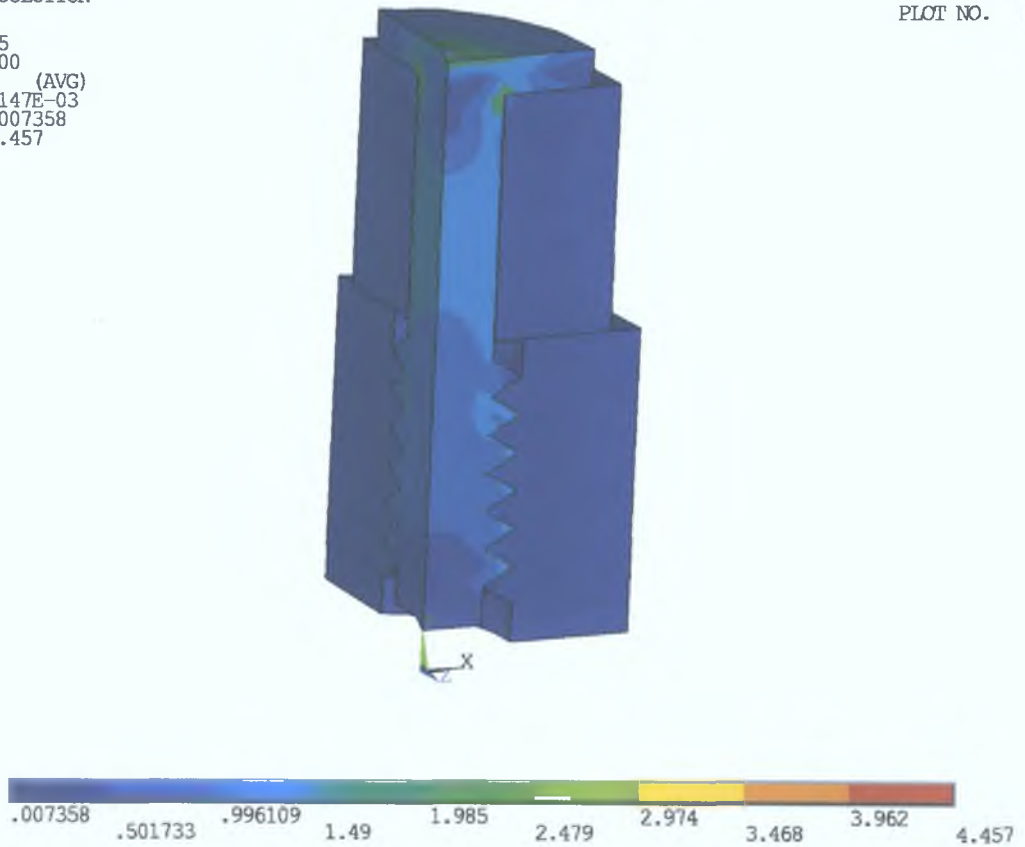


Figure 3.16 von Mises Plot of the Quarter Volume Prosthesis, Screw and Bone Area (MPa)

This stress plot was very similar to the stress plot for the 2D axisymmetric plot in Figure 3.12. It has the same high stress spot resulting from the lack of a fillet between the screw and the prosthesis, and the stress gradients are almost the same.

As with the axisymmetric model, we were only interested in the stress in the threaded area. A selection of the elements around the threaded area was selected and the von Mises stress was plotted again, which can be seen in Figure 3.17.

NODAL SOLUTION  
 STEP=2  
 SUB =15  
 TIME=200  
 SEQV (AVG)  
 DMX =.147E-03  
 SMN =.007358  
 SMK =1.772

ANSYS  
 PLOT NO. 1

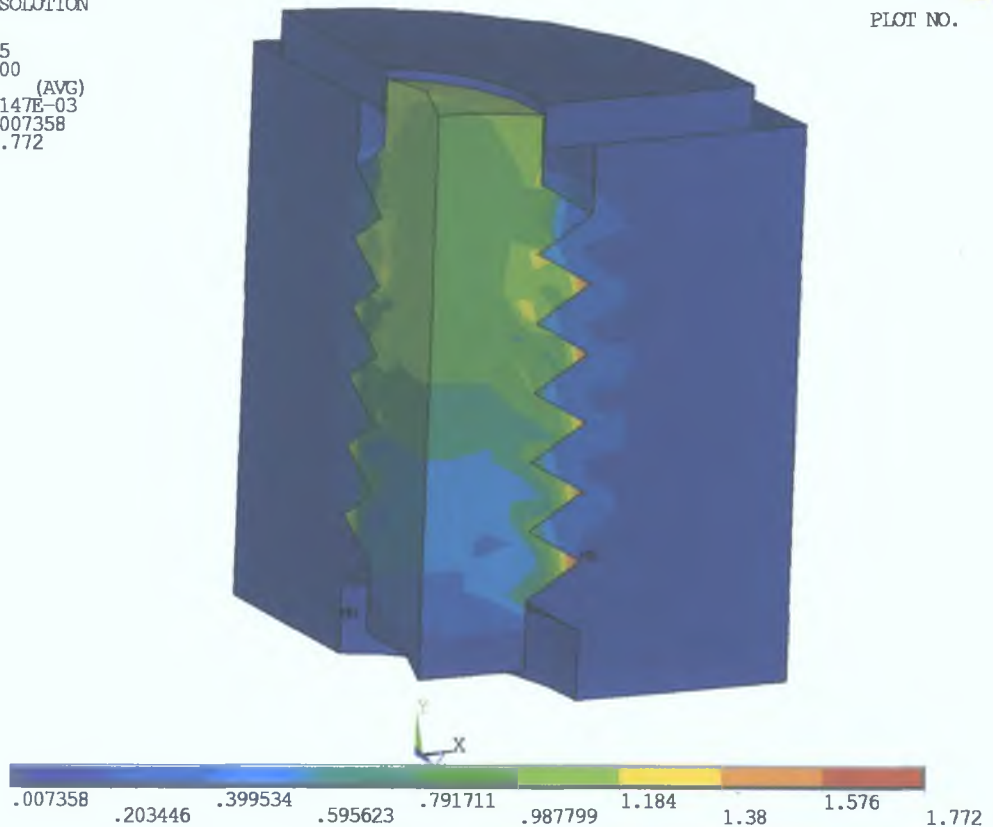


Figure 3.17 von Mises Plot of the Thread Area (MPa).

The Maximum von Mises stress was 1.772 MPa, which is an 11.2 % increase from the axisymmetric value of 1.593 MPa in Figure 3.13. This is explained by the use of the helical path as opposed to the circular rings that are assumed in an axisymmetric model. As expected again, the von Mises stress plot showed a high level of stress around the first engaged thread then tapering off on the remaining threads. Figure 3.18 shows the highest contact pressure at the first engaged thread and the pressure decreasing in the remaining engaged threads.

NODAL SOLUTION  
 SUB =1  
 TIME=200  
 COMPLENE (AVG)  
 DMX =.147E-03  
 SMX =.561E-05

ANSYS  
 PLOT NO. 1

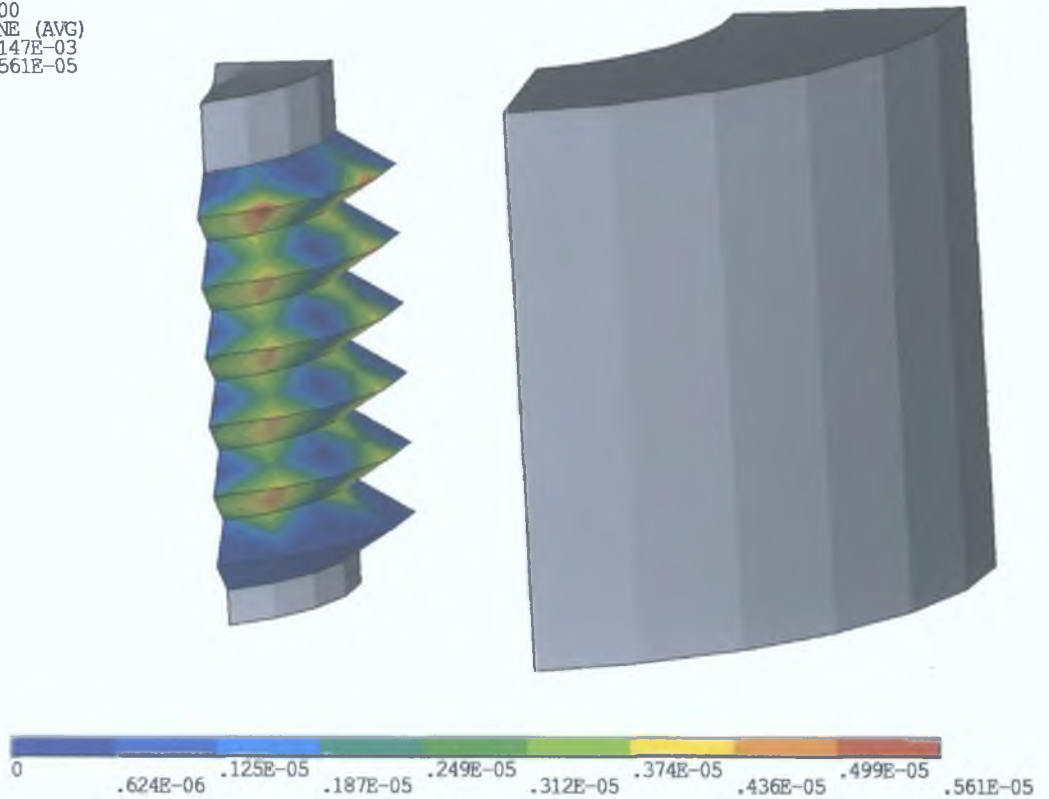


Figure 3.18 Contact Pressure Plot on Quarter Volume Screw and Bone Area (Pa).

The quarter volume three-dimensional model, while more accurate than the axisymmetric model, does not consider the fact that helical shape of the thread flank is continuous about the longitudinal axis of the bolt. To allow this simulation to occur a 360-degree three-dimensional model was needed.

### 3.4.3 Three Dimensional Model. (Full Volume)

The third logical step in this analysis was to model a full volume of the prosthesis, screw, and bone. The full volume was created by sweeping the same profile from the quarter volume about a 360° helical path, with a 3mm diameter and a 0.6mm pitch. This left a hole in the centre of the screw, as shown in Figure 3.19, which proved to be very difficult to mesh with hexahedral elements.





Figure 3.19 Full Volume Bone, Screw and Prosthetic with a Hole at the Centre of the Screw.

The helical path was divided into two halves that resulted in the prosthesis, bone, and screw volumes also divided in two. This volume split was to be used later to plot the von Mises stress gradients on the inside of the model.

As with the quarter volume the plane and contact elements of the 2D model were deleted, and the new full volume was meshed with solid 20 node brick elements.

The same elastic modulus, Poisson's ratio, multilinear elastic properties, constraints, contact elements and displacements, applied to the quarter volume were applied to the full volume.

The hole at the centre of the screw still needed to be filled. Two volumes were created to fill the hole for the top and bottom halves, when these volumes were meshed with solid elements and joined together the elements did not match with each other, but the nodes on the elements did match up, as shown in Figure 3.20.

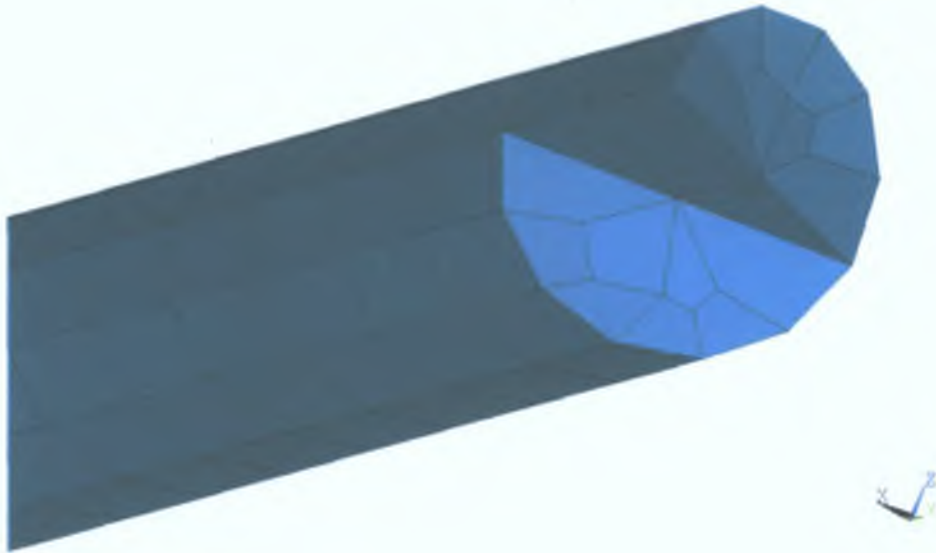


Figure 3.20 Finite Element Volume Mesh at the Centre of the Screw.

As long as the nodes at the centre of the screw matched up the analysis would be a good representation of the screw-bone-prosthesis interface and the analysis could continue.

The contact elements that were included to allow sliding and opening of the bone-screw and screw-prosthesis interfaces, are shown in Figure 3.21



Figure 3.21 Full Volume Contact Elements.

After the volume was modelled and meshed successfully and contact elements were applied, the bone areas were constrained with no displacements in all degrees of freedom. Because this model was a full 360°, symmetry constraints need not be applied, so zero displacement constraints were also applied to the outside area of the prosthesis in the X and Z directions to prevent rigid body motion. At this point the first load step to allow the contact elements to obtain equilibrium was carried out in one substep. The second load step involved a pressure of 130 Pa applied to the area at the top of the screw in the negative Y direction. This was applied using 15 substeps and the non-linear solution algorithm. The result of the von Mises stress in this analysis is plotted below. For clarity only half of the volume is shown in Figure 3.22.

```

NODAL SOLUTION
STEP=2
SUB =15
TIME=200
SEQV      (AVG)
DMX =.223E-03
SMN =.626E-03
SMX =8.824

```

ANSYS  
PLOT NO. 1

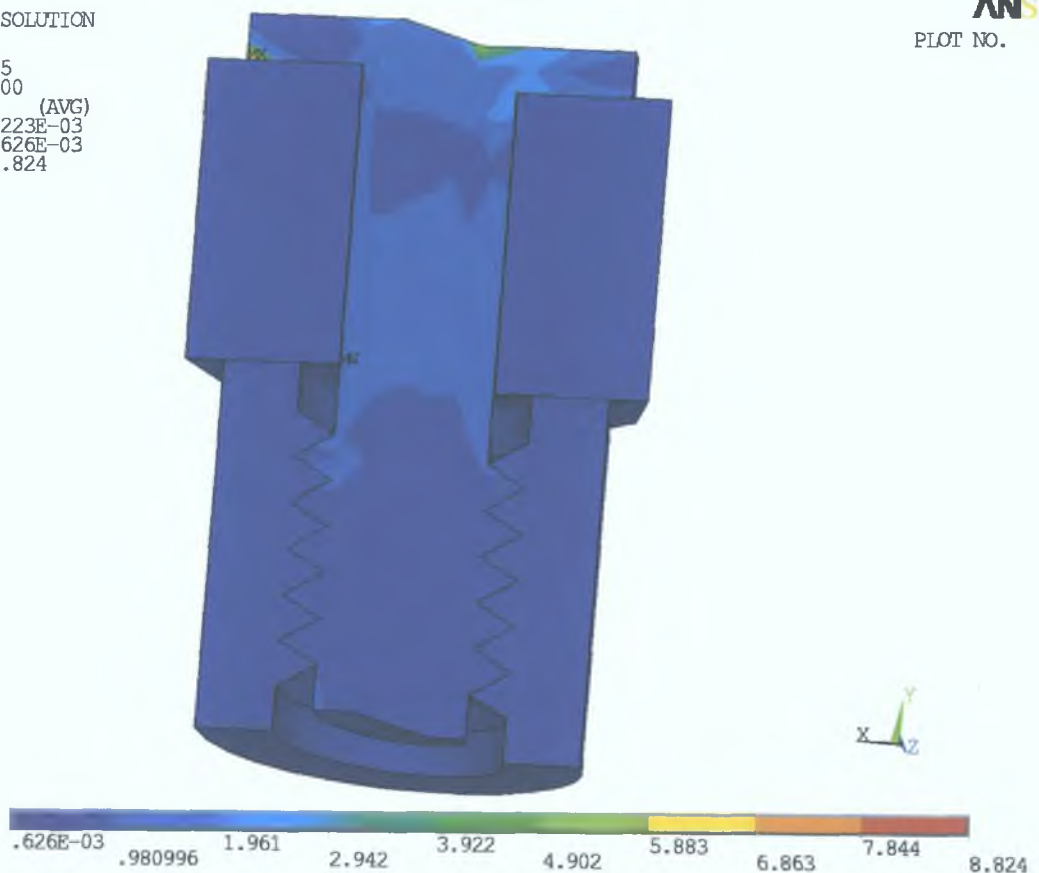


Figure 3.22 von Mises Stress Plot of the Screw-Bone-Prosthesis Connection (MPa).

Again the stress gradient is very similar to the stress plot for the axisymmetric model in Figure 3.12 and quarter volume model in Figure 3.18,

As with the 2D axisymmetric and quarter volume models, we were only interested in the stress at the threaded area. A selection of the elements around the

threaded area was taken, and the von Mises stress gradient was plotted again, which can be seen in Figure 3.23.

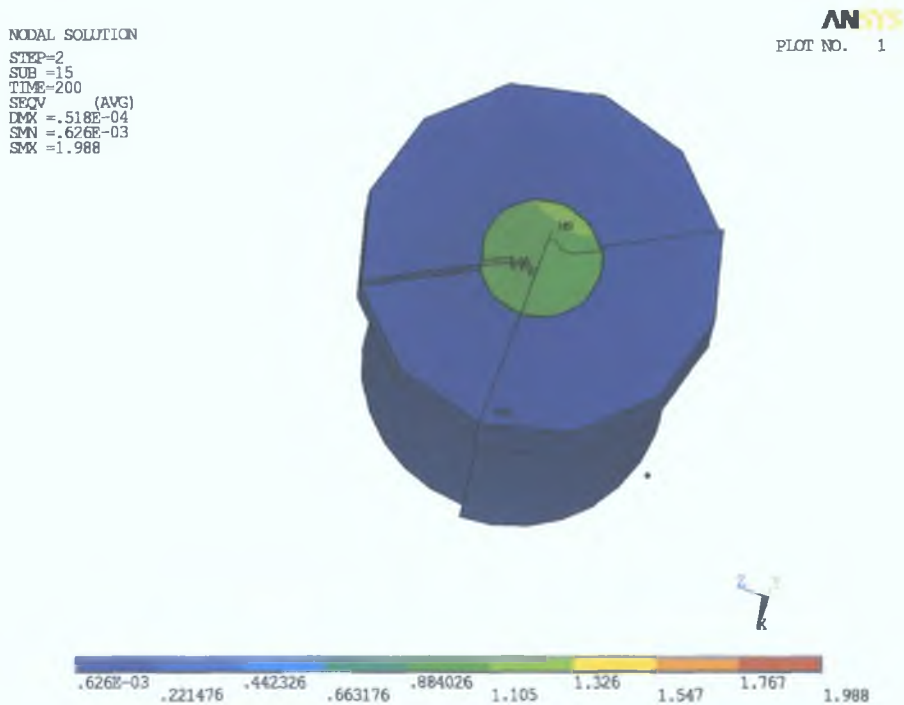


Figure 3.23 von Mises Plot of Full Volume Threaded Area (MPa).

The Maximum von Mises stress at the thread area was 1.988 MPa, which is an increase of 24.8 % compared to the axisymmetric value of 1.593 MPa, this is again explained by the use of the helical path as opposed to the circular rings that are assumed in the axisymmetric model. The comparison between the von Mises plots of the thread areas for the quarter volume 1.772 MPa and the full volume 1.988 MPa (an increase of 12.2 %) suggest that when the threads are the only area of interest the difficulties of a full body analysis could be avoided with a quarter model, and still generate relatively accurate results. For the results to have a high degree of accuracy the full volume screw should be modelled. These values are tabulated below.

	Maximum von Mises stress MPa	% Difference from axisymmetric	% Difference from $\frac{1}{4}$ Volume
2D Axisymmetric model	1.593 MPa		
$\frac{1}{4}$ Volume model	1.772 MPa	+11.2%	
Full Volume model	1.988 MPa	+24.8%	+12.2%

Table 3.3 Summary of Maximum von Mises Stress Analysis Results.

Excessive micromotion is directly implicated in the formation of fibrous encapsulation<sup>13</sup>. Sahin [11] suggests that there is a critical threshold of micromotion above which fibrous encapsulation prevails over osseointegration. Sahin found that the tolerated micromotion threshold lies somewhere between  $50 \cdot 10^{-6}$  and  $150 \cdot 10^{-6}$ mm.

The maximum displacement at the bone was  $26 \cdot 10^{-6}$ mm at the tip of the first thread as seen in Figure 3.24. This micromotion was below Sahin's critical level, it was so small that osseointegration should not be hindered by it.

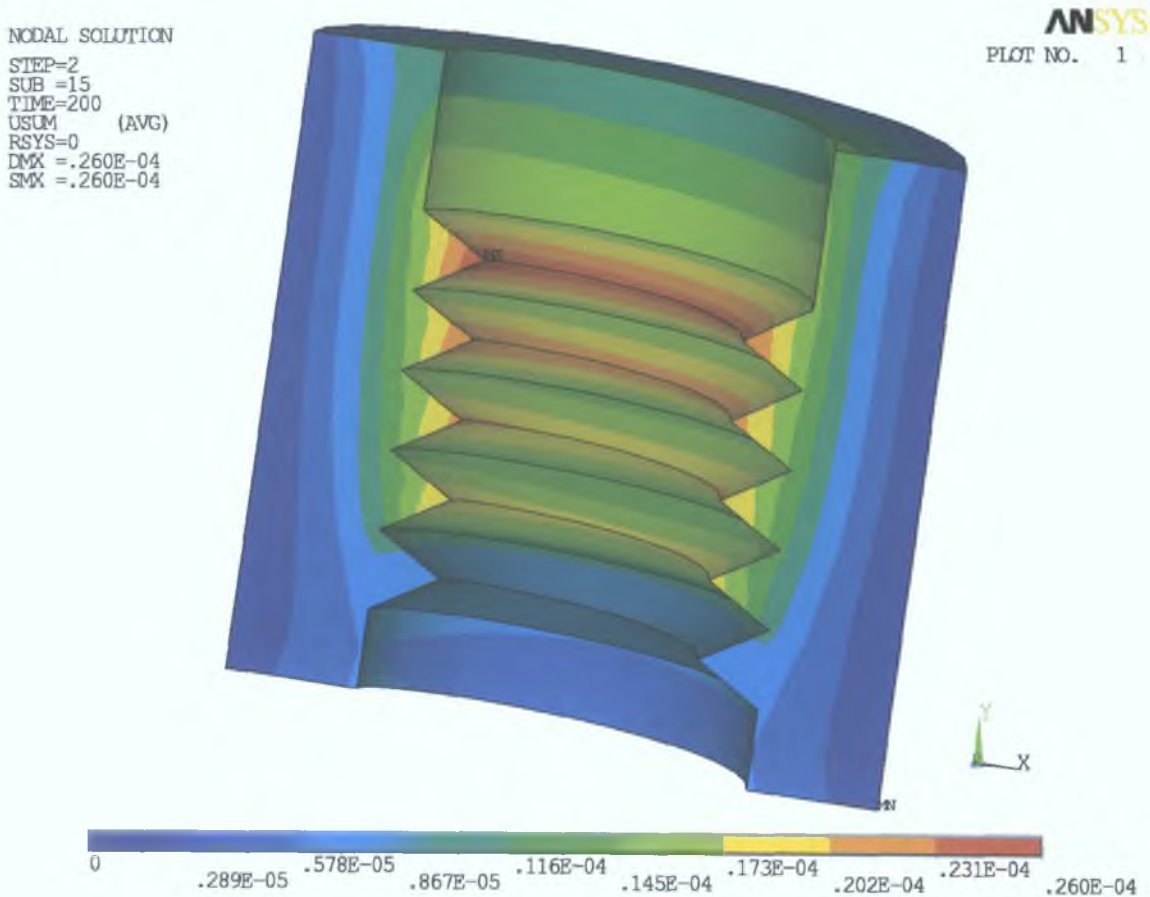


Figure 3.24 Maximum Displacement of the Bone Area (mm).

<sup>13</sup> **Fibrous encapsulation:** Encapsulation of a mass of dead cells and debris that may accumulate at a site of infection or inflammation. If untreated leads to an abscess.



### 3.5 Screw-Preload Analysis.

The preload in a screw has a significant effect on the performance of the bolted connection. The screw preload comes from the installation torque applied when a screw is tightened.

The objective of this analysis was to determine what were the stress distributions on the prosthesis and bone when the preload was applied to the screw.

The first step of the preload analysis was to apply the material properties. The material of the screw and the prosthesis was Titanium with an elastic modulus of 114,000 MPa, a Poisson's ratio of 0.3 [8,19,72], a coefficient of friction of 0.2, and a thermal expansion coefficient of  $13 \cdot 10^{-6}/K$ . The bone was given an elastic modulus value of 13,400 MPa a Poisson's ratio of 0.3 [52] and a thermal expansion coefficient of  $12.43 \cdot 10^{-6}/K$  [8]. A typical reference temperature of 70°F was applied [64], and the same structural multilinear plastic properties from the contact analysis were also included.

A three-dimensional model of the 3mm diameter, 0.6mm pitch threaded screw, prosthesis and bone was created. Ten node tetrahedral elements were used, which allowed the author to create a more geometrically accurate model represented in Figure 3.25.

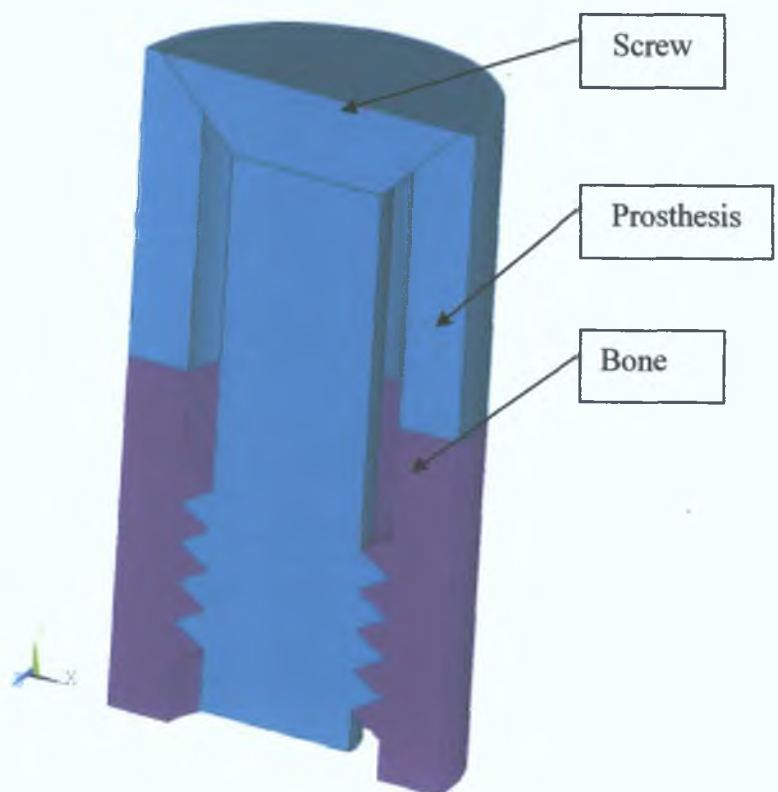


Figure 3.25 Screw, Prosthesis and Bone Volumes for Preload Analysis.

The volumes were glued together so that when it was meshed the connecting surfaces would have matching mesh patterns detailed in Figure 3.26.



Figure 3.26 Finite Element Volume Mesh.

A pretension force of 0.64 kN, which represents the equivalent preload torque from Eq (2) was halved to 0.32kN because the volume was halved, and applied to the preload elements in the screw volume along the Y-axis, between the threads and the countersunk head, see Figure 3.27.

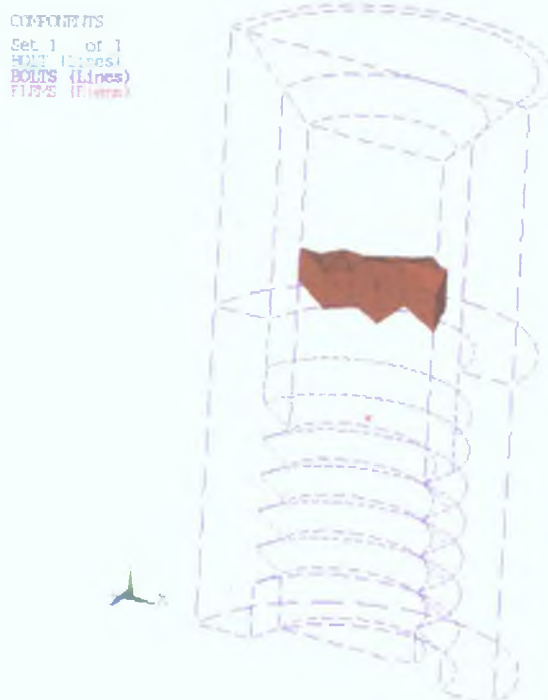


Figure 3.27. Preload Elements on the Screw.

Symmetry boundary condition displacements were applied to the front section areas. Zero displacements were put on the keypoint at the bottom centre of the screw in the X and Y directions, and another zero displacement was put on the keypoint at the top centre of the screw in the X direction, to suppress rapid body motion, as shown in Figure 3.28.



Figure 3.28. Preload Constraints.

A fixed loadstep was applied using a small displacement with 10 substeps. The stability of the three dimensional stress state was evaluated according to the von Mises hypothesis.



The result of the von Mises stress from the last substep in this analysis is plotted below.

```
NODAL SOLUTION
STEP=1
SUB =1
TIME=1
SEQV      (AVG)
DMX =.226E-04
SMN =.001144
SMX =.357024
```

ANSYS  
PLOT NO. 1

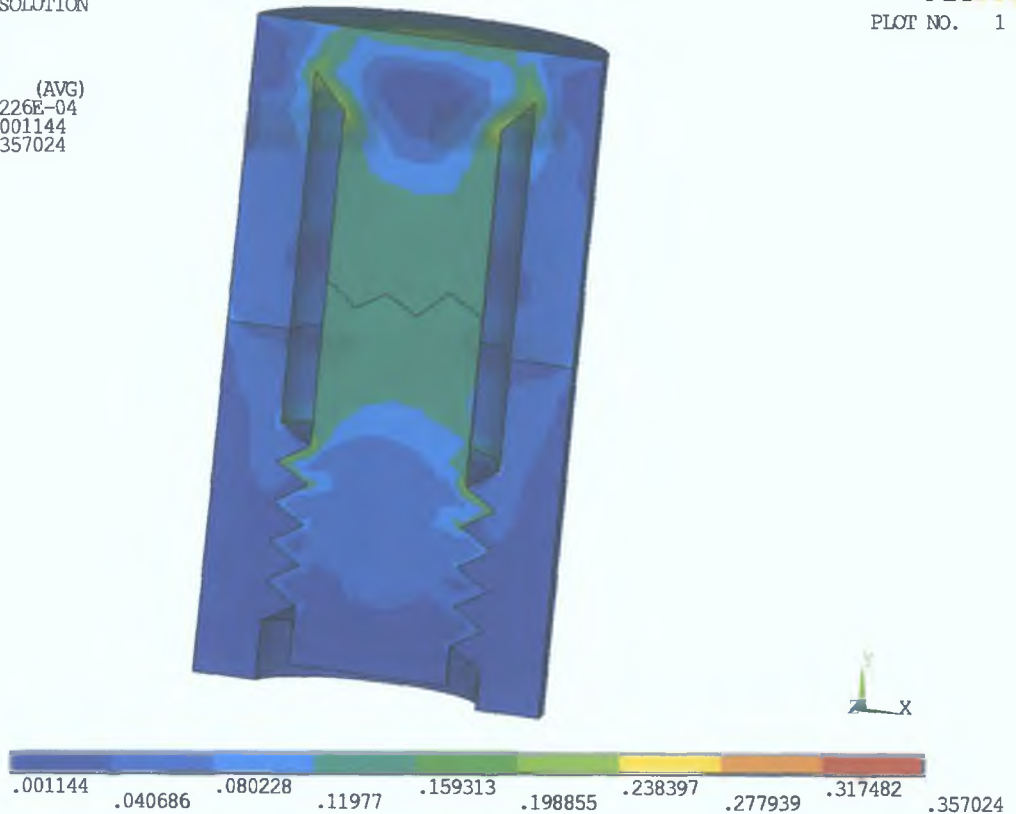


Figure 3.29 Full Model von Mises Plot of the Preload.

The Maximum von Mises stress was 0.357024 kPa. The plot also lists a maximum degree of freedom displacement of  $22.6 \times 10^{-6}$  mm which is well below the critical threshold of micromotion (between  $50 \times 10^{-6}$  and  $150 \times 10^{-6}$  mm.) that Sahin [11] suggests.

The stress gradient was as expected very similar to the screw contact analysis with high stress spots at the joints between the screw shank and head. These stress spots can be seen more clearly when only the von Mises plot of the head of the screw is shown. Illustrated in Figure 3.30.

NODAL SOLUTION

STEP=1  
 SUB =1  
 TIME=1  
 SEQV (AVG)  
 DMX =.226E-04  
 SMN =.001175  
 SMX =.3064

ANSYS  
 PLOT NO. 1

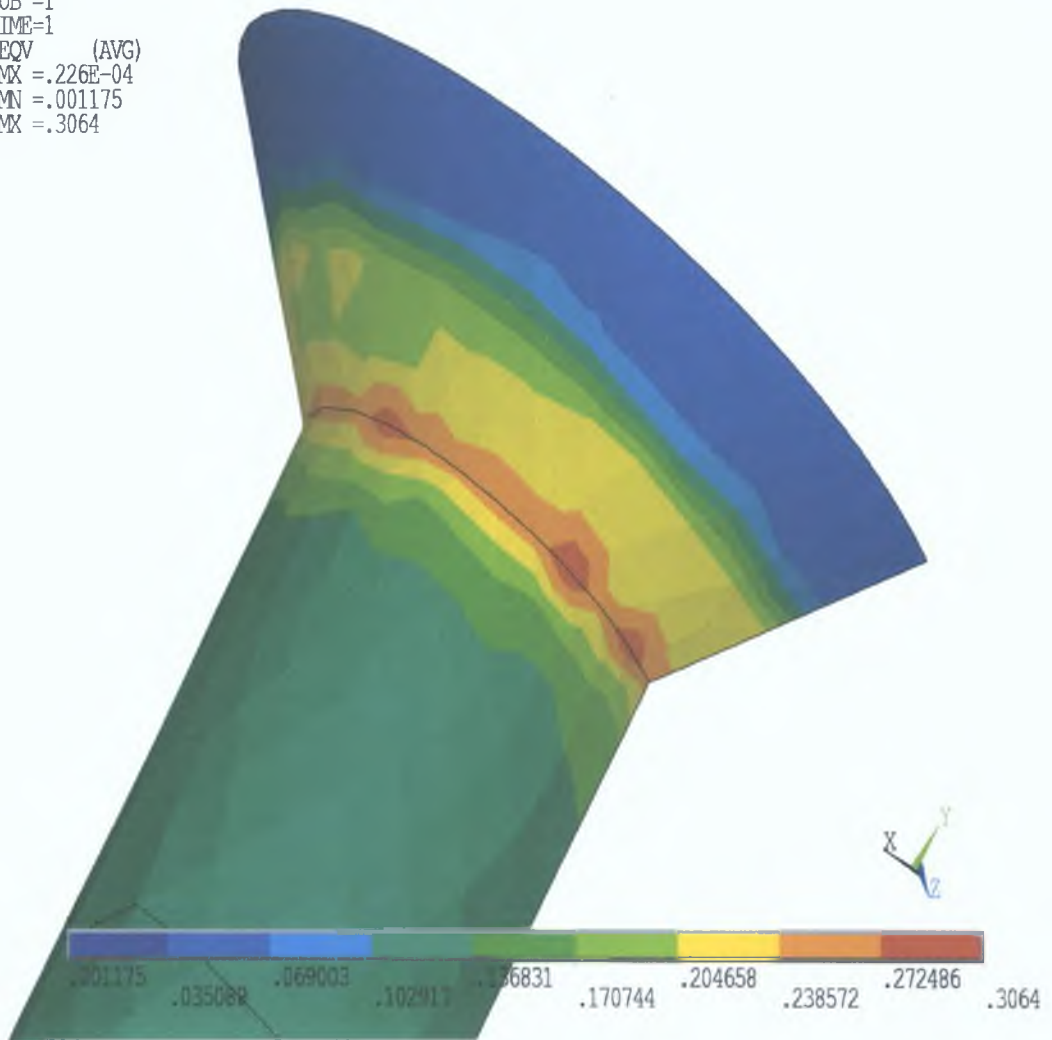


Figure 3.30 von Mises Plot of the Screw Preload.

To fix the problem of these high stress spots the area between the shank and head would need to be filleted.

The von Mises stress plot of the bone volume, as expected showed the highest level of stress around the first engaged thread then tapering off on the remaining threads, detailed in Figure 3.31.

NODAL SOLUTION

```
STEP=1
SUB =1
TIME=1
SEQV (AVG)
DMX =.108E-04
SMN =.003238
SMX =.148663
```

ANSYS

PLOT NO. 1

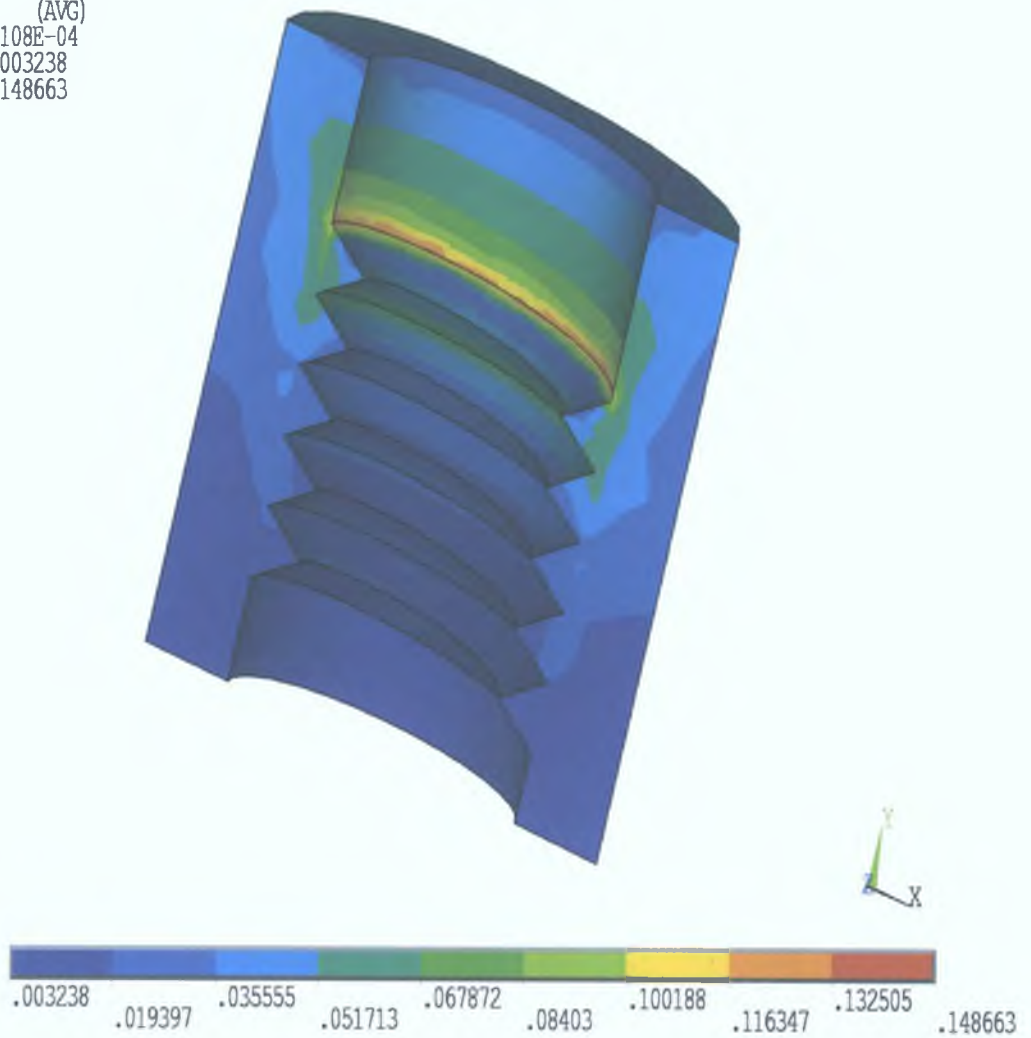


Figure 3.31 von Mises Plot of the Preload on the Bone Area.

The maximum von Mises stress in the bone area was 0.148663 Pa, and the maximum degree of freedom displacement of  $10.8 \cdot 10^{-6}$  mm is well below the critical threshold of micromotion that Sahin [11] suggests.

### 3.6 Second Modification.

The second modification was to replace the detachable abutments in Figure 3.32 with a similar design that was to be an integral part of the prosthesis. This eliminated the need to precisely drill and tap holes in the prosthetic and prevented four possible incubation sites for bacteria [18].

#### 3.6.1 Design Criteria

The design criteria for the second modification were:

1. The abutment geometry should be as close as possible to the standard abutment design.
2. The final prosthesis should be designed for manufacture. The geometry should lead to reduced manufacturing set up times.
3. The abutments should function within their elastic range during normal mastication, and at the same allow the over denture to be removed without causing undue stress on the screws that anchor the prosthesis to the maxilla bone.



Figure 3.32 Examples of Abutment Design from Lifecore Biomedical, Inc. USA [63].

#### 3.6.2 Abutment Design

The analysis of the abutments consisted of creating a model similar to those in Figure 3.32, in order to find the pull out and push in force needed to remove the over denture from the prosthesis. It was thought very early in the analysis that it would be physically impossible to manufacture the round abutment because the only CNC milling machine available was a three-axis machine. Using this machine the other abutments would get in the way of the cutting tools. For this reason a new design had to be considered. Several different designs were looked at but the one that was considered

most suitable was a hexagonal shape detailed in Appendix B, which was similar in size and shape to the round design represented in Figure 3.32.

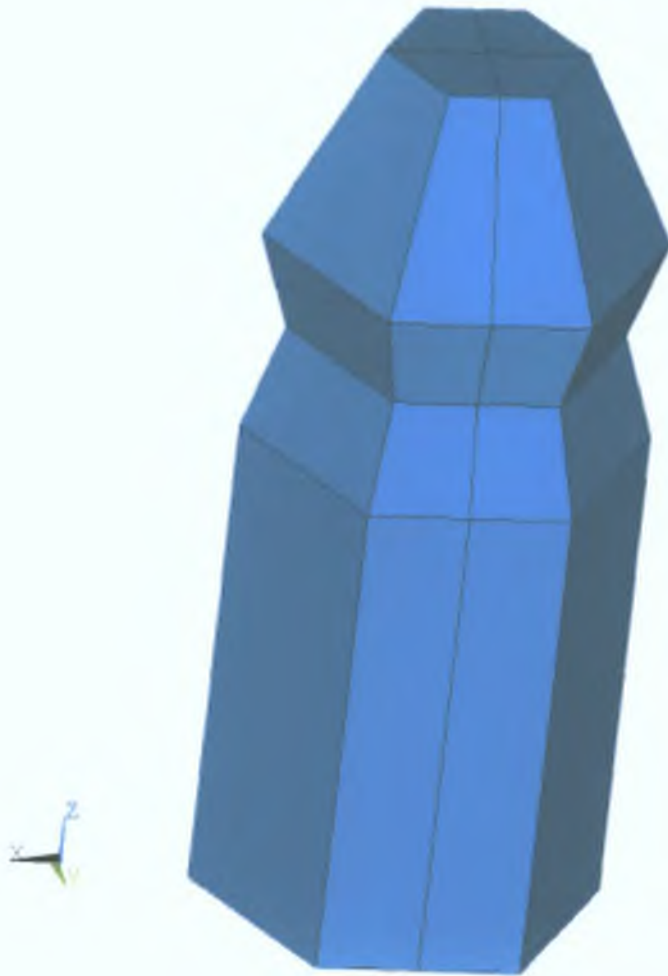


Figure 3.33 Hexagonal Abutment.

A requirement for this new hexagonal abutment was that it would have to have a push in and pull out reaction force similar to the original round abutment. The reaction force would also need to be less than the preload on the titanium screws anchoring the abutment to the bone, otherwise the whole prosthesis might give way and be pulled out of position when it was only intended to remove the over denture. At the same time it was important that the reaction forces were large enough that the over denture did not dislodge during normal mastication.

The round abutment in Figure 3.34 was based on a design from Lifecore Biomedical Inc. [63]. The model has an interference fit of  $-0.03\text{mm}$ , which removed the possibility of incubation sites for bacteria. The model could be quartered because it is



symmetric about the XY, and YZ planes which saved a lot of computational time due to the reduced number of nodes needed for the mesh.

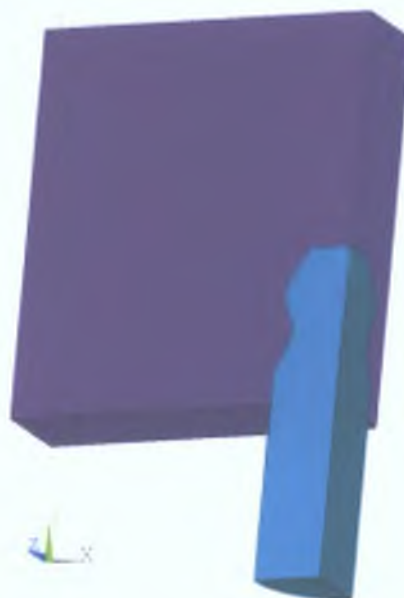


Figure 3.34. Round Abutment and Over Denture Material Quartered Volume.

### 3.6.2.1 Mesh

The volumes were meshed with 10 node tetrahedral elements and contact elements were included to allow sliding and opening of the abutment-dental material interface.

### 3.6.2.2 Material Properties.

The first step of the preload analysis for the round abutment was to apply the material properties. The material of the abutment was titanium with an elastic modulus of 114,000 MPa, a Poisson's ratio of 0.3 [8,19,72], a coefficient of friction of 0.2, and the same structural multilinear plastic properties from the prosthesis analysis were also included.

From the Murata et al [50], Heckmann et al [57] and Lassila et al [68], experiments, the dental material was given a standard elastic modulus value of 3,000 MPa and a Poisson's ratio of 0.3. To allow for the plastic properties of the dental material, structural plastic isotropic multilinear properties were included. These properties, like the titanium properties were not in the literature, so the author had to make an educated guess as to what they might be.

The linear region of the stress strain curve had to equal the elastic modulus value, (3000 MPa) given by Heckmann et al [57]. A value of 300 MPa was chosen for the yield stress, which gives a yield strain of 0.1mm.

$$\text{Elastic modulus (E)} = \frac{\sigma}{\varepsilon} = \frac{\text{Stress}}{\text{Strain}} \quad (5)$$

$$\text{First data point} = 3000 \text{ MPa} = \frac{300 \text{ MPa}}{\varepsilon} \quad (6)$$

$$\varepsilon = 0.1 \text{ mm} \quad (7)$$

The rest of the data points were chosen arbitrarily by the author to model what the denture material might look like. The values chosen are listed in table 3.4 below

Strain (mm)	Stress (MPa)
0.1	300
0.2	550
0.3	770
0.4	970
0.5	1170
2.5	1330
6	1470
10	1580
15	1670
20	1710

Table 3.4 Dental Material Multilinear Plastic Values.

These values produced the following stress strain plot.

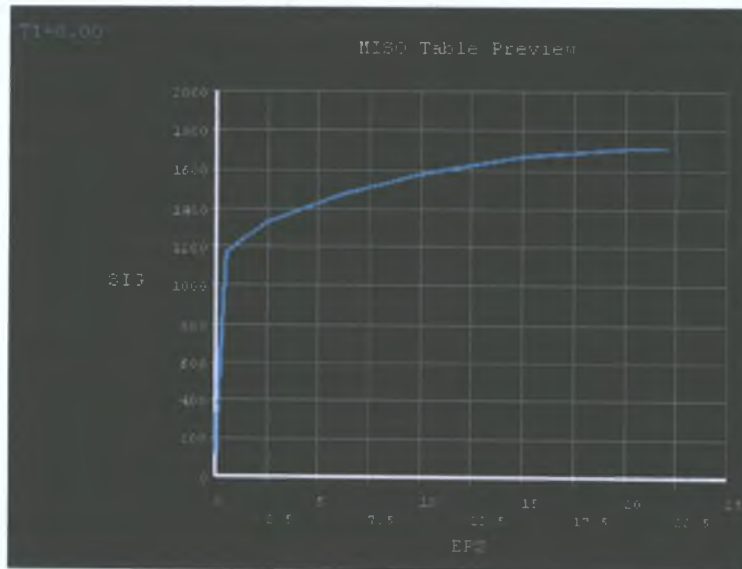


Figure 3.35 Denture Material Stress Strain Curve.

### 3.6.2.3 Boundary Conditions.

Zero displacement constraints were applied to the top surface area of the denture material in all degrees of freedom, and symmetry constraints were applied to the sliced sections of both the denture material and the abutment volumes. In addition, a

displacement of 2.3mm was placed on the bottom surface of the abutment in the Y direction to move the abutment relative to the denture material as shown in Figure 3.36.

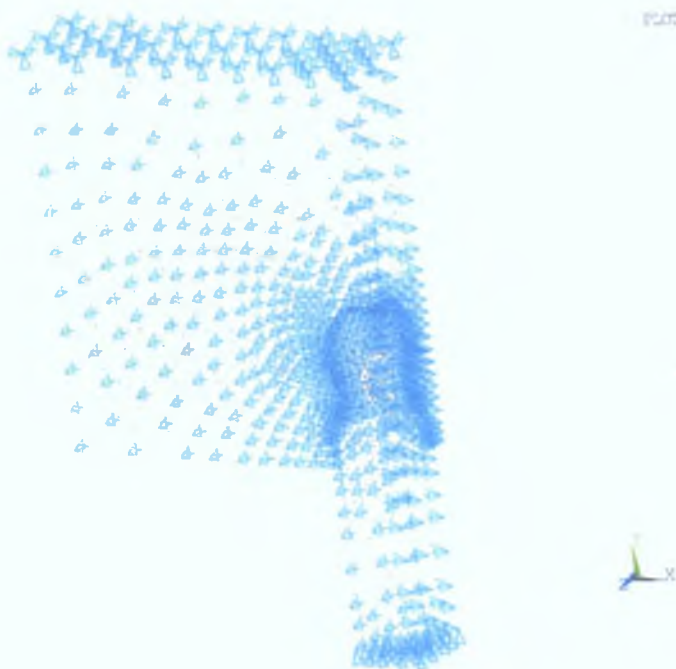


Figure 3.36. Boundary Conditions of the Abutment and Denture Material.

#### 3.6.2.4 Load Step Options.

There were three load steps in this analysis the first load step was to allow the contact elements to reach a state of equilibrium. In the second load step, the round abutment was pulled out of the dental material by a displacement of 2.3mm on the bottom surface of the abutment in the negative Y direction, which was just enough movement for the abutment to clear the dental material. This was a large displacement and needed fifty substeps to complete it successfully. The third loadstep involved pushing the abutment back home into the dental material 2.3mm in the positive Y direction, again with a large displacement and fifty substeps

The reaction forces from the following analyses were only gathered from the nodes on the areas at the bottom of the abutments where the displacements were applied. The results of the analysis listed a total reaction force of -159.24 N when the abutment was pulled out, and a total reaction force of 158.58 N when the abutment was pushed back in to the dental material. These Figures were multiplied by 4 because the abutment was quartered which gives a total reaction force of -636.96 N when the abutment was pulled out and a total reaction force of 634.32 N when the abutment was pushed back in to the dental material.



The new hexagonal design provided access to all areas of the abutment for machining. It was very similar in shape and also had similar total push in and pull out reaction forces to the round abutment detailed in Appendix C, including the same -0.03 interference fit with the over denture material. This was achieved by manipulating the angle of the taper and the thickness of the hexagon.

The results of the final hexagonal abutment structural stress analysis listed a total pull out force of -164.23N and a total push in force of 161.72 N.

	<b>Total Reaction Pull out force (N)</b>	<b>Total Reaction Push in force</b>
<b>Round Abutment</b>	-159.24	158.58
<b>Hexagonal Abutment</b>	-164.23	161.72

Table 3.5 Abutment Total Reaction Forces.

At this stage of the analysis the author was advised by Gabriel Costello the project supervisor that indeed it was possible to mill the round abutments on the 3-axis CNC milling machine with a custom made form tool. The round abutments would also save several machine set-ups, so at this stage it was decided to abandon the idea of a hexagonal abutment.

The author decided to examine how much the interference affected the reaction forces. A number of new models of the round abutments were created which ranged from -0.03mm interference fit, from Table 3.5. To 0.03mm clearance fit.

Again, the bottom surfaces of the abutments on these models were pulled out to clear the material and pushed back home 2.3 mm. The total reaction forces of these models are presented as a percentage of the original -0.03mm interference fit abutment, and tabulated in Table 3.6

<b>Clearance / Interference</b>	<b>Total Reaction Pull out force (N)</b>	<b>Total Reaction Push in force (N)</b>
<b>-0.03 Interference</b>	<b>-159.24</b>	<b>158.58</b>
-0.02 Interference	-6.80%	-6.42%
-0.01 Interference	-10.97%	-10.51%
0.00	-18.35%	-18.04%
0.01 Clearance	-21.14%	-20.45%
0.02 Clearance	-26.14%	-25.77%
0.03 Clearance	-30.67%	-29.84%

Table 3.6 Total Reaction Forces for Different Quarter Abutment Models.

These results were then used to produce the following chart.

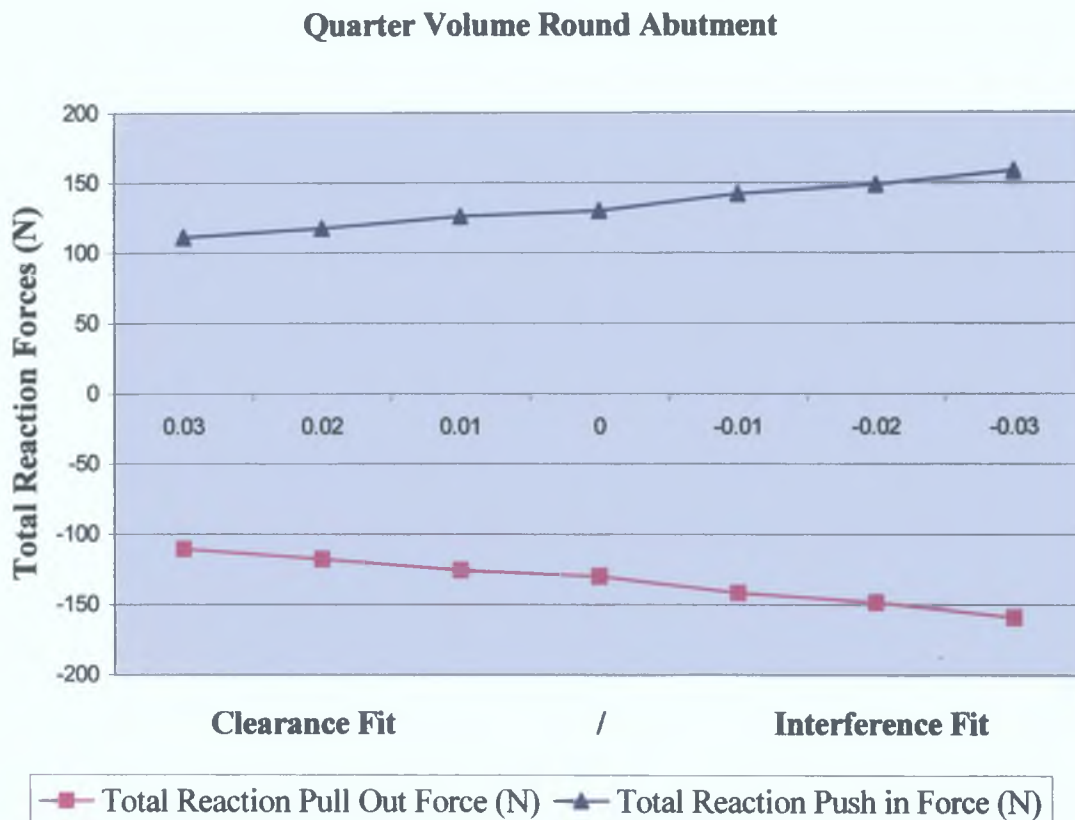


Figure 3.37 Total Reaction Forces for the Quarter Volume Abutments with Different Clearances.

It was noted from the chart that reducing the interference to 0.0 and then increasing the clearance seems to have an almost linear relationship to the total reaction forces.

At this stage of the abutment analyses it was decided to investigate what would be the effect on the total reaction forces if the coefficient of friction was changed.

For this analysis the -0.03 mm interference model was used and the problem was run eleven times with a coefficient of friction between 0.0 and 1.0 in increments of 0.1mm. It was noted that the higher the coefficient of friction on this model, the longer the FEA program took to solve the problem, up to a point at a coefficient of 0.7 where the program convergence criteria could not solve the analysis. The results of the successful analyses are presented as a percentage of the original -0.03mm interference fit abutment with a coefficient of friction of 0.2, and tabulated in Table 3.7.

Coefficient of Friction	Total Reaction Pull out force (N)	Total Reaction Push in force (N)
0	-42.59%	-46.13%
0.1	-22.21%	-24.01%
0.2	-159.24	158.58
0.3	+23.51%	+24.97%
0.4	+47.98%	+51.25%
0.5	+73.49%	+78.72%
0.6	+99.43%	+106.97%

Table 3.7 Total Reaction Forces with Different Coefficients of Friction.

The results were then used to produce Figure 3.38, which shows again a very linear trend with the increase in the coefficients of friction.

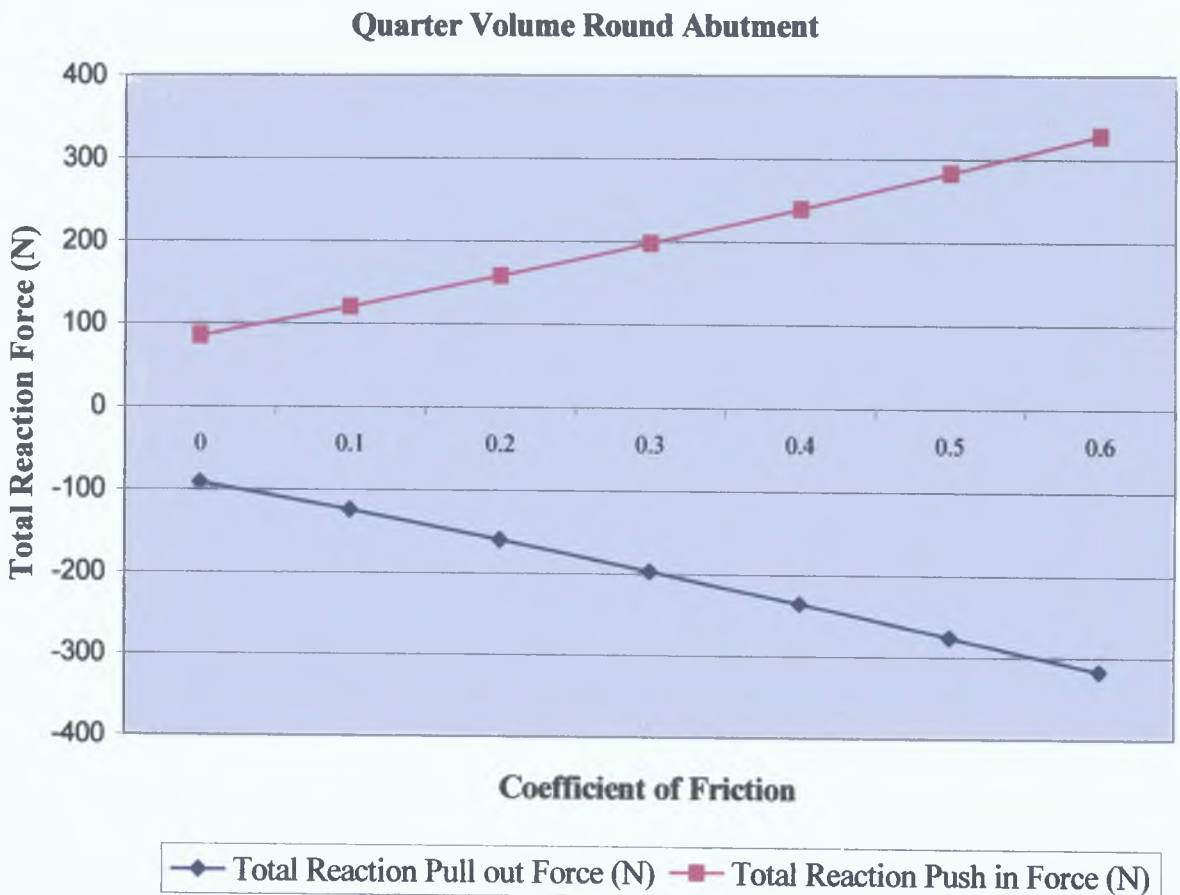


Figure 3.38 Total Reaction Forces for the -0.03 mm Interference Fit Abutment with Increasing Coefficients of Friction.

The results of these analyses suggest logically that, the higher the interference between the abutment and the dental material and the higher the coefficient of friction the higher the reaction forces will be.

### 3.7 Final Design

Gathering the results from these analyses, a final design was created, as shown in Figure 3.39. A detailed drawing of the design may be seen in Appendix D.

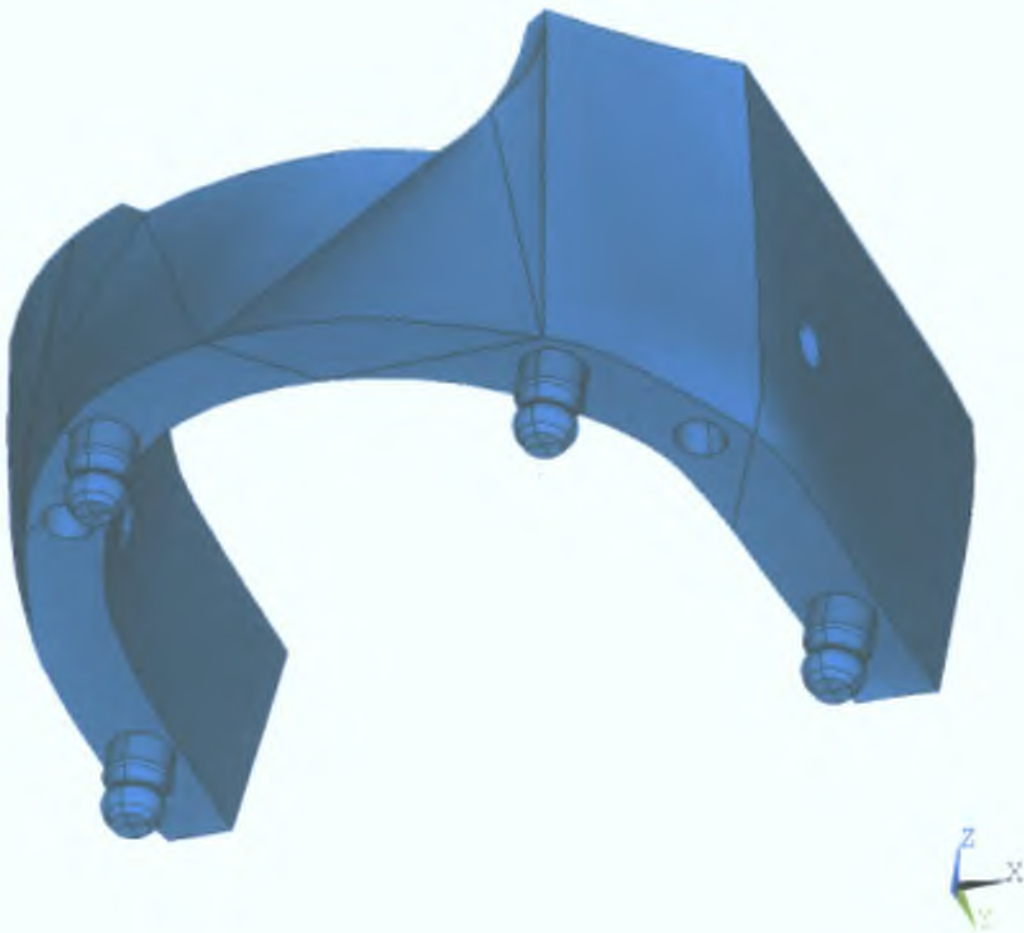


Figure 3.39 Final Prosthesis Design and Overdenture.

It should be noted that the abutments were intentionally placed a safe distance from the screws, while at the same keeping a regular pattern.

### 3.8 Discussion.

In the analyses of the two modifications to the design of the prosthesis, the FEA program has shown the new design will work within the limits of stress allowed.

The first modification in the redesign, to remove the wings and replace them with four holes proved successful, resulting in a reduced von Mises stress of 63.63%, and a reduced micromotion at the prosthesis interface of 99.914%. This modification more importantly also removed the necessity for mutilation of the face during surgery, because the screws could be attached to the skull through the open mouth.

In the prosthesis screw and bone contact analysis there was a 12.2% difference in the von Mises stress at the thread area between the  $\frac{1}{4}$  volume screw and the full screw analysis, and a 24.8% difference between the axisymmetric screw and the full screw. These results indicate that an axisymmetric model should not be used to replicate the helical thread, and a  $\frac{1}{4}$  volume will only achieve relatively accurate results. For the results to have a high degree of accuracy the full volume screw should be modelled, however it must be noted that the design of the full volume screw was compromised due to the difficulties in meshing hexahedral elements.

The maximum micromotion at the bone screw interface was  $26 \cdot 10^{-6}$ mm, well below the critical threshold of between  $50 \cdot 10^{-6}$  and  $150 \cdot 10^{-6}$ mm. This indicates that the 3mm diameter holes that the screws were designed to fit are large enough to prevent fibrous encapsulation of the prosthesis bone interface. The preload on the bolt produces a maximum micromotion of  $22.6 \cdot 10^{-6}$ mm, which again is well below Sahin's [11] critical threshold for micromotion.

The second modification to the prosthesis was the addition of the abutments as an integral part of the prosthesis. The function of the abutments is to aid in the location and retention of the overdenture, while at the same time allowing the overdenture to be removed without causing undue stress on the screws anchoring the prosthesis to the maxilla bone. W.S.L Winson et al [69], Studied the factors affecting the human handgrip force exertion capabilities of 27 men with an average age of 24 years old and a range of 20-30, and found that the average force exerted was 235.12 N. When the

reaction force for abutment 4 (the flush fit abutment) is multiplied by 4 the resulting reaction force for the full abutment was

$$-130.02 \times 4 = -520.08 \text{ N Pull out force}$$

$$129.98 \times 4 = 519.92 \text{ N Push in force}$$

The reaction force for the full prosthesis was

$$-520.08 \times 4 = -2.08 \text{ kN Pull out force.}$$

$$519.92 \times 4 = 2.08 \text{ kN Push in force.}$$

These results far exceed what W S L Winson et al [69] have suggested an average man might be physically be able to exert. After reviewing this analysis it became clear to the author that the reason for the discrepancy was that the assumed multilinear plastic properties for the titanium and dental material were not correct. These properties are a closely guarded proprietary secret [57].

To conduct the analyses with an acceptable level of accuracy a tensile test on the titanium and dental material would have to be made to discover what exactly are their multilinear plastic properties. The author felt that there was no point in guessing what the values might be as no analysis based on a guess could be trusted.

Even though the results of the analyses are under suspicion, the author feels it is safe to determine that an increase from clearance to interference fit between the abutment and the overdenture will increase the push in and pull out reaction forces, and an increase in the coefficient of friction will also increase the push in and pull out reaction forces.



## Chapter 4

### Machining

- 4 1 Introduction
- 4.2 CAD/CAM Software.
- 4 3 CNC Machining Centre.
- 4 4 GMIT Machining Strategy
  - 4 4 1 First Operation.
  - 4 4.2 Second, Third, Fourth, and Fifth Operations
  - 4 4 3 Sixth Operation.
  - 4 4 4 Seventh Operation
  - 4 4.5 Eight Operation
- 4.5 Outsourced Vendors.
- 4 6 Pallet Indexing System.
- 4 7 Vendor Machining Strategy
  - 4 7.1 First Operation
  - 4.7 2 Second, Third, Fourth, and Fifth Operations.
  - 4 7 3 Sixth Operation.
  - 4 7 4 Seventh Operation
- 4 8 Costing.
- 4.9 Discussion.

#### 4.1 Introduction.

CAD/CAM (computer-aided design/computer-aided manufacturing) systems are software packages used to design and manufacture products. Once a design has been produced with the CAD component, the design itself can control the machines that construct the part [66]

A DNC (Direct Numerical Control) is a computer software package that is networked to the CNC (Computer Numerical Control) machine. The CNC program is written using the CAM software and outputted in the form of a text file that can be transferred via the DNC to the CNC machine.

Prosthetics generated by CAD/CAM are more precise than those created using traditional casting technology [67]. This increased accuracy has specific benefits, including

increased longevity, and improved success. This cutting edge technology will become the standard in prosthetic dentistry for the foreseeable future [67].

## 4.2 CAD/CAM Software.

The final prosthetic design created in the finite element software from Chapter 3 was exported as an IGES file. This IGES file was imported into the CAD/CAM ProEngineer software. As a default setting, ProEngineer uses the imperial system when importing files, before the model could be manipulated these setting had to be changed to the metric system.

The four holes in the prosthetic were located at compound angles in the coordinate system, so an axis had to be created along the centre line of each hole to provide a path for them to be drilled. See Figure 4.1. When these modifications were made the model was saved as a ProEngineer .prt file, and at this point could be used to plan the machining strategy.

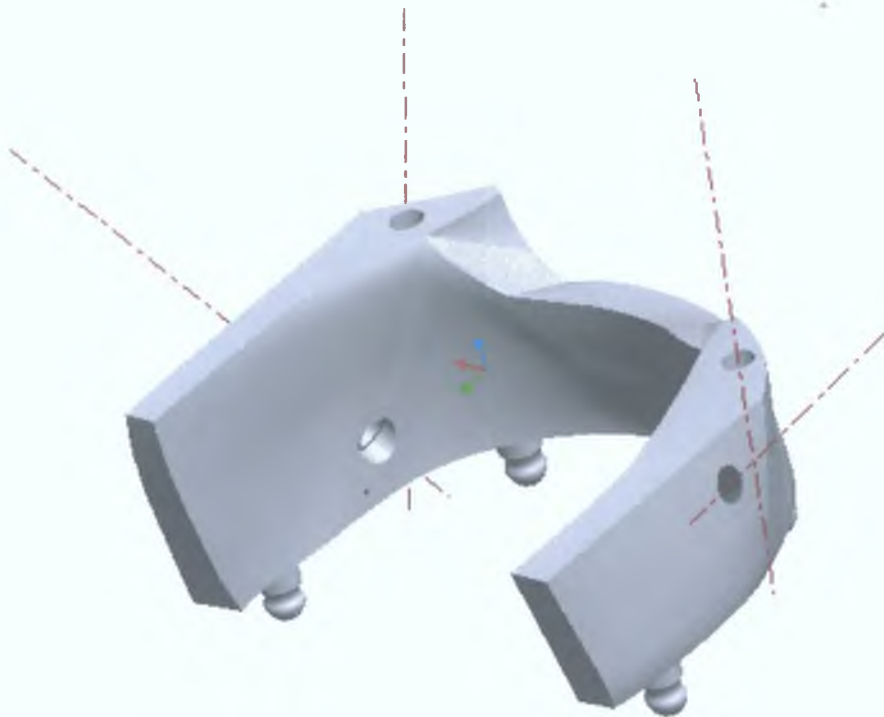


Figure 4.1 Prosthetic Model with Hole Drill Paths.

To write the numerical control program to machine the prosthetic, the ProEngineer CAM software was used. A new empty .mfg file was created and the prosthetic model saved as a prt file was used as a reference model. To create the model of the titanium blocks from which the prosthetic would be milled, a datum plane was created through the bottom flat areas of the abutments on the reference model. A number of other planes were created, which were offset and normal to this plane, to replicate the sides of the work piece.



Using these datum planes the author was able to model a work piece 50mm \* 50mm \* 40mm which surrounded the prosthetic, as seen in Figure 4.2.

The extra height on the work piece above the prosthetic was needed to grip the work piece in the bench vice.

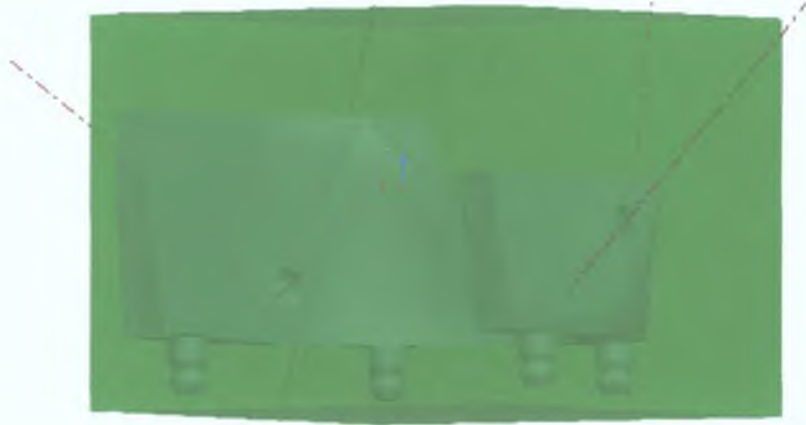


Figure 4.2 Prosthetic Surrounded by Work Piece Model.

### 4.3 CNC Machining Centre.

The CNC machining centre used in this project was a Bridgeport Interact 412 Vertical Machining Centre, as shown in Figure 4.3. The author had very limited experience in working with CNC machinery so a considerable amount of time had to be spent becoming familiar with the capabilities and limitations of the Interact 412. The author spent several weeks practicing on increasingly more complex designs before attempting to machine the prosthesis.



Figure 4.3 Bridgeport Interact 412 Vertical Machining Centre.

The Bridgeport Interact 412 CNC Machining Centre is an industry standard 3 axis vertical milling machine. It has a spindle speed range of 40 – 4000 rpm, a BT40 taper tool holder, and a 12-tool automatic tool changer. The axes of travel are;

- X = 450mm
- Y = 310mm
- Z = 300mm

Before machining could start the work pieces were machined square to 50mm \* 50mm \* 40mm on a manual milling machine, clamped in the bench vice ready for the first operation, and a number of preliminary procedures were checked [68]. These procedures are listed below.

- The machine start up

The 3 axes were set to zero using the Zrn (Zero Return) option.

- The tool magazine was loaded according to the tool set up plan in the ProEngineer CAM software, as shown in Table 4.1

Tool Number	Tool Name	Tool Offset
1	63mm Carbide fly cutter	1
2	20mm Slot mill	2
3	12mm Ballnose mill	3
4	5mm Form tool	4
5	4mm Slot mill	10
6	3mm Centre drill	11
7	3mm Drill	12

Table 4.1 GMT Tools and Offsets

- The X and Y offsets were set for the first operation
- The Z offset was set for the first operation
- The tool length offsets were set for each tool used in the first operation
- The NC program was loaded onto the machining centre in edit mode, from the CAM software, using the DNC
- The machining centre was changed to auto mode, and the coolant hose was pointed towards the work piece

The machining centre was ready at this stage to begin machining the first operation on the prosthetic

#### 4.4 GMIT Machining Strategy.

To machine the prosthetic the workpiece would have to be machined from 8 directions (bottom, top, front, back and along the axes of each of the 4 holes. Each machining direction would be a different operation, and each operation would be made up of several sequences. Because the author had a limited supply of titanium blocks to work with, aluminium was used to plan the machining strategy, and to create dummy runs.

The first attempt at machining the prosthetic was to mill from the top. The sequences of this operation were to face mill the top flat surface, volume mill the inside area down as far as the abutments and then profile cut the inside, outside and top surfaces. This first operation was successful, but the next operation requiring the four holes to be drilled could not be completed because there was no access to the holes, which had to be drilled from below. It would also mean that the four corners of the workpiece would be milled away leaving no points of reference for tool offsets in any subsequent operations. It thus became apparent that the sequence of milling operations was going to be a critical factor in successfully completing the project. After several variations, it became clear that the following sequence of operations was the only viable solution to complete the prosthetic successfully on a 3 axis-machining centre. A process plan of the operations can be seen overleaf.

Op #	Op Type	Feature	Tooling	Cutting Feed (mm/min)	Spindle Speed (rpm)
1a	Set Coordinate System				
1b	Face Mill	Bottom Surface	63mm Flycutter	150	750
1c	Volume Mill	Bottom Surface	20mm Slotmill	150	1200
1d	Volume Mill	Bottom Inside Surface	20mm Slot Mill	150	1200
1e	Profile Mile	Bottom Inside and Outside Surface	12mm Ballnose Mill	150	1600
1f	Formtool Mill	Abutments		150	1600
2a	Set Coordinate System				
2b	Centredrill	Hole 1	Centredrill	50	2000
2c	Drill	Hole 1	3mm Drill	50	2000
3a	Set Coordinate System				
3b	Centredrill	Hole 2	Centredrill	50	2000
3c	Drill	Hole 2	3mm Drill	50	2000
4a	Set Coordinate System				
4b	Centredrill	Hole 3	Centredrill	50	2000
4c	Drill	Hole 3	3mm Drill	50	2000
5a	Set Coordinate System				
5b	Centredrill	Hole 4	Centredrill	50	2000
5c	Drill	Hole 4	3mm Drill	50	2000
6a	Set Coordinate System				
6b	Face Mill	Top Surface	63mm Flycutter	150	750
6c	Volume Mill	Bottom Surface	20mm Slotmill	150	1200
6d	Profile Mile	Top Inside and Outside Surface	12mm Ballnose Mill	150	1600
6e	Surface Mill	Top Surface	12mm Ballnose Mill	150	1600
7a	Set Coordinate System				
7b	Face Mill	Bottom Surface	63mm Flycutter	150	750
7c	profile Mill	Front Areas	12mm Ballnose Mill	150	1600
8a	Set Coordinate System				
8b	profile Mill	Front Areas	12mm Ballnose Mill	150	1600

Table 4 2 GMT Production Process Plan

#### 4.4.1 First Operation.

The first operation would have to be on the bottom of the prosthetic. The coordinate system for this operation was located at the top-left-front vertex as seen in Figure 4.4. (a). The sequences were as follows:

1. Face mill the bottom of the block using a 63mm fly cutter in one pass as shown in Figure 4.4, with a cutting feed of 150mm/min, a step depth of 4 mm and a spindle speed of 750 rpm.

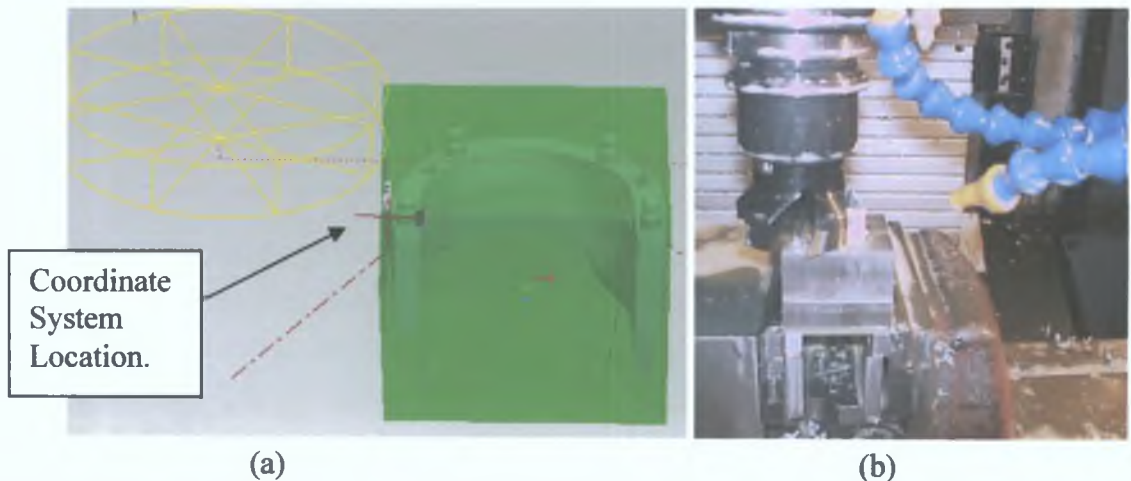


Figure 4.4 Face Mill Sequence 1. (a) ProEngineer Tool Path. (b) Machined Work Piece.

2. Volume mill down to the plane at the bottom surface of the prosthetic excluding the volumes around the abutment locations, using the 20mm slot mill in three passes, as shown in Figure 4.5. The cutting feed was 150mm/min, with a step depth of 2 mm, and a spindle speed of 1200 rpm.

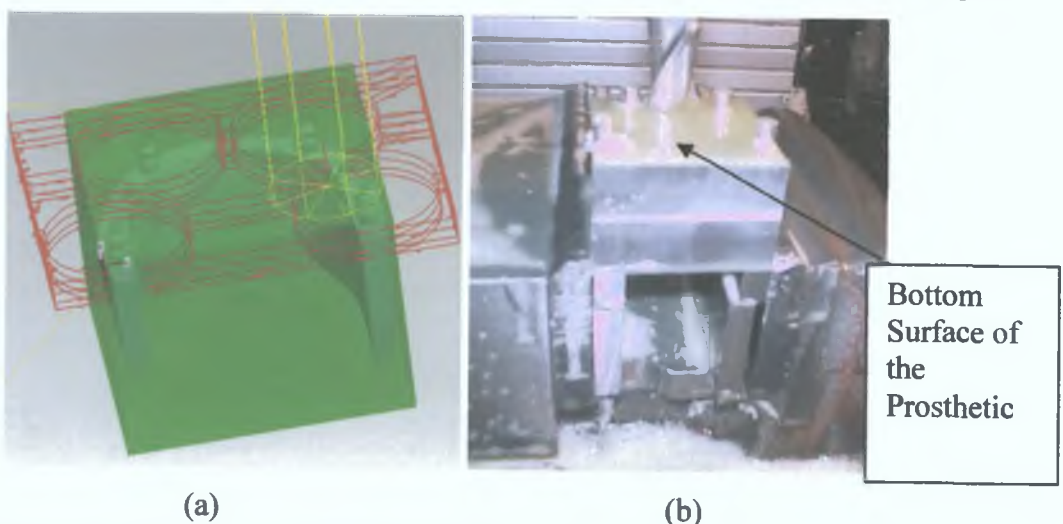
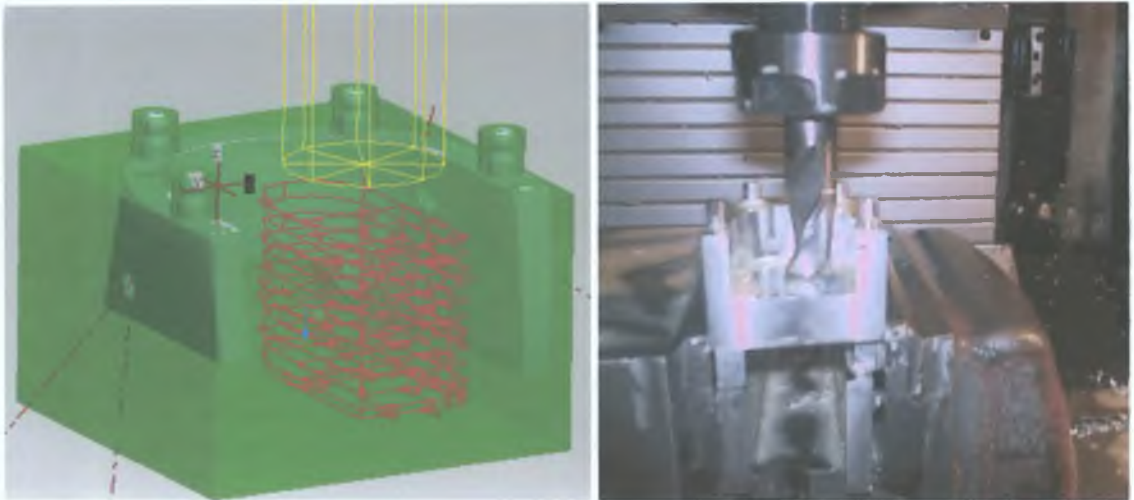


Figure 4.5 Volume Mill Sequence 1. (a) ProEngineer Tool Path. (b) Machined Work Piece.

- Volume mill the inside of the prosthetic down as far as the top surface, again using the 20mm slot mill, with a cutting feed of 150mm/min, a step depth of 2 mm, and a spindle speed of 1200 rpm, as shown in Figure 4.6.



(a)

(b)

Figure 4.6 Volume Mill Sequence 2. (a) ProEngineer Tool Path. (b) Machined Work Piece.

- Profile Mill the inside and outside left and right profiles, leaving the front block face untouched, because it will be needed to locate the coordinate system for the last operation. A 12mm ballnose milling tool was used, with a cutting feed of 150mm/min, a step depth of 2 mm, a spindle speed of 1600 rpm, and a wall scallop height of 0.225mm, as shown in Figure 4.7.

This scallop height creates a relatively coarse surface finish.

In vivo<sup>14</sup> experiments conducted by Hallgren et al [39] and Wieland [71] have shown that the surface topography of an implant may not only be too rough to promote osseointegration but it can also be too smooth. A wavelength range of 50-500 $\mu\text{m}$  (50-500 $\cdot 10^{-6}$  m) was found to be the best surface topography for osseointegration. It was decided to take a mid-range value of 225  $\mu\text{m}$ , as an average surface finish, which is the reason for the 0.225mm wall scallop height.

<sup>14</sup> **In Vivo:** refers to experimentation done in or on the living tissue of a whole, living organism as opposed to a partial or dead one.



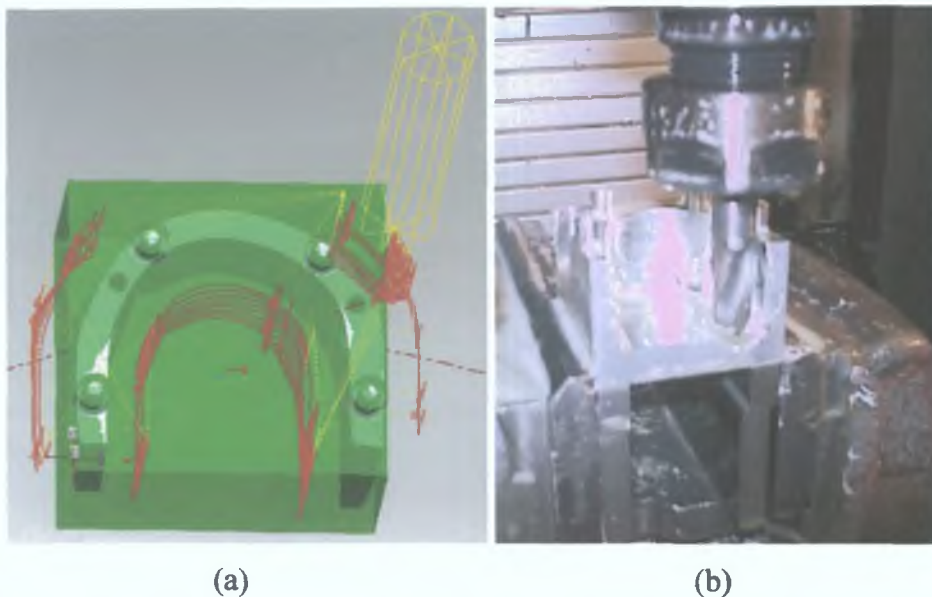


Figure 4.7 Profile Mill Sequence 1. (a) ProEngineer Tool Path. (b) Machined Work Piece.

5. At this point in the operation, it was hoped to create the profile of the abutments. A form tool was designed for this purpose, using the dimensions from the abutments in the finite element .db model seen in Appendix C. A vendor was located to manufacture the tool, but a lapse in the GMIT purchasing protocol over several months resulted in the author not receiving it in time to create these profiles.

The procedure for milling the abutment profiles would have been to use a trajectory cut using the formtool. One sequence would have been used to profile mill all four abutments, as seen in Figure 4.8.

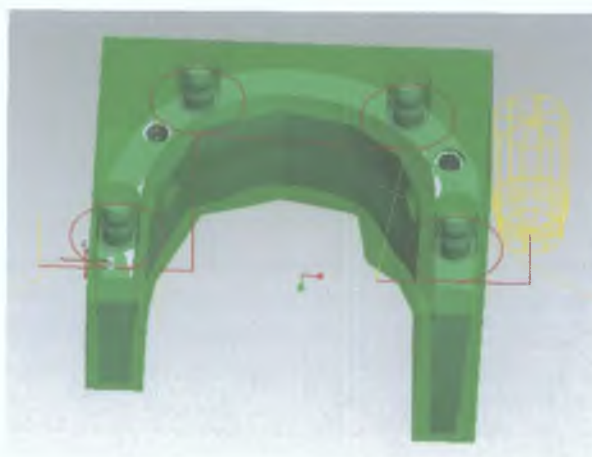


Figure 4.8 Abutment Trajectory Mill ProEngineer Tool Path.

This completed the first operation on the bottom of the prosthetic. The work piece was removed from the bench vice, cleaned and prepared for the next operation.



#### 4.4.2 Second, Third, Fourth and Fifth Operations.

The second, third, fourth, and fifth operations were to counter bore and drill the four holes. The holes were at compound angles, so the author had to manufacture four separate fixtures to hold the blocks in the correct orientation for each hole to be machined in the Z-axis. These fixtures, shown in Figure 4.9 were designed by creating a plane normal to the axis of each hole.

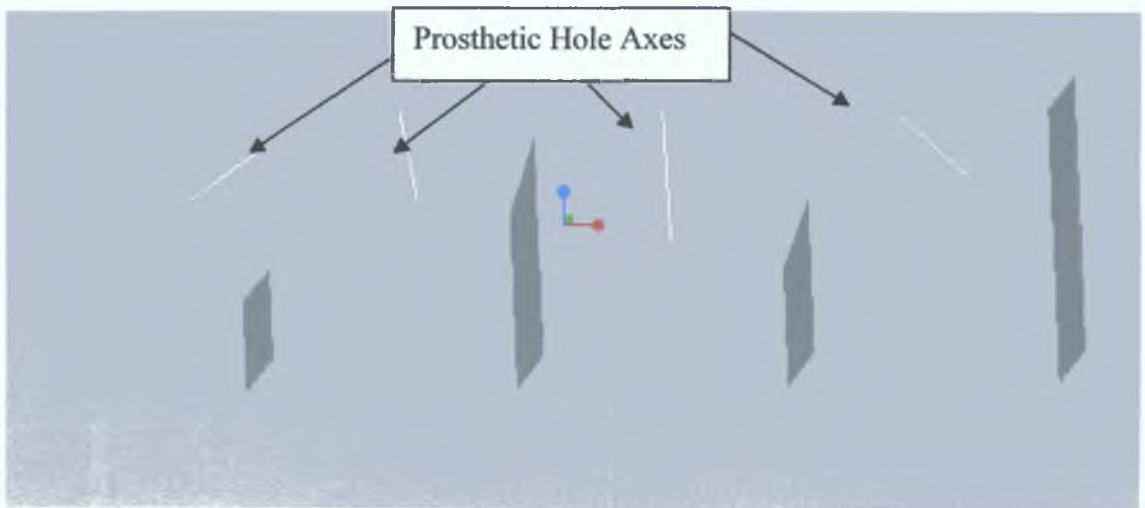


Figure 4.9 Milling Fixtures with Planes Normal to the Axes Holes.

The work pieces were located on the fixtures by means of a 6mm threaded bolt and two 5mm silver steel dowel pins, as shown in Figure 4.10

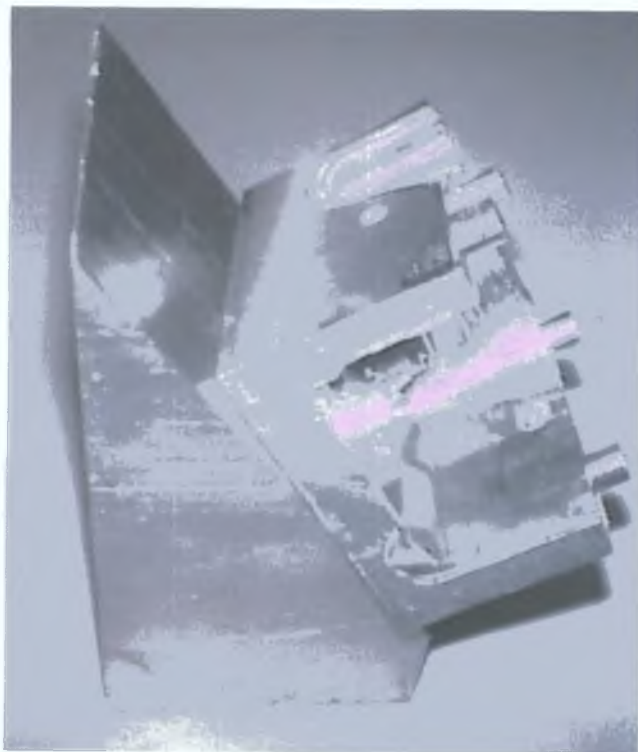


Figure 4.10 Work Piece Attached to Fixture.

Even though the work pieces were in the correct vertical orientation when attached to the fixtures, the angle of the bench vice holding the fixtures had to be adjusted manually to compensate for the horizontal aspect of the compound angles.

The bench vice angles of adjustment were;

- Hole 1 -----6.539 degrees.
- Hole 2 -----1.243 degrees.
- Hole 3 -----0.154 degrees.
- Hole 4 -----6.754 degrees.

The process of manually adjusting the vice only had an accuracy of 1 degree, which resulted in very poor hole location.

Due to the compound angle on the hole axes, there were no flat surfaces, which could be used as references for the X, Y, and Z offsets. Therefore, the coordinate system for these operations was located at the front-top vertex that provided easiest access, as seen in Figure 4.11. The 3mm centre drill was used to set the offsets by placing its tip as close as possible to the vertex in question. The author fully understands the compromise in the dimensional quality of the prosthetic that was made, but because of the limitations of a 3-axis machine, this action was unavoidable.

Once the work piece was located adequately there were three hole making sequences for these operations.

1. Counterbore the location for the head of the screw using a 4mm slot mill, with a cutting feed of 50mm/min, and a spindle speed of 2000 rpm, as shown in Figure 4.11.

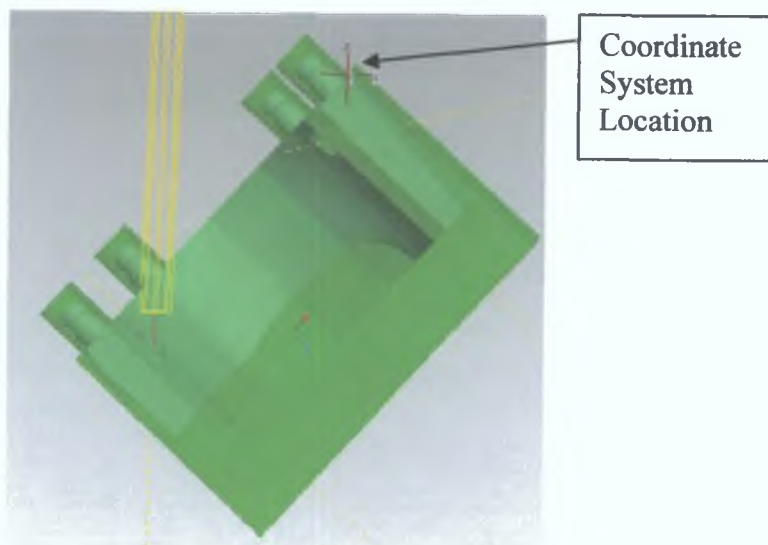


Figure 4.11 Counterbore Sequence ProEngineer Tool Path.

2. Centredrill the hole using a 3mm centredrill, with a cutting feed of 50mm/min, a spindle speed of 2000 rpm, and a breakout distance of 2mm. The centerdrill had to be attached in a long thin extension collet, as shown in Figure 4.12, because the regular collet would damage the work piece.

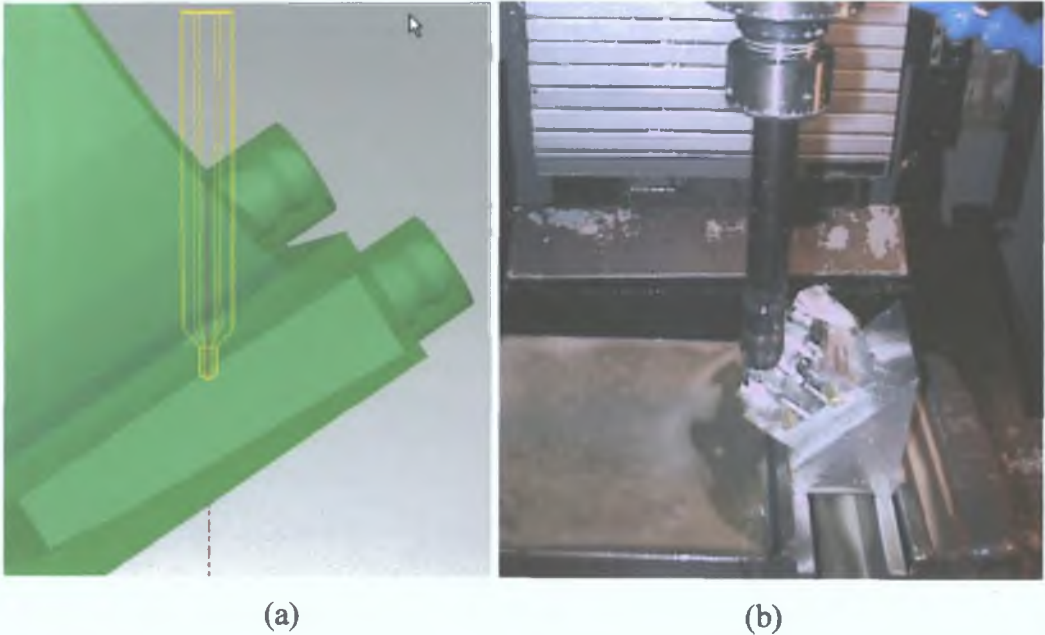


Figure 4.12 Centredrill Sequence. (a) ProEngineer Tool Path. (b) Machined Work Piece.

3. Drill the hole using a 3mm drill, with a cutting feed of 50mm/min, a spindle speed of 2000 rpm, a peck depth of 2mm, and a breakout distance of 3mm, as shown in Figure 4.13.

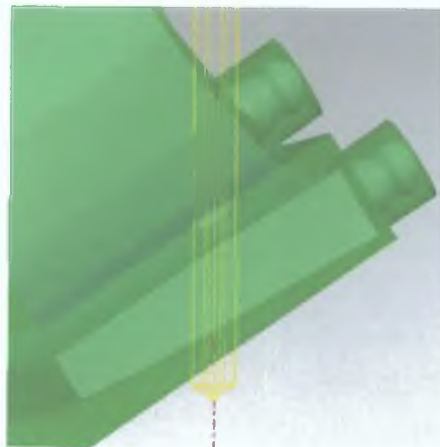


Figure 4.13 Drill Sequence ProEngineer Tool Path.

This completed the hole making operations. The work piece was removed from the bench vice, cleaned and prepared for the next operation.

#### 4.4.3 Sixth Operation.

The sixth operation was to machine the top of the prosthetic. The positioning of the prosthetic in the vice was critical for this operation. If the left and right sides of the prosthetic were gripped with the vice, excessive vibration and distortion of the prosthetic would occur. Due to the large volume that was removed from the centre of the work piece in the first operation, the only safe way to hold the prosthetic was to grip it with the front and back faces. For this reason these faces were deliberately not profile milled in the first operation as shown in Figure 4.15. The coordinate system for this operation was located at the top-left-front vertex, as seen in Figure 4.14. The sequences for this operation were as follows:

1. Face off the top of the block down to 1mm above the top surface of the prosthetic this 1mm would later be used to create the  $225\mu\text{m}$  surface finish. The 60mm fly carbide cutter was used with a cutting feed of 100mm/min, a step depth of 4mm, and a spindle speed of 750 rpm. Three passes were needed to complete the sequence, as shown in Figure 4.14.

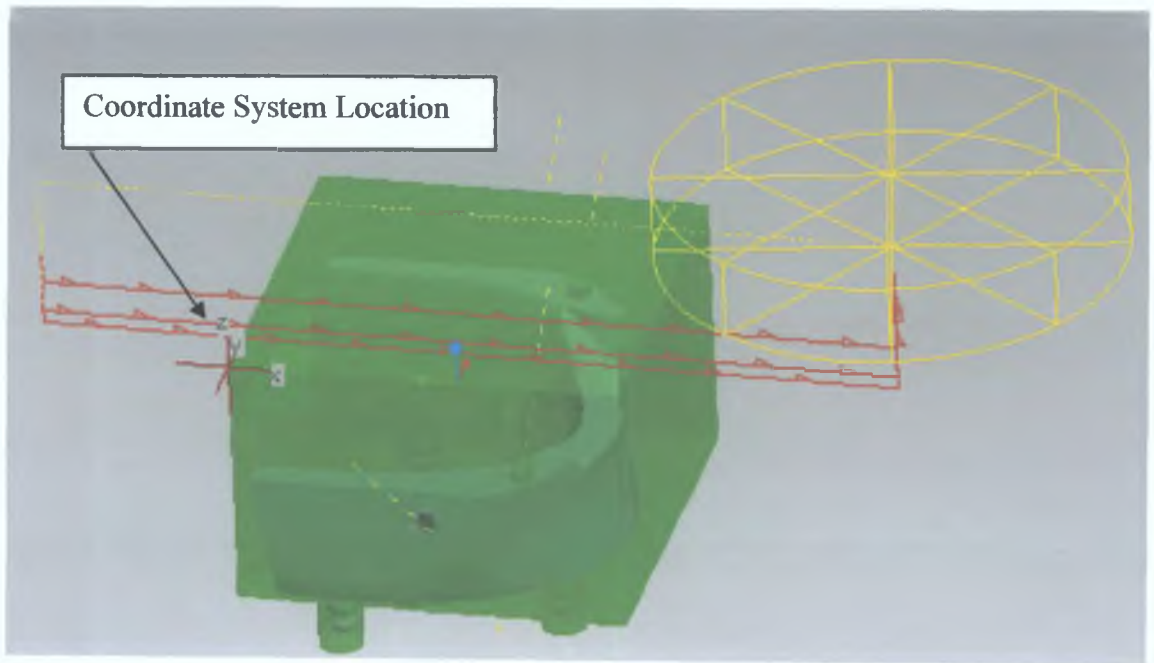


Figure 4.14 Face Mill Sequence 2 ProEngineer Tool Path.

2. Volume mill from 1mm above the upper top surface to 1mm above the lower top surface, as seen in Figure 4.15, using the 20mm slot mill, with a cutting feed of 150mm/min, a step depth of 2mm, and a spindle speed of 1200 rpm.



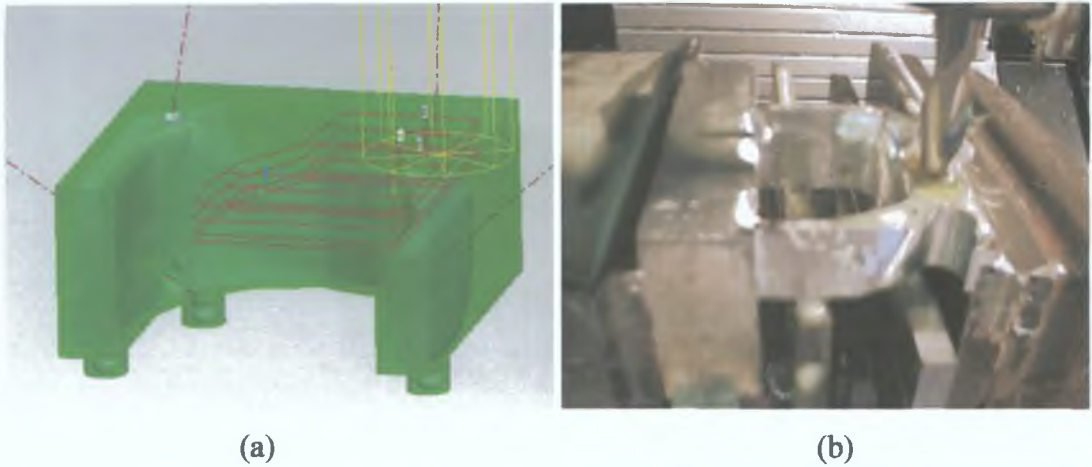


Figure 4.15. Volume Mill Sequence 3 (a) ProEngineer Tool Path. (b) Machined Work Piece.

3. Profile mill the left and right inside and outside areas, and the top-front areas of the prosthetic, using the 12mm ballnose cutter, with a cutting feed of 100mm/min, a wall scallop height of 0.225mm, and a spindle speed of 1600 rpm, as shown in Figure 4.16. The author needed to be careful at this point not to mill the front or back of the work piece as they would be needed to locate the coordinate system in the next operation.

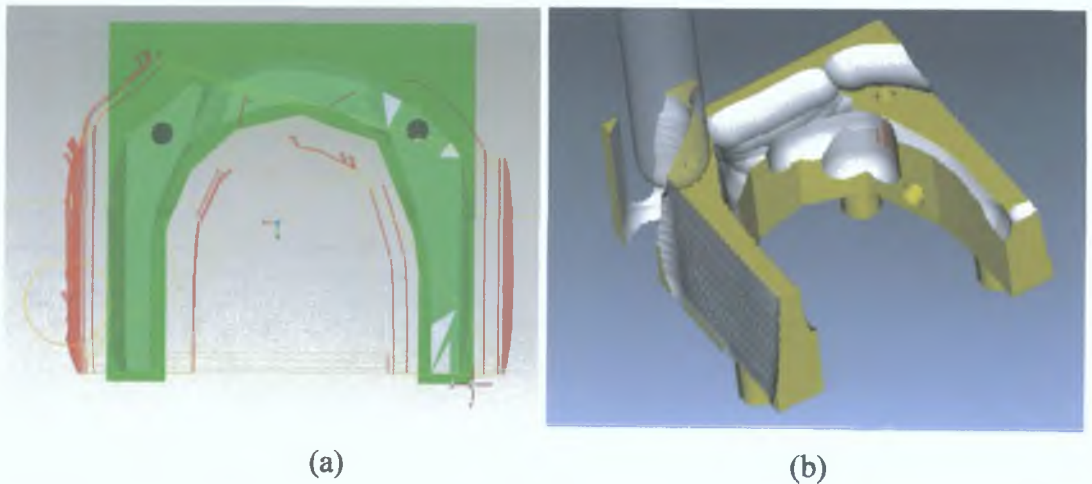


Figure 4.16. Profile Mill Sequence 2 (a) ProEngineer Tool Path. (b) NC Tool Path.

4. Surface mill the top faces with a the 12mm ballnose mill using a cutting feed of 150mm/min, a wall scallop height of 0.225mm, and a spindle speed of 1600 rpm, as seen in Figure 4.17.

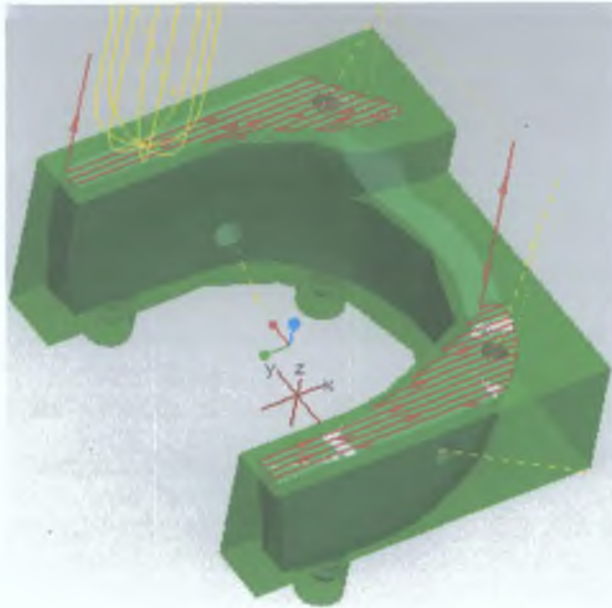


Figure 4.17 Surface Mill Sequence ProEngineer Tool Path.

This completed the sixth operation on the top of the prosthetic. The work piece was removed from the bench vice, cleaned and prepared for the next operation.

#### 4.4.4 Seventh Operation.

The seventh operation was to machine the front of the prosthetic. The coordinate system for this operation was located at the top-right-front vertex seen in Figure 4.18. The prosthesis was positioned vertically in the vice and a square bar was placed between the abutments to protect them from damage, as seen in Figure 4.19. The sequences for this operation were as follows:

1. Face mill the front of the block using the 63mm fly cutter in one pass as shown in Figure 4.18, with a cutting feed of 150mm/min, a step depth of 4 mm, and a spindle speed of 750 rpm. This sequence was included to remove material quickly, saving time on the next profile sequence.

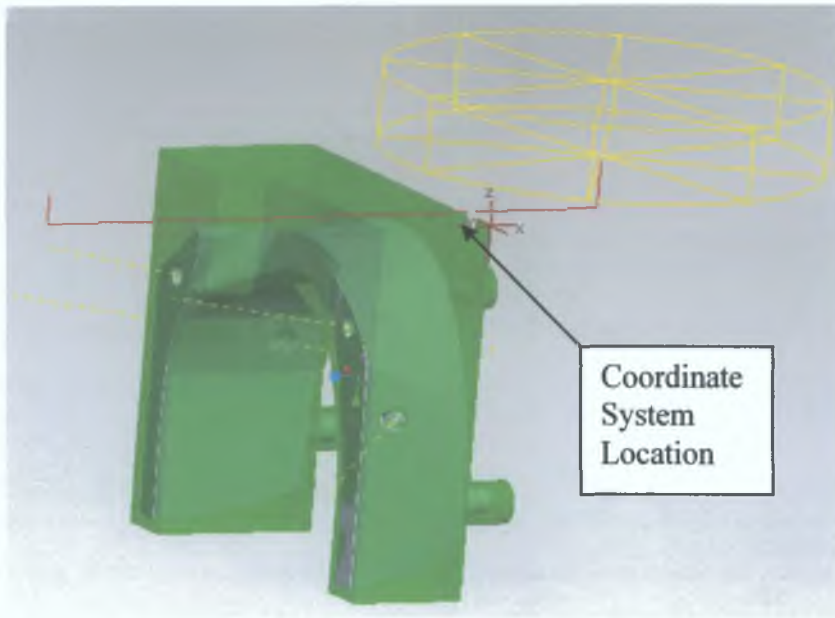


Figure 4.18 Face Mill Sequence 3 ProEngineer Tool Path.

2. Profile mill the front areas of the prosthetic with a 12mm ballnose mill, using a cutting feed of 150mm/min, a wall scallop height of 0.225mm, and a spindle speed of 1600 rpm, as seen in Figure 4.19

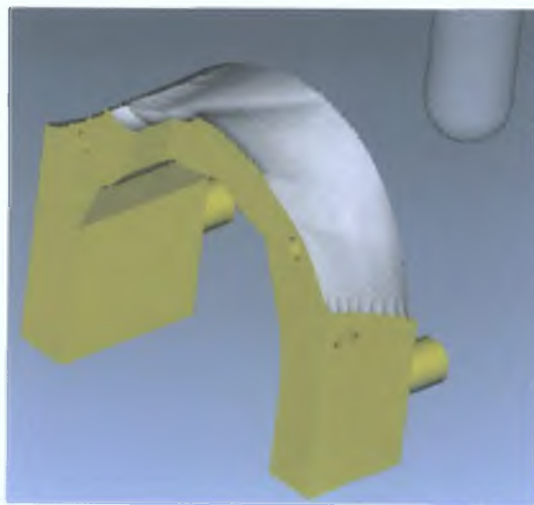


Figure 4.19 Profile Mill Sequence 3 NC Tool Path.

This completed the seventh operation on the front of the prosthetic. The work piece was removed from the bench vice, cleaned and prepared for the next and final operation.



#### 4.4.5 Eight Operation.

The final operation was to mill the back of the prosthesis. The original work piece block was purposefully located in relation to the X, Y, and Z directions of the bottom surface of the abutments. This allowed the author to use a square bar (slightly larger than the length of the abutments, to ensure they would not be damaged as the vice was tightened) placed under the abutments to locate the prosthesis in a vertical position. Slip gauges were also used between the vice and the lower top surface to locate the prosthesis, as seen in Figure 4.20. The coordinate system for this operation was located at the top-right-front vertex. There was just one sequence in this operation.

1. Profile mill the back surfaces of the prosthetic using the 12mm ballnose cutting tool, with a wall scallop height of 0.225mm, and a spindle speed of 1600 rpm, as seen in Figure 4.20.

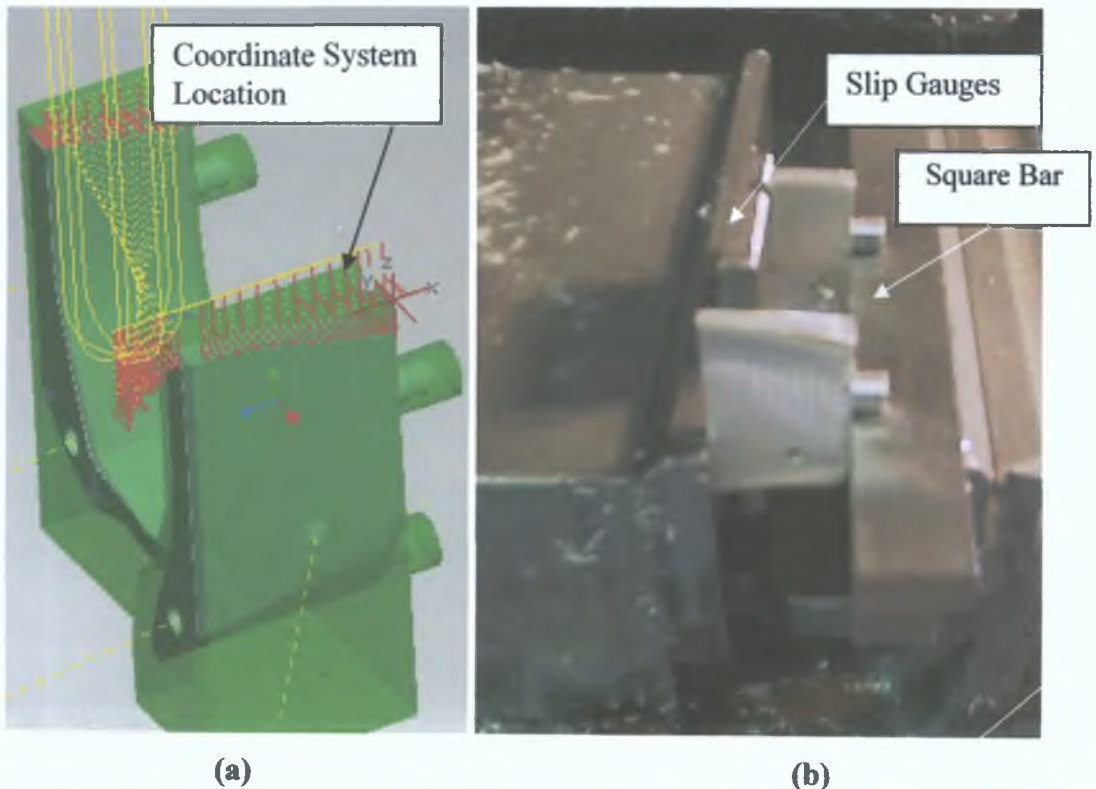


Figure 4.20 Profile Mill Sequence 4 (a) ProEngineer Tool Path. (b) Machined Work Piece.

With the milling strategy designed, the next step was to construct a prosthetic from titanium. The normal high-speed steel tools used for cutting aluminium would not be tough enough to mill titanium. To mill the prosthetic out of titanium the necessary carbide tools, and the formtool needed were ordered but never received. As a direct result of this purchasing error, the author could not machine the titanium prosthesis at GMIT. The project had to be outsourced to a toolmaking workshop.

## 4.5 Outsourced Vendors.

Two vendors were found capable of machining the titanium prosthetic, the first “Caragh Tool and Die”, a large toolroom based in Galway, quoted a price of €8,000. The second, “Prior Tool and Die”, a medium sized toolroom based in Carrick-on-Shannon, were conducting their own research into the feasibility of entering the medical device industry. They offered to machine, and verify on a CMM (Coordinate Measuring Machine), four pieces free of charge as a goodwill gesture to GMIT

Caragh Tool and Die wanted to partially outline machine the prosthetic by wire EDM (Electrical Discharge Machining). This is an easier method of machining the prosthetic, but all the definition along the profiles would have been lost For this reason Prior Tool and Die was chosen as the project vendor.

The model of the prosthetic from Figure 4.1 was saved as a parasolid file and e-mailed to them. This file type allowed them to open and manipulate it in their Unigraphics CAD/CAM software.

The milling tools used are detailed in Table 4.2

Tool Number	Tool Name	Tool Offset	Feed rate (mm/min)	Spindle Speed (Rpm)
1	17mm Carbide tee-slot mill	1	120	1600
2	8mm Carbide ballnose mill	2	400	2000
3	6mm Carbide ballnose mill	3	400	2500
4	8mm Carbide slot mill	4	400	2000
5	6mm Carbide slot mill	5	400	2500
6	2mm Carbide ballnose mill	6	200	3150
7	3mm Carbide drill	7	100	3000

Table 4 3 Milling Tools, Offsets, Feeds, and Speeds.

#### 4.6 Pallet Indexing System.

The standard 3 axis-milling machine was not appropriate for machining the prosthetic due to the compound angles of the holes and the irregular profiles. What was needed was a minimum of four axes. The fourth axis was set up by using an indexing table. Prior Tool and Die use an Erowa Swiss palletising and indexing machine shown in Figure 4.21. This system is used on both the CNC machining centre and the CMM, eliminating the need for coordinate set-ups.

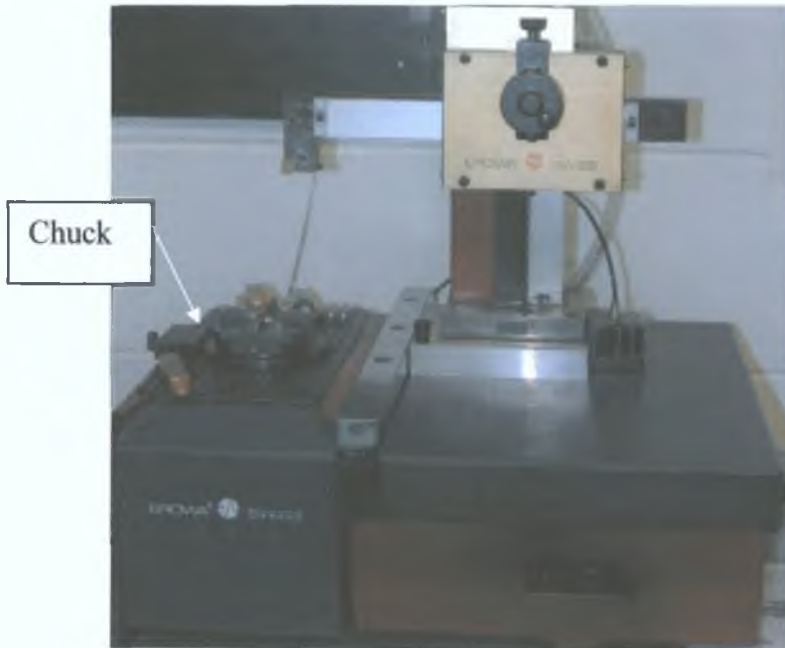
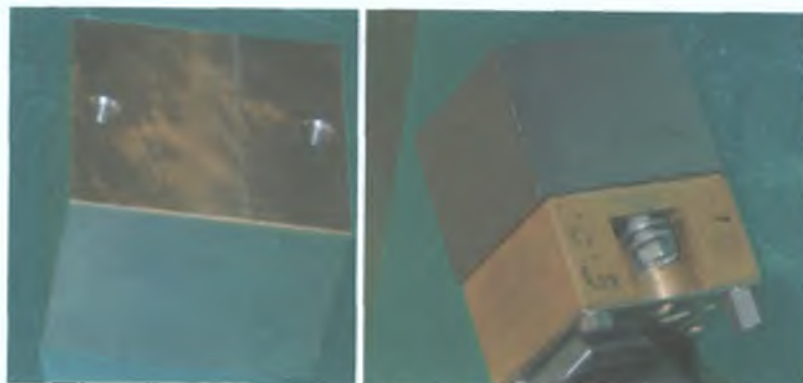


Figure 4.21 Erowa Swiss Palletising and Indexing Machine.

Palletising the work piece and fixtures on a zero point tooling system was the first step in creating the prosthetic. Two holes were drilled and tapped in the work piece, and fixed to a pallet, as seen in Figure 4.22.



(a)

(b)

Figure 4.22. (a) Work Piece Drilled and Tapped (b) Work Piece Fixed to the Pallet by Screws.

The pallet with the work piece was clamped to the chuck on the Erowa indexing machine, seen in Figure 4.21. A zero datum point created on the machine table enabled the pallet to be removed and repositioned with no realignment. This could be repeated on the milling centre and the CMM machine, allowing a standardised mechanical interface between the different processes.

#### 4.7 Vendor Machining Strategy.

At the machining centre, a horizontal and vertical portable chuck were used to orientate the work piece in the necessary position, as seen in Figure 4.23



Figure 4.23 Horizontal and Vertical Portable Chuck.

At this point, the work piece was ready for the first milling operation. The pallet was gripped in the vertical chuck shown in Figure 4.23, and clamped to the bed of the Mikron machining centre.

#### 4.7.1 First Operation.

The first operation was to machine the bottom and inside volume of the prosthetic. The sequences of this operation were:

1. Volume mill down to the plane at the bottom surface of the prosthetic excluding the volumes around the abutment locations, using the 8mm slot mill. Much the same as in Figure 4.5.
2. Volume mill the inside and outside areas of the prosthetic down as far as the top surface, again using the 8mm slot mill.
3. Profile mill the inside and outside areas with the 8mm ballnose mill.
4. Using a trajectory cut, Profile mill the abutment with the 17mm Tee slot carbide mill. This completed the first operation and resulted in the model shown in Figure 4.24.

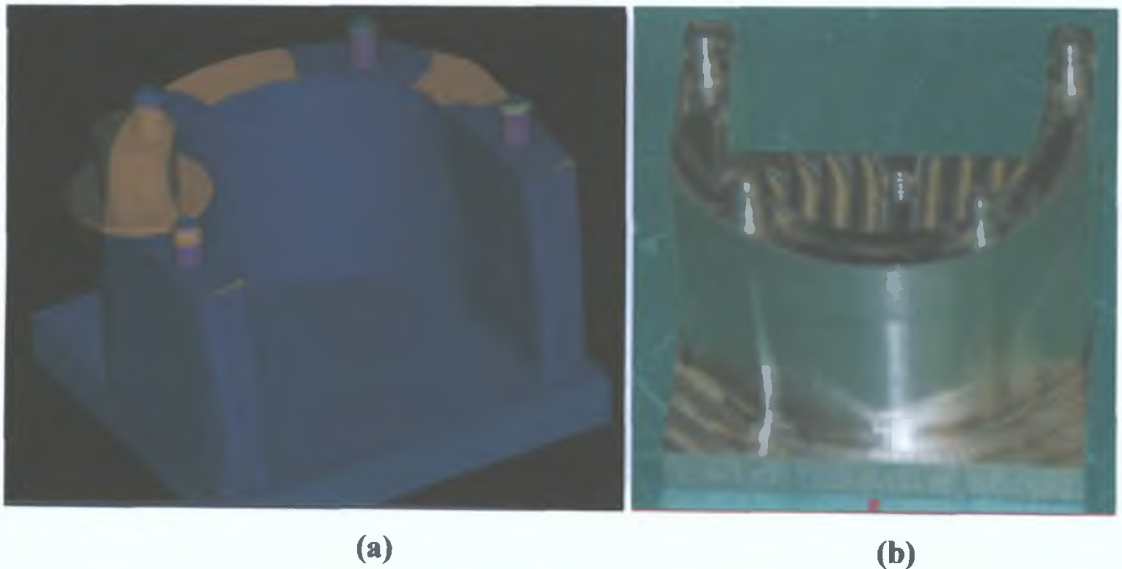


Figure 4.24. First Operation Completed. (a) Unigraphics Tool Path Model.  
(b) Machined Work Piece.



#### 4.7.2 Second, Third, Fourth and Fifth Operations.

The second, third, fourth and fifth operations were to counter bore and drill the four holes. A manual Bridgeport Vertical mill as seen in Figure 4.27, was used as opposed to the CNC mill.



Figure 4.25 Standard 3 Axis Milling Machine.

There was no particular reason that the manual mill would be a better choice for these operations, but at that particular time Prior Tool and Die were busy with other contracts from paying clients and could not spare the use of the Micron CNC machining centre, and the process of drilling is inherently simple once the locations are accurately obtained.

Unlike the GMIT method of machining the holes, Prior Tool and Die chose to secure the prosthetic in the vertical position and tilt the head of the Bridgeport milling machine to the required angle. To locate the position of the holes in the prosthetic, the fixture in Figure 4.26 was designed. This was done subsequent to the palletising operation.



Figure 4.26 Fixture Used to Locate the Prosthetic for the Manual Machining Centre.

The four holes in the fixture were located on the abutments of the prosthetic, and the sphere was centred on the zero datum point created on the Erowa palletising and indexing system.

While the head of the milling machine was in the vertical position, a lever type dial indicator shown in Figure 4.27 was used to clock the centre of the sphere.



Figure 4.27 Lever Type Dial Indicator.

The lever was offset at an arbitrary angle and the milling chuck was rotated by hand until the dial indicated zero with no movement for a  $360^\circ$  rotation about the sphere. When this neutral positioning was achieved, the head of the milling machine was tilted to the required angle for each hole in the prosthetic.

The distance from the centre of the sphere to the axis of the four holes on the prosthetic in the coordinate system was determined from the CAD model. The table bed was moved these distances, which gave the final drilling location for each hole in the prosthetic. The holes were drilled with the 3mm carbide drill bit without any further problems.



### 4.7.3 Sixth Operation.

The sixth operation was to rotate the prosthetic 45 degrees clockwise in the indexing system, as seen in Figure 4.28(a), to profile mill all the areas that are accessible with the 6mm carbide ballnose mill. The prosthetic was then rotated 90° anticlockwise on the horizontal indexing table to profile mill as much of the other side of the prosthetic as possible as seen in Figure 4.28(b). The prosthetic was rotated back 45° clockwise to a vertical position as seen in Figure 4.28(c), to mill the profile on the inside front of the prosthetic. Finally, the prosthetic was rotated 180° to mill the outside front of the prosthetic, as seen in Figure 4.28(d)

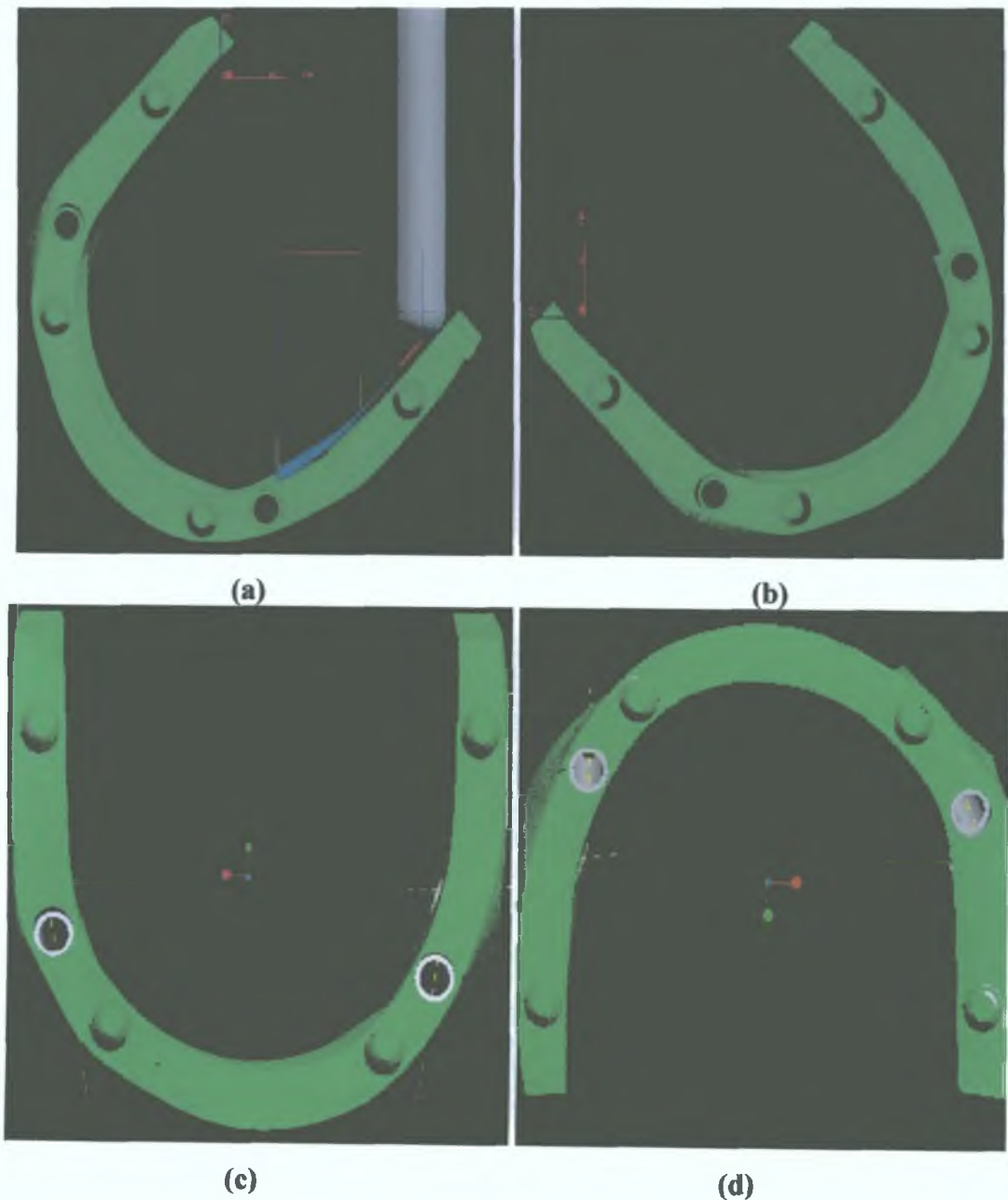


Figure 4.28 (a)(b)(c)(d) Profiling Operation.

#### 4.7.4 Seventh Operation.

The seventh and final operation was to part off the base of the block, to enable the top of the prosthetic to be machined. To machine the top of the prosthetic a second fixture was designed to secure it in the vertical position. Four holes in the fixture were used to locate the abutments in the correct position, and two clamps on the sides secured the prosthetic in position, as seen in Figure 4.29.



Figure 4.29 Prosthetic Secured to a Fixture.

The prosthetic was volume milled down to the surfaces on the top of the prosthetic with the 6mm carbide slot mill, and then the top-front of the prosthetic was profile milled with the 6mm carbide ballnose slot drill, as seen in Figure 4.30.



Figure 4.30. Unigraphics Tool Path Model Profile Milling the Top Surface.

This completed the final operation on the prosthetic. It was then taken to be analysed on the CMM.

## 4.8 Costing.

The bulk of the work required to produce the prosthetic was in planning the strategy for machining, which took two weeks. The actual machining lasted two days. The total cost of machining the first prosthetic was €8,000. This price was broken down into the cost of fixtures, and two main labour costs, the CNC machinist at a rate of € 70/ hr, and the CAD/CAM Engineer at a rate of € 80/hr

Two weeks planning	$€ 80/ hr * 80/ hr =$	€ 6,400.
Two days machining	$€ 70/ hr * 16/ hr =$	€ 1,120
Fixtures.		<u>€ 480</u>
<b>Total.</b>		<b>€ 8,000</b>

Once the staff had become used to working with this type of prosthetic, the planning phase, and the need for fixtures would be greatly reduced. The cost of any further customised, but similar prosthetics would be reduced to approximately €2,000, as detailed below

One - Two days planning	$€ 80/ hr * 10/ hr =$	€ 800
Two days machining	$€ 70/ hr * 16/ hr =$	€ 1,120.
Fixtures		<u>€ 100.</u>
<b>Total.</b>		<b>€ 2,020.</b>

Comparing these figures to the RIF project cost of € 6,000 to rapid prototype each piece [75]. The CNC milling method suggested in this research, results in a saving of approximately € 4,000 per piece

The cost involved in CNC milling each customised prosthetic on an ongoing basis is approximately €2,000 each. This represents 10% of the total costs of the surgical procedure to give a total cost of implanting the prosthesis of €22,000.

## 4.9 Discussion.

The prosthetic produced at GMIT had a number of errors in the location of the holes. It is normal practice to locate the X, Y, and Z offsets on the side, front and top of a work piece. The hole fixtures located the work piece at an angle that would only permit a vertex to be used for the offsets. This unavoidable step introduced guesswork in the holemaking sequences. In addition, the compound angle of the holes necessitated moving the bench vice at the angles listed below.

- Hole 1 -----6.539 degrees.
- Hole 2 -----1.243 degrees.
- Hole 3 -----0.154 degrees.
- Hole 4 -----6.754 degrees.

The bench vice had to be moved manually and only had an accuracy of 1 degree, compounding the hole location errors even more. These errors were unacceptable to the author, because they would in turn lead to an error on the screw location in the skull during the surgical procedure.

The author discovered after watching the operations at Prior Tool and Die that the form tool that the author ordered to machine the abutments at GMIT was in fact unnecessary, in that the abutments could have been machined quite easily with a Tee slot mill. The workshop at GMIT did not have a tee slot mill small enough for the operation, one was ordered but it was never received, for this reason the GMIT prosthetic was never completely finished.

The author did not discover about the Hallgren et al [39] and Wieland et al [71] assertion that a wavelength range of 50-500 $\mu\text{m}$  was the best surface topography for osseointegration, until after the vendor had machined their prosthetics, which was the reason that it has a very polished surface finish. One positive outcome from the GMIT prosthetic is that it displays the most appropriate surface finish for osseointegration to take place.

The palletising and indexing machine used at Prior Tool and Die, in effect converted their 3-axis Micron machining center into a 4-axis machining center, eliminating the need to reset the coordinate system for each operation. From the authors experience this is a minimum requirement when machining a complex structure such as the prosthetic. Two weeks after machining the prosthetic, the vendor had installed a 5-axis machining center. Had the prosthetic been machined on the 5-axis machining center there would have

been no need for the manual drilling operations, and the machining strategy would have been even more straightforward.

## Chapter 5

### Dimensional Analysis of the Prosthetic Using a Coordinate Measuring Machine.

- 5 1 Introduction.
- 5 2 Prosthetic Analysis.
- 5 3 Results
- 5 4 Conclusions.

#### 5.1 Introduction.

CMM's (Coordinate Measuring Machines) are mechanical systems designed to move a measuring touch probe to determine the X, Y and Z coordinates of points on a work piece surface.

There are two styles of CMM, namely bridge, and gantry. The Mitutoyo Euro-M544 absolute bridge style was used in this analysis. Some of the features of the Mitutoyo CMM are as follows

- Measuring range 400 x 600 x 300 mm
- Resolution 0.001 mm
- Guidance method: air bearings on all axes
- Table size: 900 x 900 mm – granite bed
- Operation Manual control

In the bridge style CMM, the arm is suspended vertically from a horizontal beam that is supported by two vertical posts. The machine X-axis carries the bridge, which spans the object to be measured, and a computer is networked to the CMM, as seen in Figure 5.1.



Figure 5.1 Mitutoyo Euro-M544. CMM.

The computer receives detailed dimensional data gathered by manually moving the touch probe as seen in Figure 5.2 along the work piece surfaces. The CMM CosmosV1.5 software program, manipulates this data into usable information for the user.



Figure 5.2 CMM Touch Probe.

The touch probe is isotropic [73], in that it exerts the same probing force in all three axes simultaneously. Therefore, when the probe tip touches the part surface, it is deflected along a vector that is orthogonal to the part surface at that point (see Figure 5.3). The 3-D probe head is capable of measuring the X, Y and Z coordinates of the contact point simultaneously.



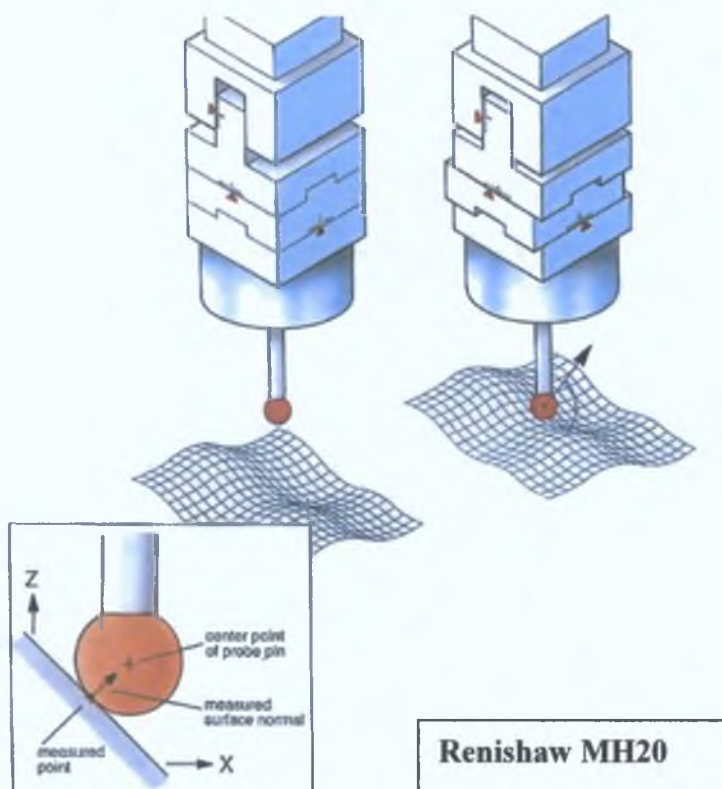


Figure 5.3 Operation of a 3-D Scanning Probe.

The readings from the probe always refer to the centre of the probe tip. The software program mathematically offsets the coordinates by the radius of the tip during the measuring operation. The vector normal to the probed surface at the point of contact determines the direction of this offset. The direction of this vector is automatically determined from the readings of the three probe axes.

## 5.2 Prosthetic Analysis.

It was hoped to investigate the dimensional quality of the machined prosthetic at GMIT, but their CMM has been out of order for the past year, and at the time of writing was still not working. John Prior performed an extensive CMM analysis at Prior Tool and Die and provided a report on completion of the investigation to GMIT.

The dimensional inspection of the prosthesis involved the process of reverse engineering or the recovering of points on the surfaces of the implant using the CMM to compare with the equivalent points in the unigraphics CAD model. Communication with the CAD software was made possible using an .iges file. An iges file is not a reliable file format to use for file transfer of a three-dimensional model because some detail can be lost. This is the reason the abutments are missing in Figures 5.4 and 5.5. It is suggested that in future a STEP or VDA file is used for file transfer, as they are more compatible with both CMM and CAD software [74].

There were 138 measurement points in total taken from the titanium prosthetic on the CMM, 120 points were taken from the surface areas, and 18 points were taken from the hole areas. Some of these points can be seen in Figures 5.4, and 5.5. A detailed list of measurements taken can be seen in the CMM report in Appendix E.

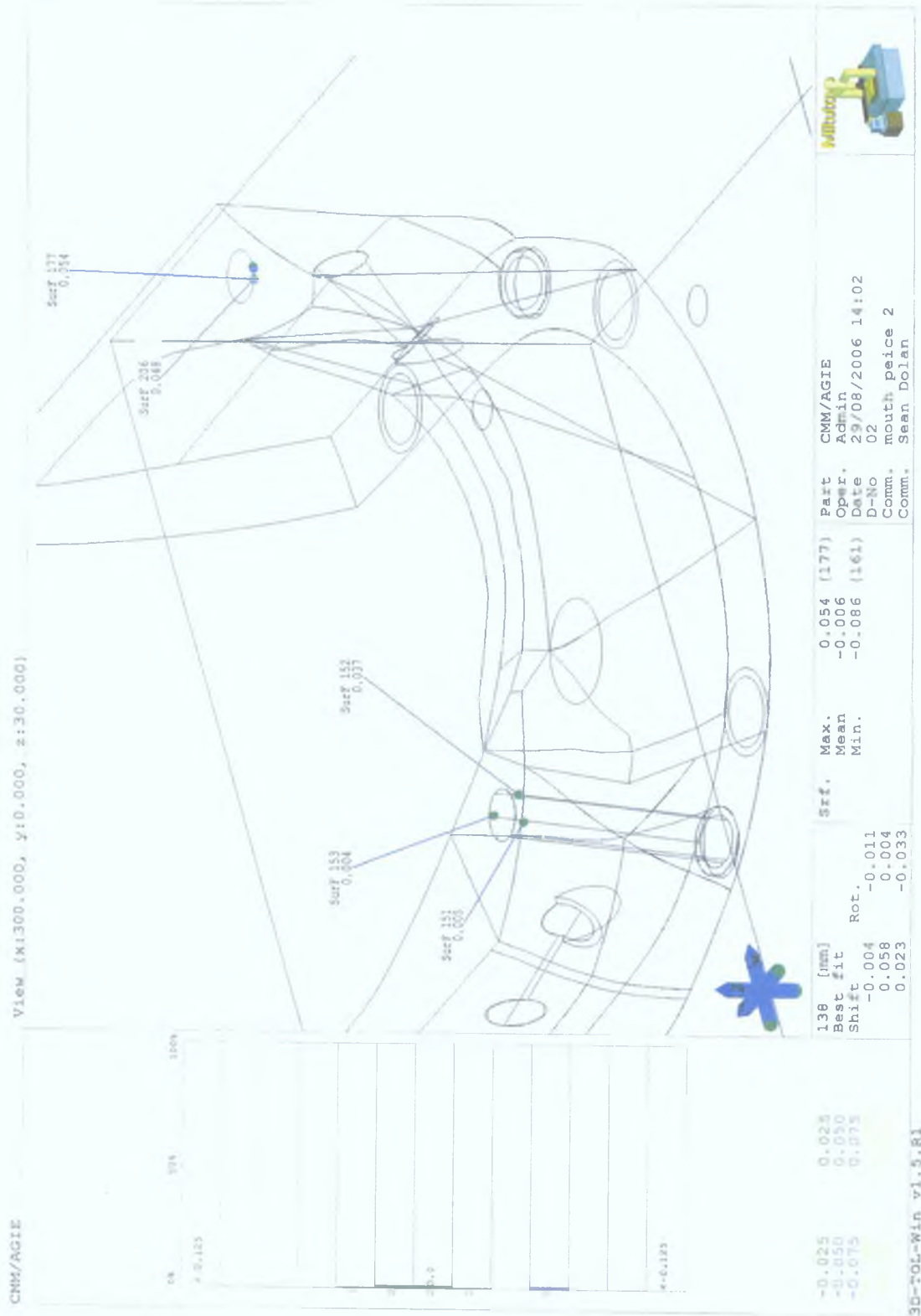


Figure 5.4 Measurements Taken from Points on the Prosthetic Hole Areas.

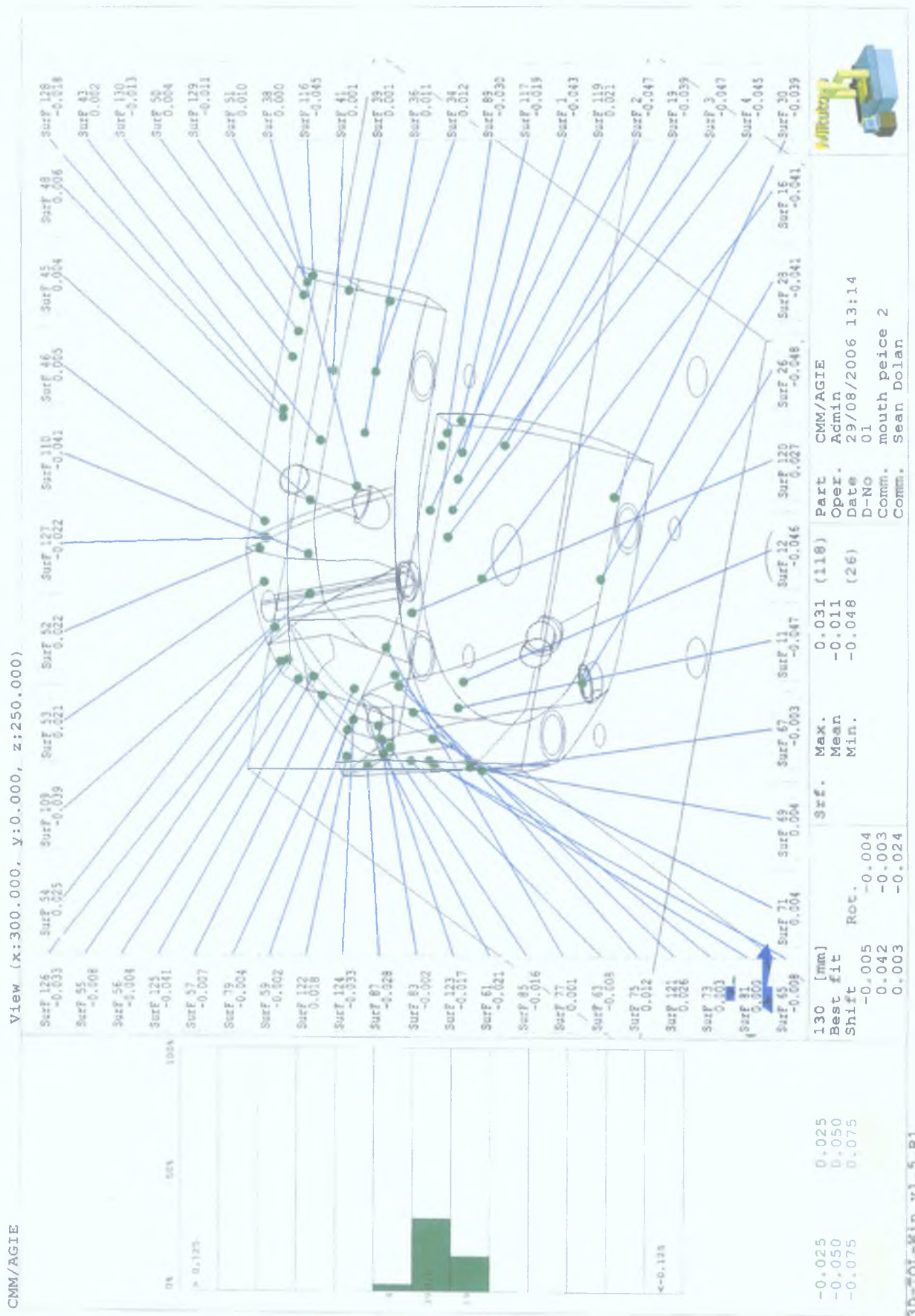


Figure 5.5 Measurements Taken from Points on the Prosthetic Surface Areas.



The Erowa Swiss palletising and indexing system described in Chapter 5 was used in conjunction with the CMM, eliminating the need for coordinate set-ups.

The CMM software measured each sample point in the X, Y, and Z-axes, and calculated the deviation from the CAD model, it also summed the deviations to give a total positive or negative orthogonal deviation.

### 5.3 Results.

From the measurement points taken on the surface areas, there was a maximum positive deviation of +0.031mm, a minimum negative deviation of -0.048 and a mean deviation of -0.011mm from the corresponding points on the CAD model.

From the 18 points taken from the prosthetic on the hole areas, there was a maximum deviation of +0.054mm, a minimum deviation of -0.086 and a mean deviation of -0.006mm from the corresponding points on the CAD model.

The orthogonal deviations of all 138 points in Appendix E from a maximum positive deviation of +0.054mm to a maximum negative deviation of -0.086mm, with a mean deviation of -0.020mm were plotted on the chart below.

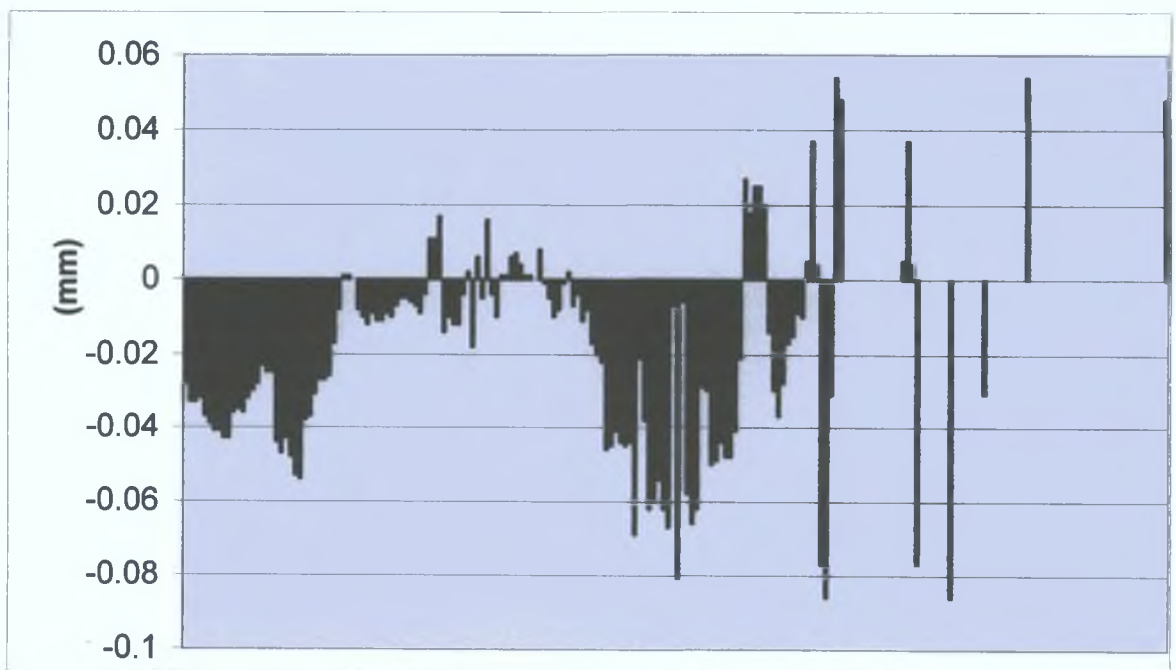


Figure 5.6. Total Orthogonal Deviation of Each Measurement Point.

From this chart, and Appendix E, it can be seen that near the end of the sampling points the CMM operator made a number of accidental errors. These errors were rejected, and did not affect the final result of the analysis.

## 5.4 Conclusions.

From Figure 5.4 and 5.5, it may be concluded that most of the positive deviations occurred at points taken from around the hole areas, while the points on the surface areas had mostly negative deviations. This suggests that the drilling operations carried out on the manual milling machine as described in Chapter 4 did not have as tight a tolerance as the other machining operations carried out on the micron CNC machining centre, as could be expected.

Figure 5.4 and 5.5 only show 65 of the 138 measurement point locations. While the CMM report in appendix E gives the X, Y, Z and total deviations of the missing 73 measurement points, the author cannot determine where they were taken from, and thus cannot comment on the localised effect of these deviations on the prosthetic.

In comparison with the originally designed rapid prototyping prosthetic described in [19], listing a mean deviation of +1.83mm when it was analysed with the CMM. The new CNC milled prosthetic established a mean deviation of -0.02mm. The original prosthetic was stated to be within the tolerance of those in the literature, and was assessed as feasible engineering and suitable for surgery. Therefore it may be concluded that the milled prosthetic is well within the tolerance in the literature. This factor alone suggests that the prosthetic should be milled rather than rapid prototyped.

The relative type CMM measurement system (point to point) used in the original prosthetic analysis, was not a good method for analysing the prosthetic, because of the difficulty in identifying and locating the landmarks used for measuring. The absolute (point measurement relative to a fixed coordinate) system used in this project, on the other hand did not rely on landmarks, and had no difficulty in choosing points to measure.

## Chapter 6

### Physical Testing of the Prosthesis

- 6.1 Introduction
- 6.2 Aluminium Physical Test.
- 6.3 Aluminium FEA Analysis
  - 6.3.1 Mesh.
  - 6.3.2 Material Properties
  - 6.3.3 Boundary Conditions
  - 6.3.4 Load Step Options
- 6.4 Titanium Physical Test
- 6.5 Titanium FEA Analysis
  - 6.5.1 Mesh
  - 6.5.2 Material Properties
  - 6.5.3 Boundary Conditions
  - 6.5.4 Load Step Options
- 6.6 Conclusions.

#### 6.1 Introduction.

The purpose of this section was to compare the results of the deformation from a bending test of the aluminium and titanium over time on an Instron tensile testing machine, to the deformation generated from aluminium and titanium models of the prosthetic under the same loading conditions in a finite element analysis

The tensile tester used was an Instron 5544-H1861, servo hydraulic testing system with a 2 kg axial load cell. The bottom grip of the tester was fixed and the top grip induced a displacement on the prosthetic. The tensile tester is networked to a personal computer enabling the user to control the displacement, bending load, speed of the displacement, and frequency of the measurements. The prosthetics were held in the testing machine by two angle brackets attached to the top and bottom grips, as shown in Figure 6.1.



Figure 6.1 Instron Tensile Testing Machine.

The rate of prosthetic deformation was controlled by the speed imposed on the top grip. The tests were conducted under static loading at a rate of 2mm/min, with a capture interval of 15 seconds. For safety reasons, there was a limit of 5mm displacement applied to the analysis, to prevent the prosthetic eventually dislodging from the brackets and flying off the machine.

## 6.2 Aluminium Physical Test.

The first test conducted, was on the aluminium prosthetic. It was gripped in the Instron machine. A static loading at a rate of 2mm/min, with a capture interval of 15 seconds was applied as described above. The machine measured the load exerted (N) and the displacements (mm) as the prosthetic was deformed. The data was saved as a .raw file, and opened in Microsoft Excel. The resulting data of this aluminium test are listed in Table 6.1 overleaf.



Aluminium Physical Testing		
Time (sec)	Displacement (mm)	Load (N)
0.0	0.0	0.00
15	0.5	73.74
30	1.0	153.92
45	1.5	240.87
60	2.0	330.90
75	2.5	421.36
90	3.0	513.32
105	3.5	607.75
120	4.0	702.36
135	4.5	797.25
150	5.0	892.23

Table 6.1 Aluminium Physical Testing Results.

The maximum load of the prosthetic for a displacement of 5mm was 892.23 N over a period of 150 seconds.

### 6.3 Aluminium FEA Analysis.

The model used in the FEA analysis, illustrated in Figure 6.2 was created from the redesigned prosthesis in Chapter 3, and two angle brackets modelled from those used in the physical test.

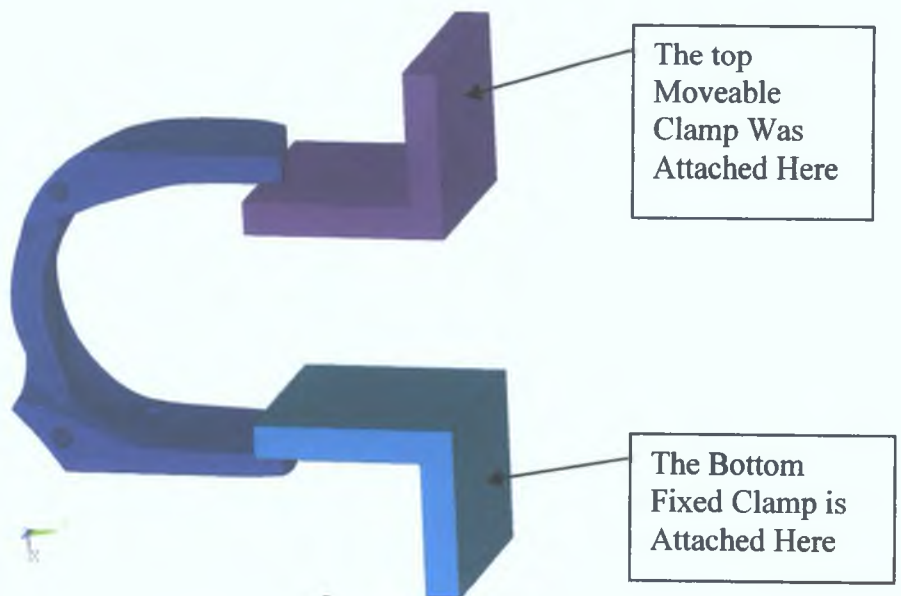


Figure 6.2 FEA Bending Test Model.

### 6.3.1 Mesh.

The prosthetic was meshed with ten node tetrahedral elements with an element edge length of 2.5mm. There were contact element pairs between the bottom bracket and the prosthetic, and the top bracket and the prosthetic to allow sliding and opening of the interfaces. The contact elements included a coefficient of friction of 0.2.

### 6.3.2 Material Properties.

The material of the first prosthetic model was aluminium with an elastic modulus of 71,000 MPa, and a Poisson's ratio of 0.3 [59]. To allow for the plastic properties, structural plastic multilinear properties for aluminium were used [70]. These values are listed in Table 6.2 below.

Strain (mm)	Stress (MPa)
0.001	71
0.007	496
0.0082	524
0.0094	538
0.012	552

Table 6.2 Aluminium Isotropic Multilinear Plastic Values.

The mild steel angle brackets used to grip the prosthesis were given a modulus of elasticity of 207,000 MPa, and a Poisson's ratio of 0.3 [59].

### 6.3.3 Boundary Conditions.

The model was constrained with zero displacements in all degrees of freedom on the two areas of the bottom bracket, which replicated where the bottom grip held the bottom bracket.

The top bracket was constrained on the front area with zero displacements in the Y and Z directions only, to prevent it from slipping off the prosthetic. It also had a displacement of 5mm in the positive X direction on the two areas that would be held by the top grip to simulate movement. The prosthetic was constrained on one node near the bottom grip, in all degrees of freedom to prevent the prosthetic from slipping off the brackets, as shown in Figure 6.3.



Figure 6.3. Loads and Degree of Freedom Constraints on the Prosthesis and Brackets.

#### 6.3.4 Load Step Options.

The model was solved in a non-linear static analysis. There were two stages in the analysis, the first stage had only the zero constraints applied and was to allow the contact element pairs to obtain an equilibrium position. The second loadstep had the 5mm displacement applied to the top bracket in the positive X direction over a period of 150 seconds. This axial displacement was incremented linearly over 10 substeps. No solution convergence problems were encountered.

The reaction forces from the analyses were only gathered from the nodes on the areas at the bracket where the 5mm displacements were applied. The results of the analysis are tabulated in Table 6.3 below.

<b>Aluminium FEA Analysis</b>		
<b>Time (sec)</b>	<b>Extension (mm)</b>	<b>Reaction Force (N)</b>
0.0	0.0	0.00
15	0.5	77.80
30	1.0	166.12
45	1.5	256.61
60	2.0	348.14
75	2.5	441.19
90	3.0	535.14
105	3.5	629.60
120	4.0	723.76
135	4.5	813.54
150	5.0	895.10

Table 6.3 Aluminium FEA Analysis.

The FEA results along with the results from the physical testing were plotted in Figure 6.4. Both results display similar linear trends, indicating the FEA analysis confirm the results obtained in the physical test.

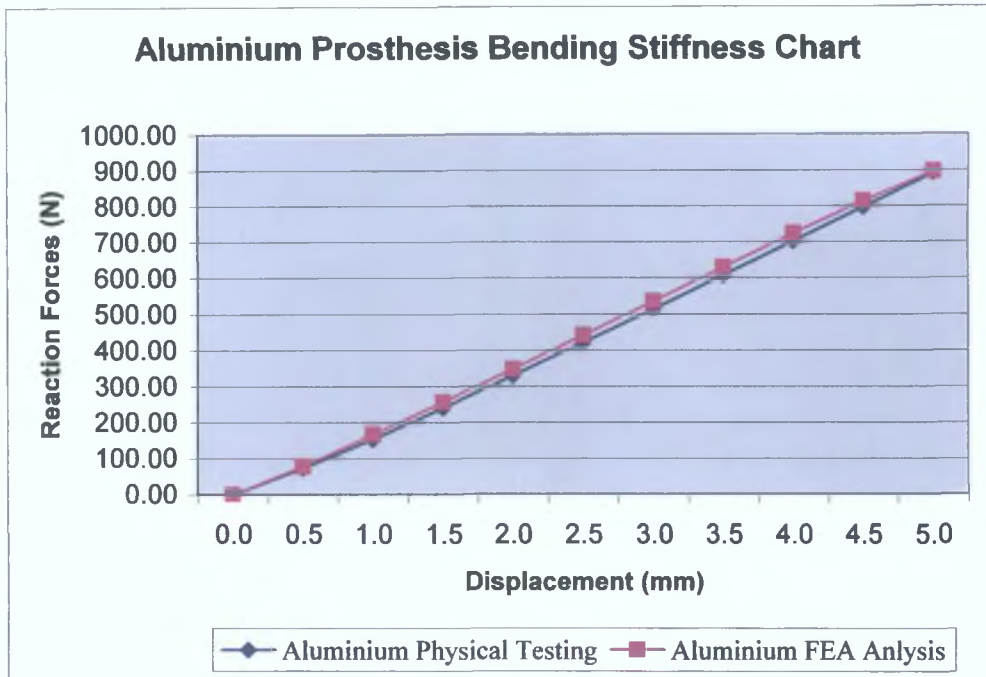


Figure 6.4 Aluminium Physical Testing And FEA Analysis.

#### 6.4 Titanium Physical Test.

The physical testing of the titanium prosthetic was conducted in the same way, and under the same loading conditions as the previous aluminium prosthetic detailed earlier in this chapter. The Instron machine measured the load exerted (N) and the displacements (mm) as the prosthetic was deformed. The data was saved as a .raw file, and opened in Microsoft Excel. The resulting data of this titanium test are listed in Table 6.4 below.

<b>Titanium Physical Testing</b>		
<b>Time (sec)</b>	<b>Displacement (mm)</b>	<b>Load (N)</b>
0.00	0.00	0
15.00	0.50	78.27
30.00	1.00	158.53
45.00	1.50	241.13
60.00	2.00	325.22
75.00	2.50	411.11
90.00	3.00	498.36
105.00	3.50	585.01
120.00	4.00	672.43
135.00	4.50	760.14
150.00	5.00	848.67

Table 6.4 Titanium Physical Testing Results.

The maximum load of the titanium prosthetic for a displacement of 5mm was 848.67 N over a period of 150 seconds.

## 6.5 Titanium FEA Analysis.

The model used in the titanium FEA analysis, shown in Figure 6 2 above, was again made up from the redesigned prosthetic from Chapter 3, and two angle brackets modelled from those used in the physical tests

### 6.5.1 Mesh.

As with the aluminium prosthetic, the titanium prosthetic was meshed with ten node tetrahedral elements with an element edge length of 2.5mm. There were contact elements pairs between the bottom bracket and the prosthetic, and the top bracket and the prosthetic to allow sliding and opening of the interfaces, the contact elements included a coefficient of friction of 0.2.

### 6.5.2 Material Properties.

The material of the second prosthetic model was titanium with an elastic modulus of 144,000 MPa, and a Poisson's ratio of 0.3 [8,19,72]. To allow for the plastic properties of the titanium, structural plastic multilinear properties were used. As discussed in Chapter 3, there was no information on the plastic properties of titanium in the literature, so the author had to make an educated guess as to what they might be. These suggested values are listed in Table 6.5 below

Strain (mm)	Stress (MPa)
0.001	114
0.002	225
0.003	337
0.004	360
0.005	375
0.025	450
0.06	532
0.1	585
0.15	630
0.2	652
0.25	673
0.275	675

Table 6.5 Titanium Isotropic Multilinear Plastic Values

Once again, the mild steel angle brackets used to grip the prosthesis were given a modulus of elasticity of 207,000MPa, and a Poisson's ratio of 0.3 [59]

### 6.5.3 Boundary Conditions.

The model was constrained under the same conditions described in the aluminium FEA boundary conditions

### 6.5.4 Load Step Options.

The model was solved in the same non-linear static analysis described in the previous aluminium analysis

The reaction forces from the analysis were gathered from the nodes on the areas of the top bracket where the 5mm displacements were applied. The results of the analysis as seen in Table 6.6 listed a maximum reaction force of 867.49 N

<b>Titanium FEA Analysis</b>		
<b>Time (sec)</b>	<b>Displacement (mm)</b>	<b>Reaction Force (N)</b>
0 00	0 00	0.00
15 00	0 50	130.53
30 00	1 00	270.18
45 00	1 50	412.29
60 00	2 00	549.46
75 00	2 50	656.33
90 00	3 00	729.77
105 00	3 50	780.07
120 00	4 00	816.19
135 00	4 50	844.15
150 00	5 00	867.49

Table 6.6 Titanium FEA Analysis

This result is relatively close to the maximum load from the Instron physical test 848 67 N seen in Table 6.4 above.

When all the titanium reaction forces were plotted against the displacements at 0.5 mm intervals, a different picture emerges, as illustrated in Figure 6.5



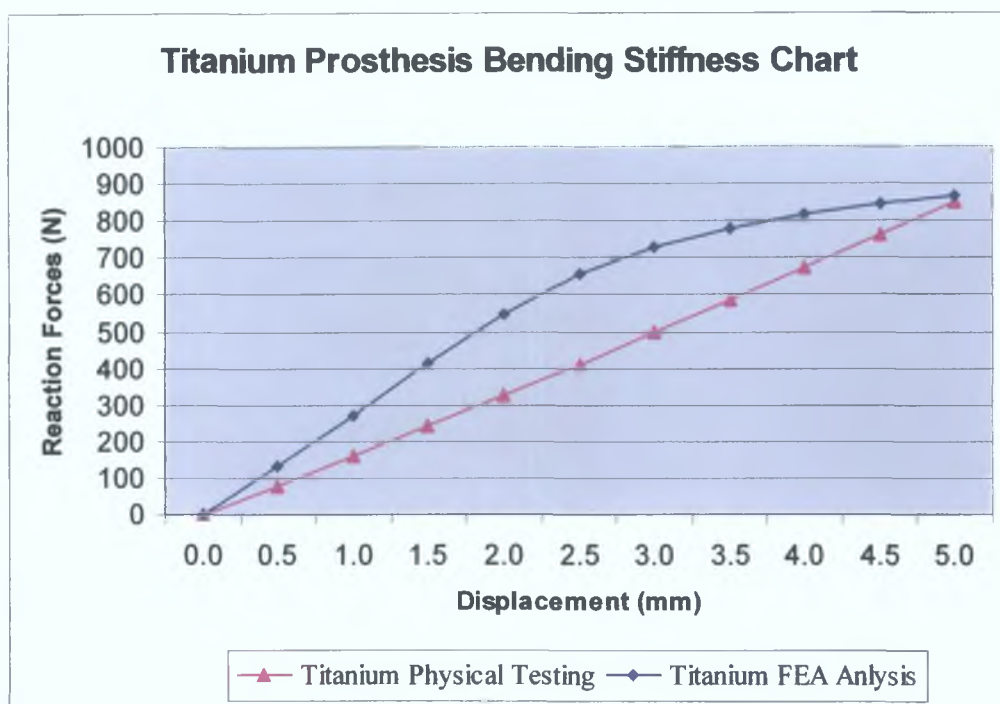


Figure 6.5 Titanium Physical Testing and FEA Analysis.

## 6.6 Conclusions.

Unlike the aluminium analysis, the titanium FEA analysis results do not confirm the physical test results. The only differences between the aluminium and titanium analyses were the elastic modulus, and the multilinear properties. The results of the aluminium bending test, and FEA analysis are relatively similar, therefore it may be concluded that they have the correct multilinear plastic properties. This indicates that there were significant errors in the multilinear properties for titanium that were suggested in Chapter 3. Given that there were no values for titanium multilinear properties in the literature, the author had no choice but to speculate as to what they might be.

When the stress strain graphs for the aluminium and titanium used in this project were plotted against each other, as illustrated in Figure 6.6, it became apparent where the problem lies. The titanium properties initially in the elastic phase appear correct, but the yield point is too low, driving the titanium into the plastic phase much too early, thus generating inaccurate reaction forces.

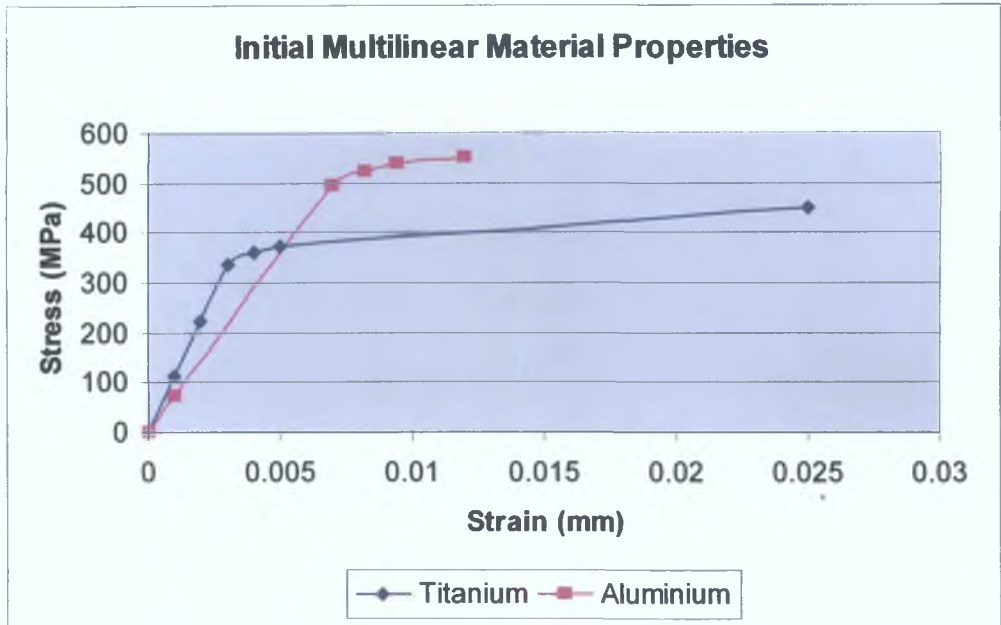


Figure 6.6 Aluminium and Titanium Multilinear Properties.

There was no information on the multilinear plastic properties of titanium in the literature, so the author had to make an educated guess as to what the correct values for the titanium multilinear properties might be, based on Figures 6.5 and 6.6, and given an ultimate tensile strength of 900MPa. These figures are purely speculation and therefore cannot be trusted. The revised values are plotted in Figure 6.7 below

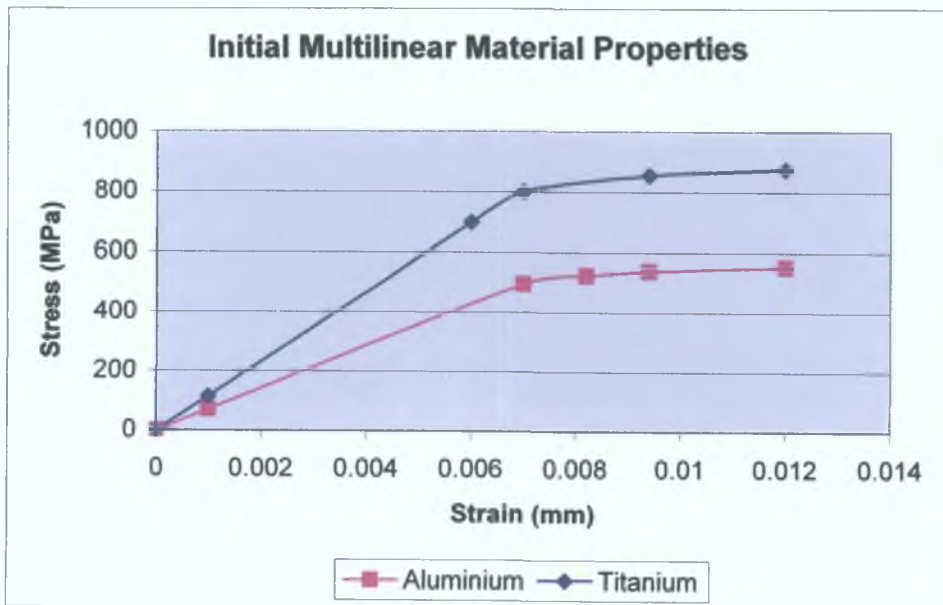


Figure 6.7 Revised Titanium Multilinear Properties.

It was considered a futile exercise to reassess all the FEA analyses made previously with these new properties, as only the correct multilinear properties would be acceptable for an accurate analysis.

After consideration of the (RIF) project, values for the multilinear properties of titanium were found. Figure 6.8 details these values, plotted with the values for aluminium, and the proposed values for titanium from Figure 6.7 above.

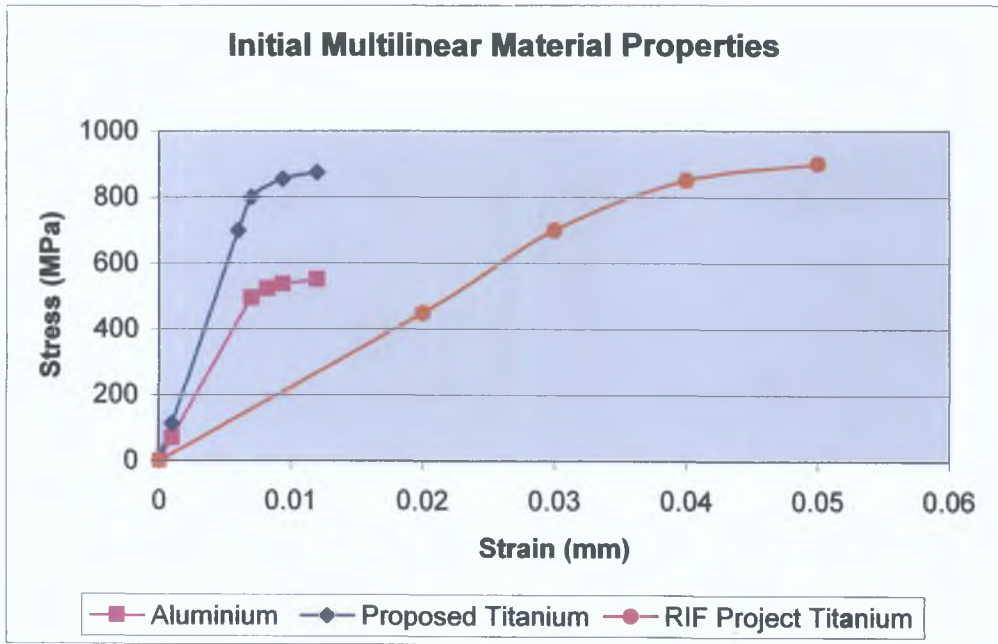


Figure 6.8 Aluminium, Proposed Titanium, and RIF Titanium Material Properties.

Assuming the aluminium material properties are correct, then the RIF project titanium has a greater elastic phase than aluminium. In reality this is not true, and for this reason the RIF project titanium multilinear properties were dismissed as erroneous.

## Chapter 7

### Animation

- 7.1 Introduction.
- 7.2 Sectioning the Prosthesis.
- 7.3 The Prosthesis Moving Into Position
- 7.4 The Screws Moving Into Position
- 7.5 Presentation

#### **7.1 Introduction.**

The objective of this animation was to develop a resource to provide a comprehensive 3D animated video of the surgical procedure involved in the replacement of the damaged maxilla. Computer generated animated graphics can help clinicians and operating room personnel learn the detailed progression from sectioning the maxilla to inserting, positioning and attaching the prosthesis replacement. The animated video is also helpful to prospective patients as it provides information on what to expect when they undergo this particular procedure.

The animation virtually removed the tumoured portion of the maxilla, animated the insertion path of the prosthesis, and visualised the placement and tightening of the restraining screws [18]. It was broken in to three separate animations so that if an adjustment had to be made, the whole animation would not have to be rendered again. The animation was prepared and powered by the Bryce 5.5 software program. The skull, prosthesis, screws, cutting tool, and background were rendered with colours obtained from the Bryce material library. The simple green background was chosen so as not to distract from the animation in the foreground.

## 7.2 Sectioning the Prosthesis.

For the first part of the animation sequence only the skull, cutting tool and the prosthesis (hidden), were needed, they were imported directly into the Bryce animation software from proEngineer .prt files as seen in Figure 7.1.

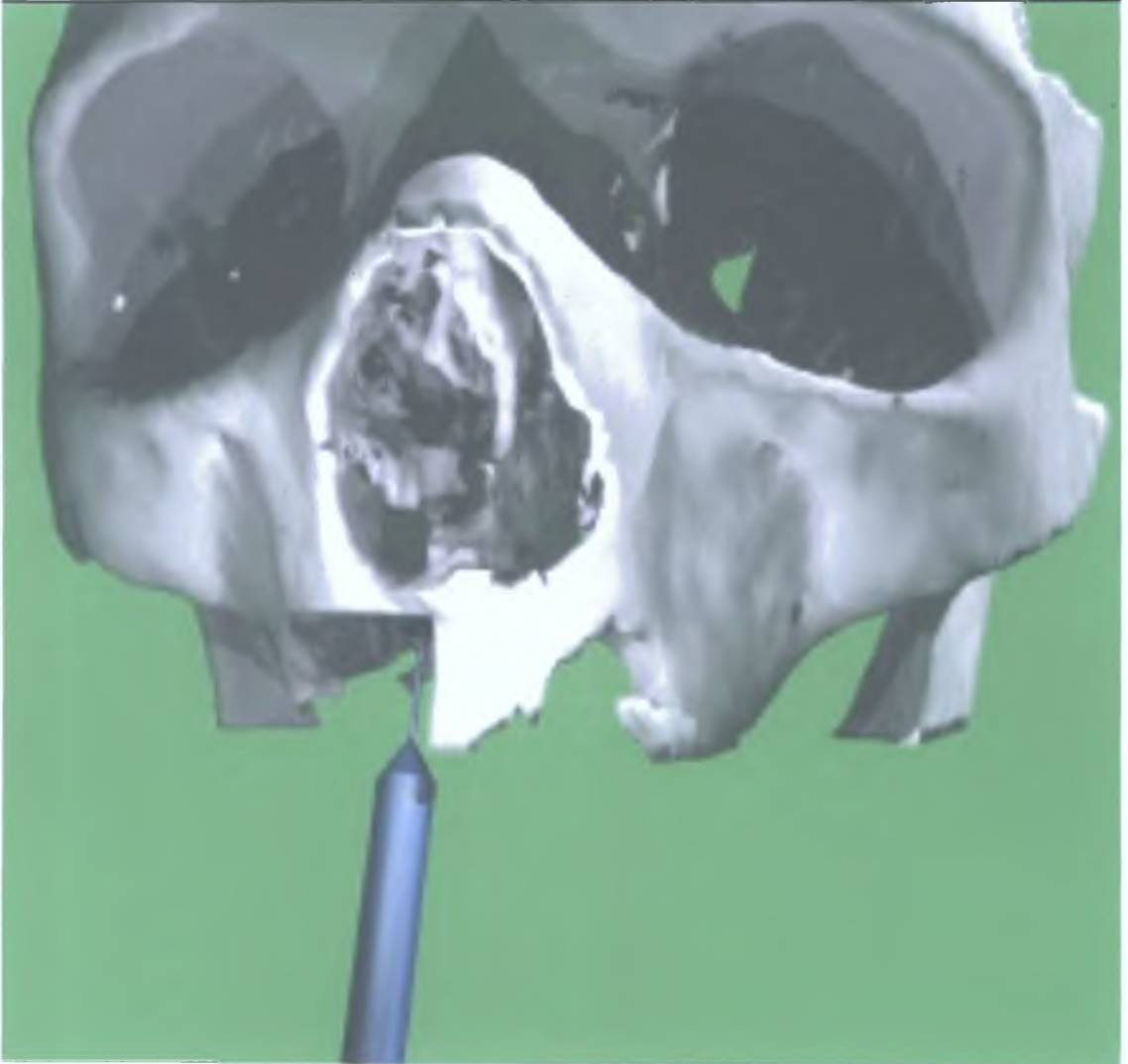


Figure 7.1 First Rendered Animation Sequence. Sectioning the Skull.

The top of the prosthesis was located at a position predefined by the surgeon as where the maxilla bone would be sectioned from the skull. The prosthesis was given a negative attribute, which means that while it can still be manipulated it would not be part of the rendered animation. Its purpose was to provide the location for the cutting tool. The cutting tool was placed an arbitrary distance away from the skull at the zero keyframe<sup>15</sup>, as shown in Figure 7.2.

---

<sup>15</sup> Zero Keyframe: The start of an animation.



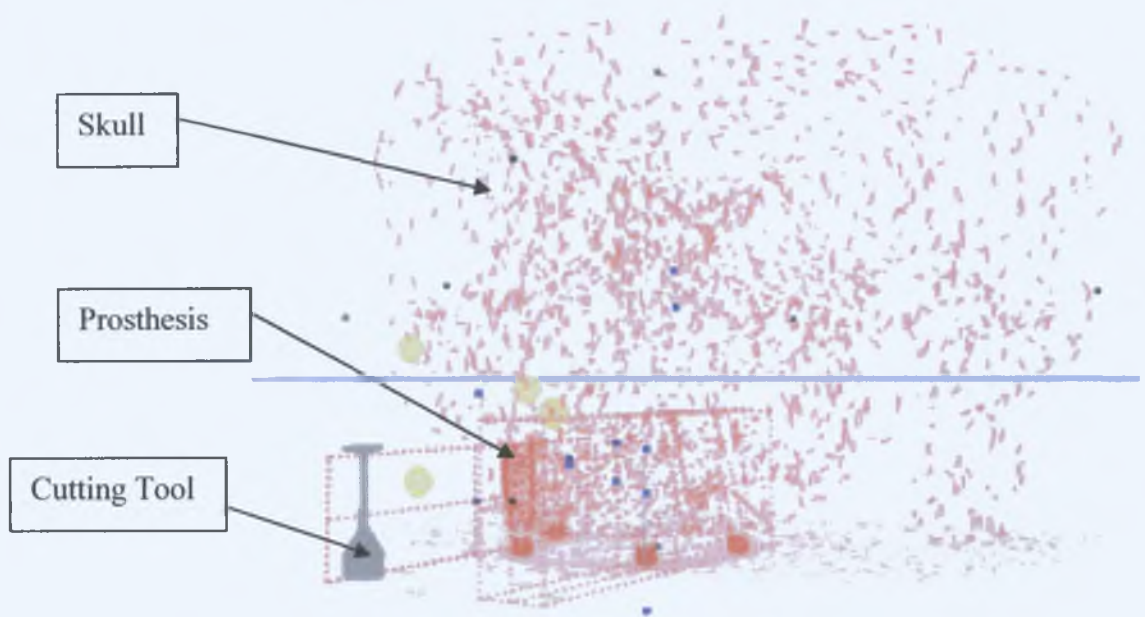


Figure 7.2. Zero Keyframe Location.

The camera was grouped with the cutting tool, so that as the cutting tool moved, the camera focused on it. There were four stages in sectioning the prosthesis.

#### Stage One.

The cutting tool was moved to the left hand side of the skull at the top of the negative prosthesis and given a second keyframe<sup>16</sup> time of 5 seconds. This is detailed in Figure 7.3.

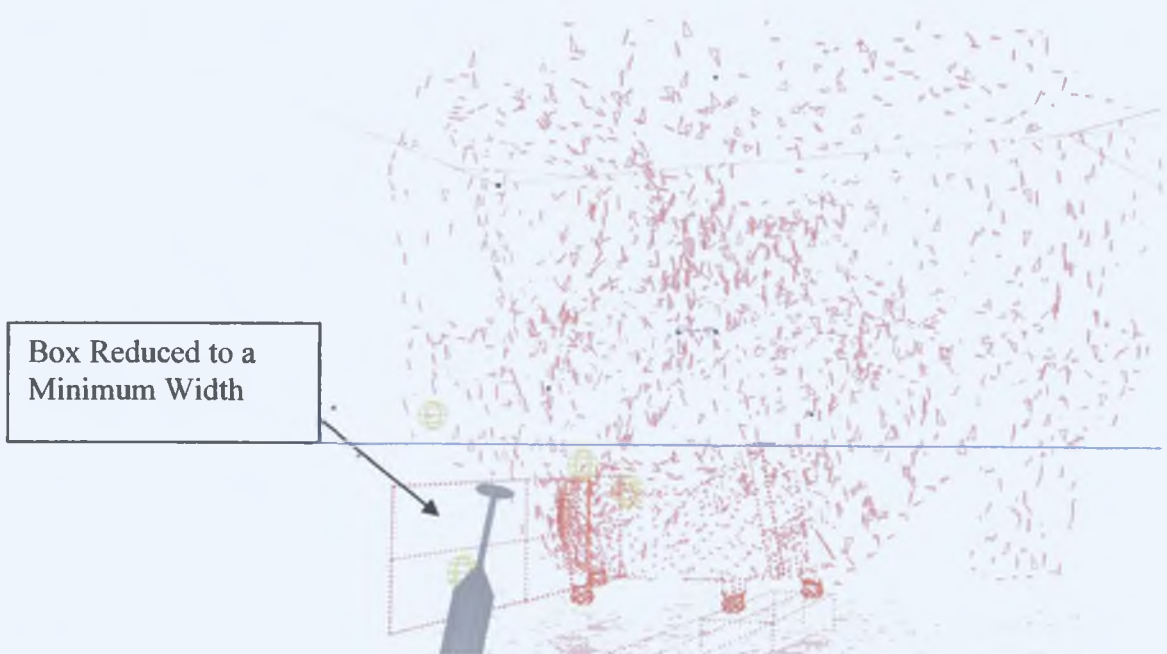


Figure 7.3. Second Keyframe Location.

<sup>16</sup> Keyframe: A snapshot of objects at key moments during a sequence of movement or change.



### Stage Two.

A box with its width reduced to a minimum was created on the left hand side of the skull as seen Figure 7.3, in the volume of the negative prosthesis. This box was grouped with the skull. The skull was given a positive attribute, and the box was given a negative attribute. The cutting tool was grouped with the right hand side of the box and given a neutral attribute. The box was elongated to the right hand side of the skull over a period of fifteen seconds, at which point a third keyframe was created, as seen in Figure 7.4.

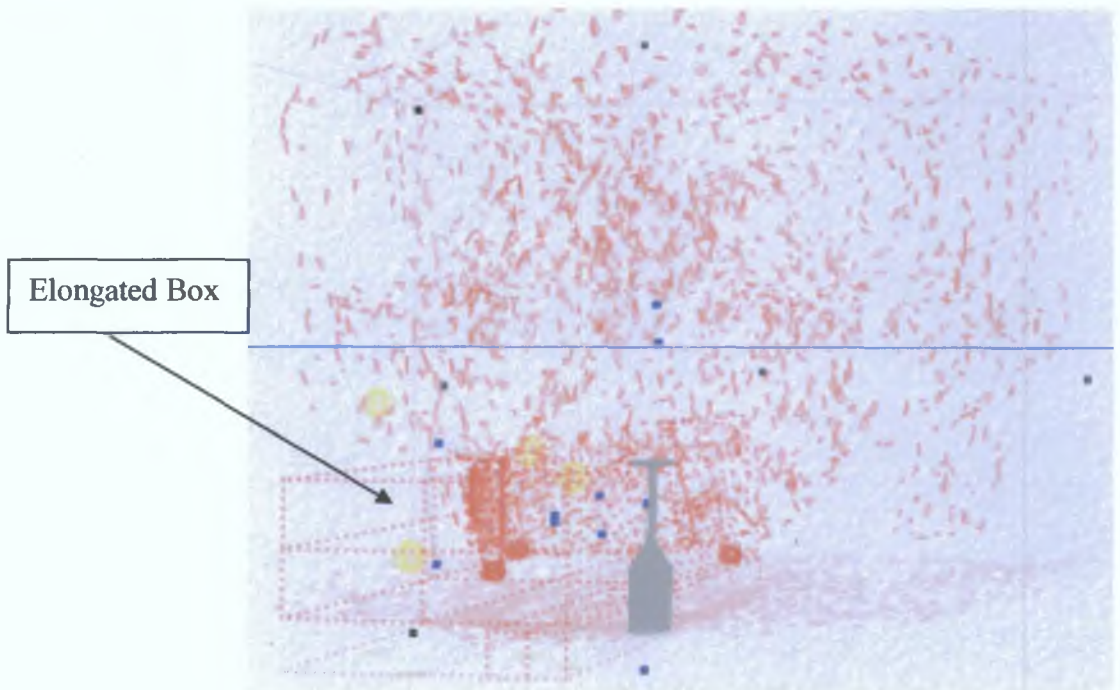


Figure 7.4. Third Keyframe Location.

As the box was widened and the (neutral) cutting tool followed the edge of the (negative) box, the part of the skull enveloped by the box disappeared, giving the illusion of a cutting operation.

### Stage Three.

At the third keyframe where the cutting tool reached the right hand side of the skull, a second box was created. The cutting tool was ungrouped from the first box, and grouped with the top of the second box. The skull was ungrouped from the first box, and grouped with the second box, with the skull having a positive attribute and the second box having a negative attribute. The second box was elongated in the

vertical direction to the top of the negative prosthesis, over a period of five seconds. At this point the fourth keyframe was created, as illustrated in Figure 7.5.

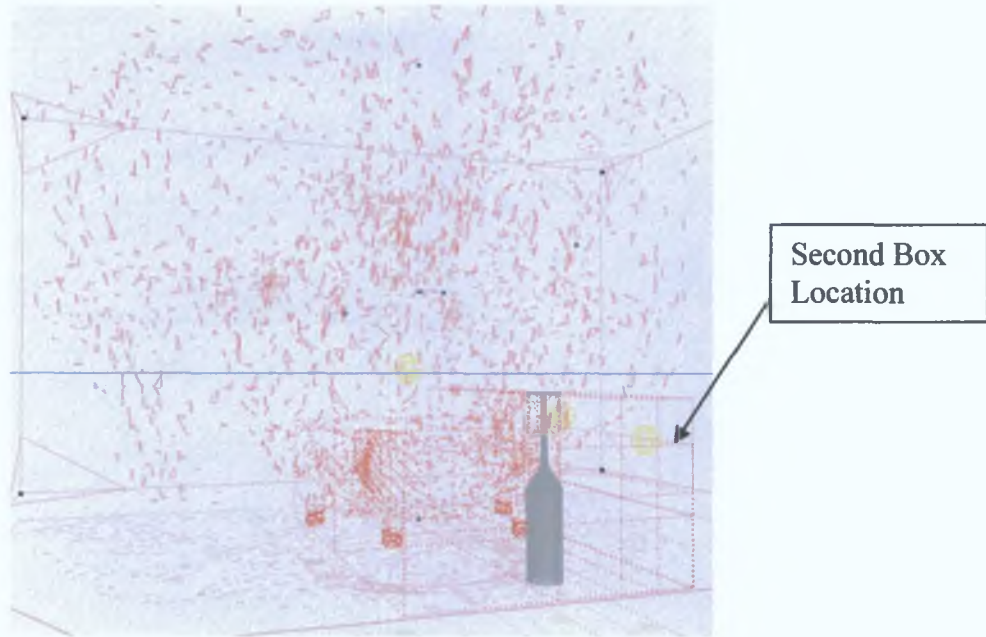


Figure 7.5. Fourth Keyframe Location.

As the second box was elongated and the (neutral) cutting tool followed the top of the second (negative) box, the volume of the skull enveloped by this box disappeared. This operation gave the appearance of the skull after sectioning.

#### Stage Four.

From this Fourth keyframe at 25 seconds, the cutting tool was ungrouped from the second box and moved an arbitrary distance away from the skull at which point the last keyframe in this sequence was created at 30 seconds, as shown in Figure 7.6.

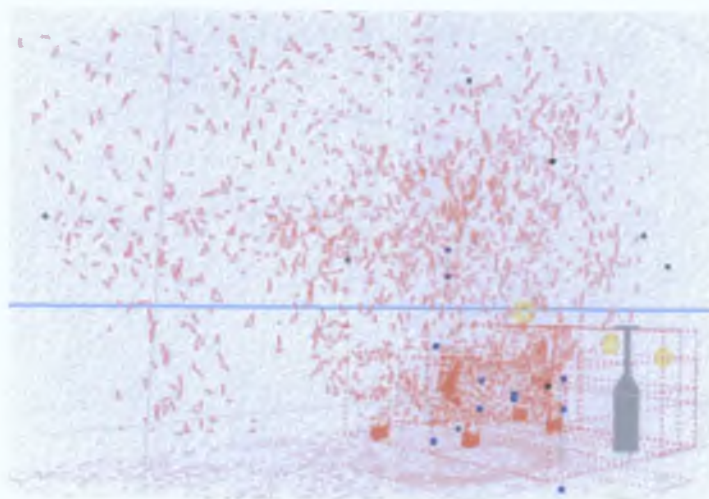


Figure 7.6. Fifth Keyframe Location.

This animation was saved as a video .avi file, and a new file was opened to animate the prosthesis moving into position.

### 7.3 The Prosthesis Moving Into Position.

For the second part of the animation sequence only the skull and the prosthesis were needed. The first animation section was copied to a new file and the cutting tool, no longer needed, was hidden, as shown in Figure 7.7.

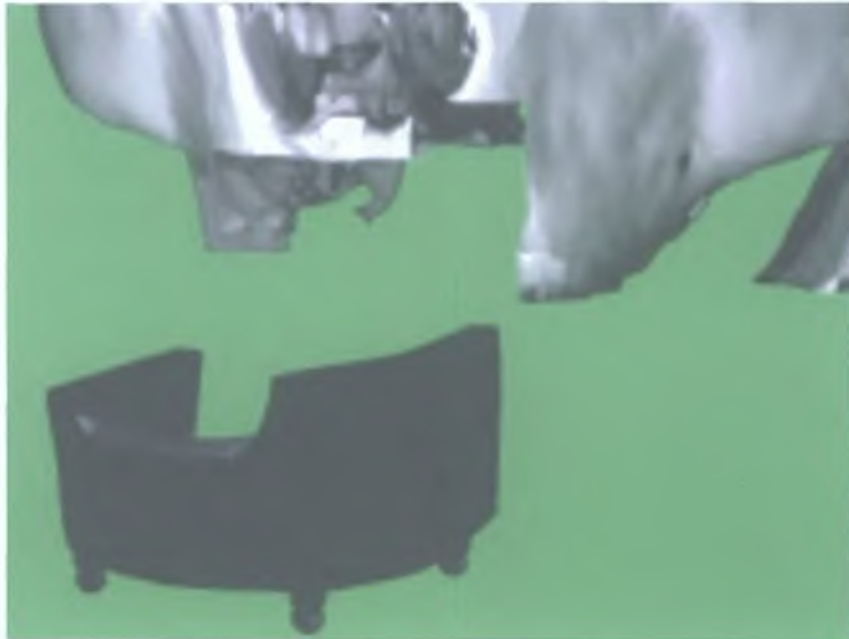


Figure 7.7. Second Animation Sequence. Locating the Prosthesis.

The negative prosthesis was duplicated, and this new prosthesis was displaced an arbitrary distance from the skull. This position was designated as the zero keyframe for the second animation. The new prosthesis was given a neutral attribute meaning it could be seen in the rendered animation. The absolute coordinates of the first (negative) prosthesis were noted and given to the second (neutral) prosthesis. A keyframe was given a time of ten seconds, during this period the (neutral) prosthesis moved from its arbitrary position to the exact (negative) prosthesis position predefined by the surgeon.

The camera view was linked to the prosthesis so that it would focus on the prosthesis as it moved. The camera view started at the front of the skull at the zero keyframe, and slowly panned to the right at the ten-second keyframe.

When this sequence was rendered the software produced an animation of the prosthesis moving from an arbitrary position to the position predefined by the



surgeon, over a period of ten seconds, as the camera view slowly panned around the skull. The prosthesis was then locked in this position.

The animation was saved as a .avi file and a new file was opened to animate the screws moving into position.

#### 7.4 The Screws Moving Into Position.

For the third part of the animation sequence the sectioned skull, prosthesis and screws were needed, as seen in Figure 7.8.

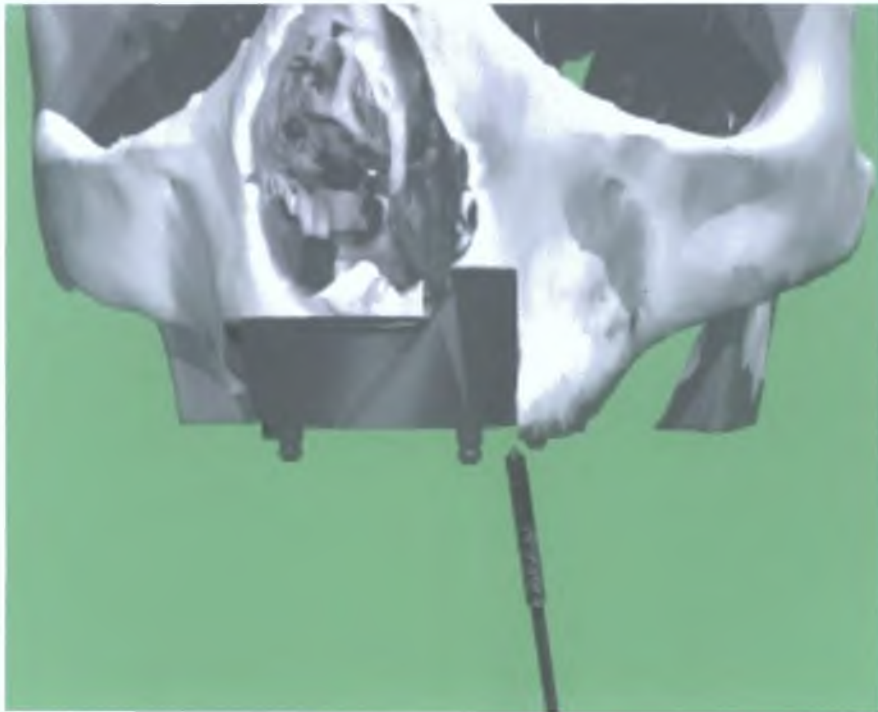


Figure 7.8. Third Animation Sequence. Locating the Screws.

The second animation sequence containing the sectioned skull and the prosthesis was simply copied to a new file, the screws on the other hand proved a challenge in modelling and manoeuvring.

The Bryce software is not a good modelling package, the author found it difficult to model and orientate the screws in the correct hole locations, for this reason a screw was modelled in proEngineer and saved as a .prt file. An assembly (.asm) file was opened in proEngineer and the prosthesis and screw .prt files were imported into it. The screw was duplicated three times to produce four screws; these screws were manoeuvred into the holes in the prosthesis to their final positions. When the author was satisfied with the final location of all the screws in the prosthesis, the assembly

was exported as an object file. An object file was chosen because it allows an assembly to be exported as separate parts. The object file was imported into the Bryce file containing a copy of the second animation.

There were now three prostheses in this animation the (negative) prosthesis from the first animation sequence, the (neutral) prosthesis from the second animation sequence, and the prosthesis imported with the screws as an object file. The neutral prosthesis from the second animation section was not needed, and was deleted.

The imported prosthesis and screws were grouped, so that they would move together. The absolute coordinates from the negative prosthesis were noted and applied to the grouped prosthesis and screws. This located the prosthesis and screws in their final position and it was given a keyframe of 20 seconds. The screws and prosthesis were ungrouped to allow them to move separately. One screw was moved out of the prosthesis to an arbitrary position and a keyframe was set at 15 seconds, a second screw was moved out of the prosthesis, and a keyframe was set at 10 seconds. The third screw was moved out of the prosthesis and a keyframe was set at 5 seconds, and finally the last screw was moved out of the prosthesis and set as the zero keyframe. This zero keyframe is seen in Figure 7.9.

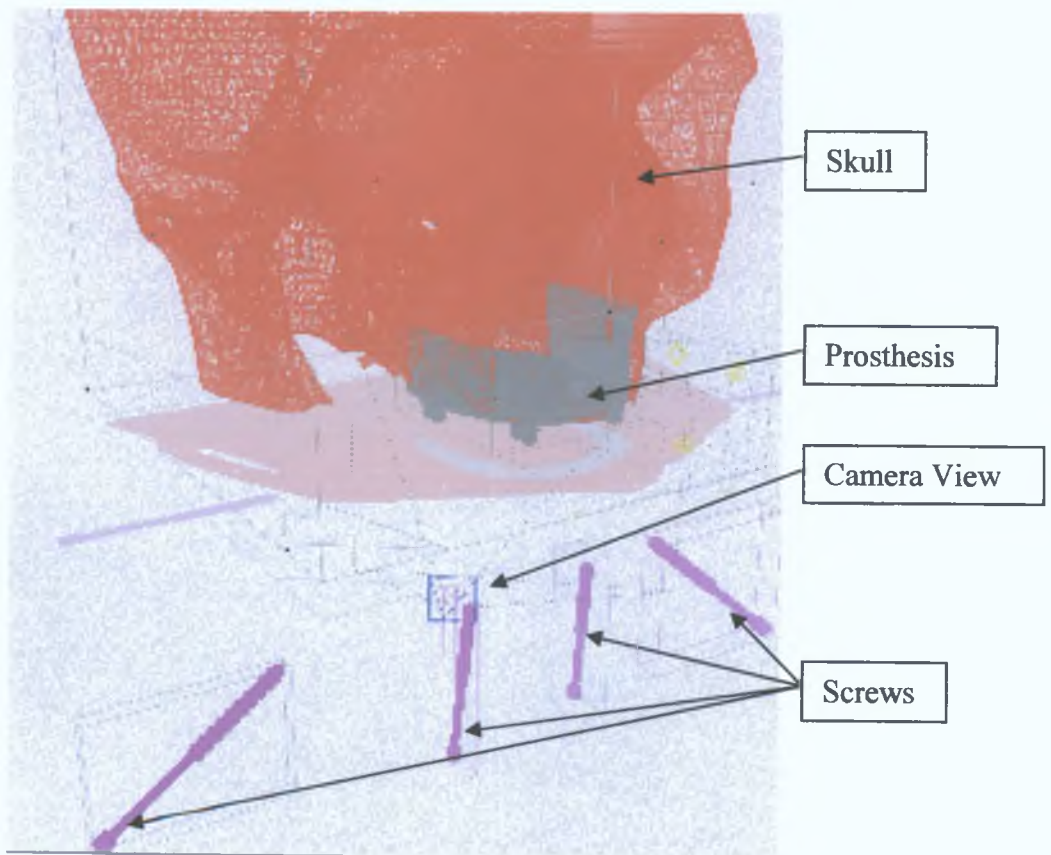


Figure 7.9. Third Animation Zero Keyframe.

These keyframes resulted in an animation where the four screws moved into their final position in the prosthesis, one at a time over a period of 20 seconds.

The camera was also moving along a path to give a good view of each screw as it moved. The camera was linked to each screw as it moved so that at all times it was focused on each screw directly, even though it was also moving on its own path.

## **7.5 Presentation.**

The Proshow gold presentation software was used to organise the animations. To start the presentation a black screen was used, from this black screen an image of the opening credits appeared, the credits faded to black again, and from this second black screen, the opening animation with the cutting tool appeared and ran for 30 seconds. This animation blended into the second animation, the second animation played for 10 seconds and blended into the third animation, the third animation played for 20 seconds and faded to black. From this black screen, the closing credits appeared before fading to black again to close the presentation. Background music was also included in the presentation to give it a sense of continuity. The whole presentation lasted for 95 seconds.

When the author was satisfied with the final presentation an executable .exe file was created. This was a simple PowerPoint slide showing a picture of the skull and prosthesis displayed at the start of the presentation, when the picture is clicked on the presentation begins.



## Chapter 8

### Discussion and Conclusions

- 8 1 Main Findings of the Research.
  - 8 1.1 Finite Element Analysis
  - 8.1.2 Machining.
  - 8 1.3 Coordinate Measuring Machine
  - 8.1 4 Physical Testing.
  - 8.1.5 Animation
  - 8.1 6 limitations
- 8 2 Conclusions
- 8 3 Recommendations for Future Study

#### 8.1 Main Findings of the Research.

This chapter concludes the thesis. It consists of the most important findings and conclusions revealed from the present study. It also suggests a list of related topics for future study in the maxillo-facial prosthesis research area.

The present research was concerned with taking the existing successful RIF prosthetic (Figure 3 2), redesigning it, and investigating an alternative manufacturing process. The redesign was achieved by integrating two main modifications.

1. Incorporating the over-denture abutments directly into the prosthetic.
2. Removing the restraining wings by the addition of screws, which affix the implant to the dense material of the jawbone.

These modifications created the possibility of using CNC machining techniques to manufacture the implant (rather than investment casting or selective laser sintering of titanium powder as used in the RIF project)

In addition to these main objectives the research was also concerned with

- Developing a computer based finite element modelling methodology for the design and optimisation of the new prosthetic by means of a static stress analysis, to verify that the maximum stress achieved with the average bite force is within acceptable limits.
- Perfecting reverse engineering and quality metrics with equipment such as a Co-ordinate Measuring Machine (CMM), which can be applied to the manufactured prosthetic.
- Performing a mechanical test on the manufactured prosthetic and comparing the results with those obtained on a finite element analysis.
- Developing 3D animated videos, which will assist the clinician in preparation for surgery. The animation was to virtually remove the tumoured portion of the maxilla, animate the insertion path of the prosthetic, and visualise the placement and tightening of the restraining screws.

### 8.1.1 Finite Element Analysis.

The principle objective, to improve the design of the current maxillo-facial implant, by incorporating the over-denture abutments directly into the implant and removing the restraining wings by the addition of holes, through which screws affix the implant to the dense material of the jawbone, was completed successfully in the ANSYS FEA software. These modifications provided a means for minimally invasive oral surgery, removing the necessity for mutilation of the face during the operation.

### 8.1.2 Machining.

It was not discovered about the Hallgren et al [39] and Wieland et al [71] assertion that a wavelength range of 0.05 - 0.5mm was the best surface topography for osseointegration, until after the vendor had machined their prosthetics with a scallop height of 0.001mm which was the reason that it has a very polished surface finish. However, the GMIT prosthetic displays the appropriate surface finish with a scallop height of 0.225mm.

The cost involved in CNC milling each customised prosthetic on an ongoing basis is approximately €2,000 each. This represents 10% of the total costs of the surgical procedure. Comparing these figures to the RIF project cost of € 6,000 to rapid prototype each piece [75], the CNC milling method suggested in this research, results in a saving of approximately € 4,000 per piece.

### **8.1.3 Coordinate Measuring Machine.**

The prosthetic produced by the machining vendor was analysed on a CMM to verify the dimensional accuracy of the model in order to check if its specifications and manufacturing tolerances had been exceeded. It became clear that the drilling operations carried out on the manual milling machine as described in Chapter 4 did not have as tight a tolerance as the other machining operations carried out on the micron CNC machining centre, as could be expected

It was discovered that the absolute measurement system used in this project had no difficulty in choosing points to measure whereas the relative type measurement system used in the original prosthetic analysis had difficulty in identifying and locating the landmarks used.

### **8.1.4 Physical Testing.**

Aluminium and Titanium bending tests were performed on the prosthetic models and compared with the FEA results to confirm the multilinear plastic properties used in the analyses. The aluminium multilinear plastic properties were confirmed with very similar results, as documented. However, with regard to the titanium, there was no information on the multilinear plastic properties in the literature, so the author had to make an educated guess as to what they might be. The bending test proved that this guess was inaccurate

### **8.1.5 Animation.**

The animation of the surgical procedure proved to be an invaluable resource in that it could demonstrate to the surgeon, operating room personnel, and the patient what to expect with this particular procedure.

The process developed in this and the preceding RIF project can be summarised as follows:

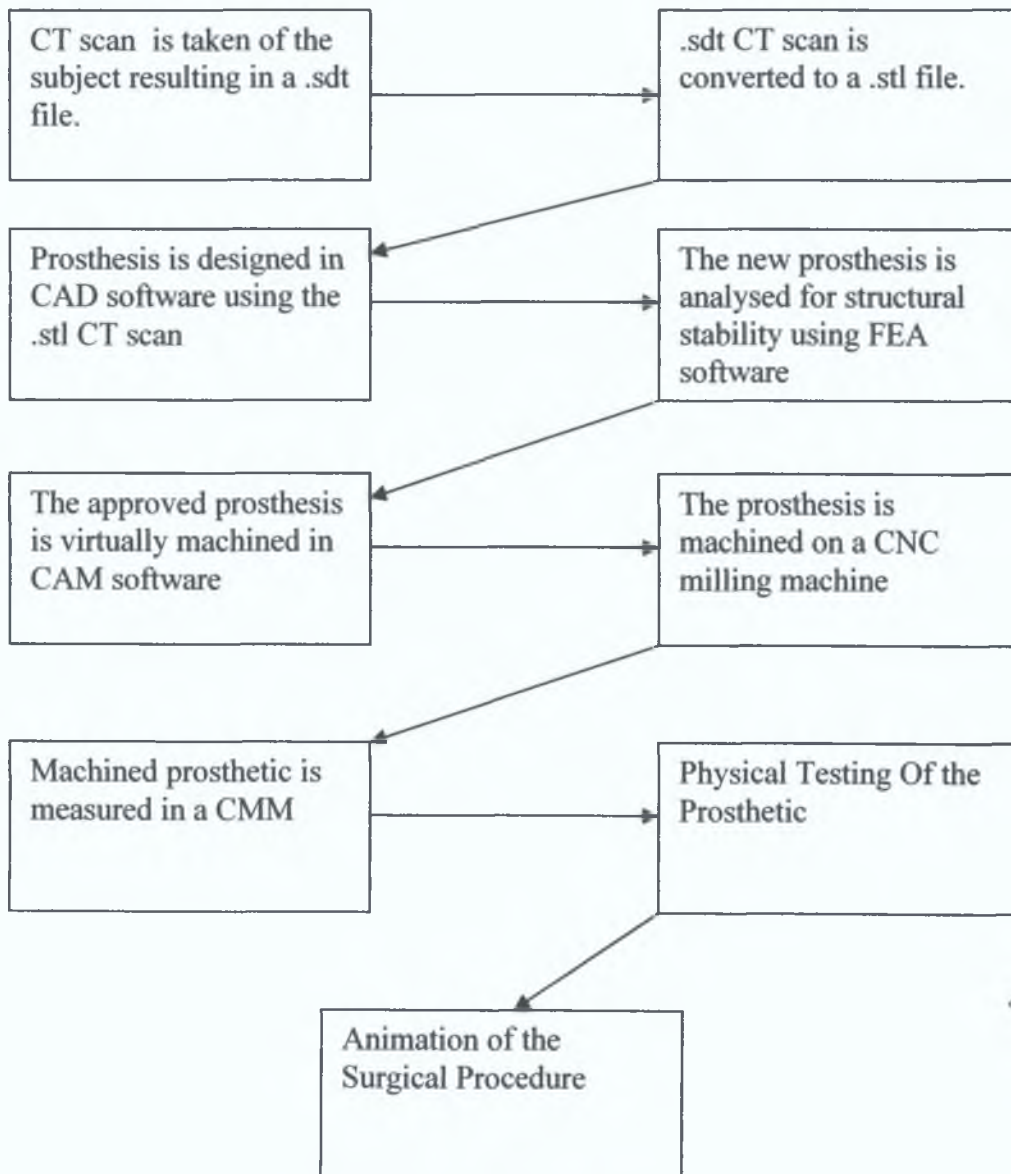


Figure 8.1 Flow Chart of the Prosthesis Manufacturing Process.

The provided CT scans of the patient are converted to .stl files using scan conversion software such as MIMICS CT. The .stl files are exported to a solid modelling package such as ProEngineer where the implant is designed on the virtual CAD representation of the skull, and is a precise custom fit. The finished design is exported to the FEA software, where it is analysed for structural stability. A program to machine the part is developed in the CAM software, and exported to the CNC milling

machine via the DNC. A titanium block is machined on the palletised 3 axis CNC milling machine, and finally it is checked for dimensional accuracy on a CMM.

### 8.1.6 Limitations.

During the course of this study the author found a new type of titanium foam which is anticipated to be a promising implant material for bone tissue engineering applications in the future due to its excellent biomechanical properties and bioactivity. However the project supervisors deemed it too late to investigate this material, so the project was limited to the standard Ti6Al4V.

The student version of the finite element analysis program used in the project was limited to 32,000 nodes. More accurate results could be generated if the more advanced professional version were to be used.

The process described in this thesis is limited for use in adults with fully formed maxilla bones. If the prosthesis was to be fitted to a child there would need to be readjustments made at several stages of the child's growth.

## 8.2 Conclusions.

- The maximum micromotion at the bone screw interface was  $26 \cdot 10^{-6}$ mm, well below the maximum critical threshold suggested by Sahin [11] of between  $50 \cdot 10^{-6}$  and  $150 \cdot 10^{-6}$ mm. This indicates that the 3mm diameter holes that the screws were designed to fit are large enough to prevent fibrous encapsulation at the prosthesis bone interface. The preload on the bolt produced a maximum micromotion of  $22.6 \cdot 10^{-6}$ mm, which again is well below Sahin's maximum critical threshold for micromotion.

- It has been proven in the research that it is possible to machine the prosthetic on a 3 axis milling machine. Although, the dimensional quality will be of a very poor standard due to the fact that the coordinate system needs to be reset for each of the eight operations, introducing a progressive error at each stage.

A palletising system is the minimum requirement if it is proposed to produce the prosthetic using a 3-axis milling machine. However, it would probably be necessary, and definitely desirable to have a 5-axis machine to manufacture the part.

- In comparison with the originally designed rapid prototyping prosthetic, listing a mean deviation of +1.83mm, the CMM results for the new CNC milled prosthetic established a mean deviation of -0.02mm. The original prosthetic was stated to be within the tolerance of those in the literature, and was therefore assessed as feasible engineering and suitable for surgery. The milled prosthetic with its even tighter mean deviation is well within the tolerance in the literature. This factor alone suggests that the prosthetic should be milled rather than rapid prototyped.

- The results achieved in this, and in conjunction with the previous RIF project, support the purpose of the research. Namely to prove the viability of the idea that by using an integrated approach with compatibility between formats, CT/MRI scans, FEA, CAD/CAM, CNC milling techniques, and CMM, realistic modelling and simulation of the body structures and the design and manufacture of the prosthetic can be easily achieved.

### **8.3 Recommendations for Future Study.**

The knowledge and experience gained from this research study has led to the following recommendations for improvements and future study.

1. The model used in the FEA analyses was assumed to be homogenous and isotropic and to possess linear elasticity. As only static stress analyses were performed, the simulated stress distribution patterns may be different to the real world application, depending on the change of the input parameters of the models used. Thus, the inherent limitations of the finite element analysis method should be considered [19]. In the current studies, only vertical loads were considered. When applying the FEA method to medical prosthesis, it is important to consider not only the axial and horizontal forces but also the combined axial and horizontal loads, which would represent more realistic occlusal directions [19].

2. There were 24,760 nodes used in the screw-preload analysis, which were mostly concentrated around the threads, however the results indicated that the elements around the thread area needed further refinement especially around the first thread. Since the



particular version of ANSYS used in this study was limited to 32,000 nodes, a more advanced version would be needed to achieve this

3. Ti6Al4V has recently been reported as toxic to the human body [31] Alternative materials for the prosthetic could be investigated such as vanadium and aluminum-free titanium. A new Ti-15Zr-4Nb-4Ta alloy with its excellent mechanical properties, corrosion resistance and corrosion fatigue properties and biocompatibility can be expected to become a new alloy for medical applications in the future Titanium (Ti), Zirconium (Zr), Niobium (Nb), and Tantalum (Ta) exhibit excellent biocompatibility [3].

4. Titanium foam is anticipated to be a promising implant material for bone tissue engineering applications in the future due to its excellent biomechanical properties and bioactivity, but further research into the area is needed [7,35].

5 The carbide tools used to mill the titanium prosthetic prototype were effective but the machining time was two days. It is recommended that any future work should use Binderless Cubic Boron Nitride (BCBN) Cutting Tools, which are more expensive but will cut titanium more efficiently

6 The new prosthetic was designed in the Ansys FEA software and exported as an iges file to ProEngineer to write the machining program When the .iges file was opened in ProEngineer it was not recognised as a volume because some of the surfaces were distorted. These surfaces had to be corrected before any manipulation of the model could take place To overcome these .iges file problems in any future work, the optimised design should be designed in ProEngineer and exported to Ansys in the compatible proEngineer prt file format

7. The conclusions drawn in Chapter's 3, and 6 highlight the need for further research into the physical testing of the titanium and denture material to determine their multilinear plastic properties, as the values proposed in the RIF project were evaluated as erroneous

8. The static analysis results described in this study were low enough that an infinite life of the prosthetic is suggested therefore a fatigue analysis was deemed unnecessary. However, for a more rounded and definitive analysis, the author recommends that this fatigue analysis should be generated at some stage.

## References

- [1.] Hausamen, J.E. (February 2001). "*The scientific development of maxillo-facial surgery in the 20th century and an outlook into the future.*" Journal of Cranio-Maxillofacial Surgery. Vol.29(1): p2-21.
- [2.] Wang, Z.G., et al. (January 2005). "*High-speed milling of titanium alloys using binderless CBN tools.*" International Journal of Machine Tools and Manufacture. Vol.45(1): p105-114.
- [3.] Okazaki, Y. (January 2001). "*A New Ti-15Zr-4Nb-4Ta alloy for medical applications.*" Current Opinion in Solid State and Materials Science. Vol.5(1): p45-53.
- [4.] Hassan, A. and Yao, Z. (December 2004). "*Dry face milling of titanium alloys.*" Journal of University of science and technology Beijing. Vol.11(6): p545-548.
- [5.] Guimu, Z., et al. (July 2003). "*Experimental study on the milling of thin parts of titanium alloy (TC4).*" Journal of Materials Processing Technology. Vol.138(1-3): p489-493.
- [6.] The Titanium Information Group "*Titanium Alloys in Medical Applications*" Accessed on April 19, 2005. from <http://www.azom.com/details.asp?ArticleID=1794>.
- [7.] Wen, C.E., et al. (October 2002). "*Novel titanium foam for bone tissue engineering.*" Journal of Materials Research. Vol.17(10): p2633-2639.
- [8.] Alkan, I., et al. (April 2004). "*Influence of occlusal forces on stress distribution in preloaded dental implant screws.*" The Journal of Prosthetic Dentistry. Vol.91(4): p319-325.
- [9.] Koriath, T.W.P., et al. (June 1997). "*Forces and moments generated at the dental incisors during forceful biting in humans.*" Journal of Biomechanics. Vol.30(6): p631-633.
- [10.] Hylander, W.L. and Bays, R. (1979). "*An in vivo strain-gauge analysis of the squamosal-dentary joint reaction force during mastication and incisal biting in Macaca mulatta and Macaca fascicularis.*" Archives of Oral Biology. Vol.24(9): p689-697.
- [11.] Sahin, S., et al. (September 2002). "*The influence of functional forces on the biomechanics of implant-supported prostheses-a review.*" Journal of Dentistry. Vol.30(7-8): p271-282.
- [12.] Gibbs, C.H., et al. (August 1986). "*Limits of human bite strength.*" The Journal of Prosthetic Dentistry. Vol.56(2): p226-229.

- [13.] Haraldson, T., et al. (1979). "*Bite force and oral function in complete denture wearers.*" *Journal of Oral Rehabilitation.* Vol.6(1): p41-48.
- [14.] Haraldson, T. and Carlsson, G.E. (1977). "*Bite force and oral function in patients with osseointegrated oral implants.*" *Scandinavian Journal of Dental Research.* Vol.85(1): p200-208.
- [15.] Carr, A.B. and W.R.Laney (1987). "*Maximum occlusal force levels in patients with osseointegrated oral implant prosthesis and patients with complete dentures.*" *International Journal of Oral and Maxillofacial Implants.* Vol.2(2): p101-108.
- [16.] Mericske-Stern, R. and Zarb, G.A. (1996). "*In vivo measurements of some functional aspects with mandibular fixed prostheses supported by implants.*" *Clinical Oral Implants Research.* Vol.7(2): p153-161.
- [17.] Wang, Z.G., et al. (February 2005). "*Tool wear characteristics of binderless CBN tools used in high-speed milling of titanium alloys.*" *Wear.* Vol.258(5-6): p752-758.
- [18.] O'Donnell, G. (2005) "*Improve the design and manufacturing process for customised, prescription fit, maxillo-facial implants*" GMIT Project proposal
- [19.] Serban, D. (2004) "*Integrated design to manufacturing process of customised maxillofacial prostheses*" GMIT Galway (M.Sc.Eng.)
- [20.] Scansite "*Reverse engineering.*" Accessed on April 22, 2005. from <http://www.scansite.com/reverse.html>
- [21.] Scansite "*CNC/Rapid prototyping guide*" Accessed on April 22, 2005. from <http://www.scansite.org/scan.php?pid=279>
- [22.] Hassfeld, S. and Muhling, J. (February 2001). "*Computer assisted oral and maxillofacial surgery- a review and an assessment of technology.*" *International Journal of oral and maxillo-facial surgeons.* Vol.30(1): p2-13.
- [23.] Sanghera, B., et al. (2001). "*Preliminary study of rapid prototype medical models.*" *Rapid Prototyping Journal.* Vol.7(5): p275 - 284.
- [24.] Sun, W., et al. (September 2005). "*Bio-CAD modeling and its applications in computer-aided tissue engineering.*" *Computer-Aided Design.* Vol.37(11): p1097-1114.
- [25.] Bezzon, O.L. (March 1993). "*Allergic sensitivity to several base metals: a clinical report.*" *Journal of Prosthetic Dentistry.* Vol.69(1): p243-244.
- [26.] Venugopalan, R. and C.Lucas, L. ( June1998). "*Evaluation of restorative and implant alloys galvanically coupled to titanium.*" *Dental Materials.* Vol.14(1): p165-172.

- [27.] Wang, R.R. and Boyle, A.M. (1993). "*A simple method for inspection of porosity in titanium castings.*" *Journal of Prosthetic Dentistry*. Vol.70(1): p275-279.
- [28.] Wataha, J.C. (February 2000). "*Biocompatibility of dental casting alloys: a review.*" *Journal of Prosthetic Dentistry*. Vol.83(2): p223-234.
- [29.] Rasmussen, E.J. (February 1987). "*Alternative prosthodontic technique for tissue-integrated prostheses.*" *Journal of Prosthetic Dentistry*. Vol.57(2): p198-203.
- [30.] Sartori, I.A.d.M., et al. (August 2004). "*In vitro comparative analysis of the fit of gold alloy or commercially pure titanium implant-supported prostheses before and after electroerosion.*" *The Journal of Prosthetic Dentistry*. Vol.92(2): p132-138.
- [31.] Okazaki, Y., et al. (June 1998). "*Corrosion resistance, mechanical properties, corrosion fatigue strength and cytocompatibility of new Ti alloys without Al and V.*" *Biomaterials*. Vol.19(13): p1197-1215.
- [32.] Li, H., et al. (2004). "*Effects of pore morphology and bone ingrowth on mechanical properties of microporous titanium as an orthopaedic implant material.*" *Materials Transactions*. Vol.45(4): p1124-1131.
- [33.] Murray, N.G.D. and Dunand, D.C. (December 2003). "*Microstructure evolution during solid-state foaming of titanium.*" *Composites Science and Technology*. Vol.63(16): p2311-2316.
- [34.] Dunand, D.C. (June 2004). "*Processing of titanium foams number.*" *Advanced Engineering Materials*. Vol.6(6): p369-376.
- [35.] Gauthier, M., et al. (September 2003). "*Properties of novel titanium foams intended for biomedical applications*" *Medical Device Materials-Proceedings of the Materials and Processes for Medical Devices Conference*. in Anaheim, CA., United States: 382-387
- [36.] Sul, Y.T. (October 2003). "*The significance of the surface properties of oxidized titanium to the bone response: special emphasis on potential biochemical bonding of oxidized titanium implant.*" *Biomaterials*. Vol.24(22): p3893-3907.
- [37.] Centre for cosmetic and reconstructive dentistry "*Types of Oral Implants*" Accessed on July 14, 2005. from [http://www.dentalinsurance.co.uk/implants/implant\\_types.htm](http://www.dentalinsurance.co.uk/implants/implant_types.htm)
- [38.] Lee, J.H., et al. (June 2005). "*Biomechanical and histomorphometric study on the bone-screw interface of bioactive ceramic-coated titanium screws.*" *Biomaterials*. Vol.26(16): p3249-3257.
- [39.] Hallgren, C., et al. (August 2001). "*The importance of surface texture for bone integration of screw shaped implants: An in vivo study of implants patterned by photolithography.*" *Journal of Biomedical Materials Research*. Vol.57(4): p485 - 496.

- [40] Simon, U., et al. (August 2003) "*Influence of the stiffness of bone defect implants on the mechanical conditions at the interface-a finite element analysis with contact.*" Journal of Biomechanics. Vol.36(8) p1079-1086.
- [41] Werner, A , et al (April 1998). "*Reverse engineering of free-form surfaces* " Journal of Materials Processing Technology Vol 76(1-3). p128-132
- [42] The learning factory "*Rapid Prototyping Primer*" Accessed on July 14, 2005 from <http://www.mne.psu.edu/lamancusa/rapidpro/primer/chapter2.htm>
- [43] Winder, J and Bibb, R. (July 2005) "*Medical Rapid Prototyping Technologies State of the Art and Current Limitations for Application in Oral and Maxillofacial Surgery* " Journal of Oral and Maxillofacial Surgery. Vol 63(7)· p1006-1015
- [44] Lex Lennings "*Selecting Either Layered Manufacturing or CNC Machining to Build Your Prototype*" Accessed on July 14, 2005 from <http://www.deskproto.com/files/cncvslmt.pdf>
- [45] VanBlarcom, C , et al (January 1999) "*The glossary of prosthodontic terms Seventh Edition* " The Journal of Prosthetic Dentistry. Vol 81(1). p39-110
- [46] Johnson, D H , et al "*Three-dimensional modeling of a bolted connection*" Accessed on January 21, 2006 from <http://www.ohiocae.com/bolt.htm>
- [47.] Englund, R.B and Johnson, D.H. (Autumn 1997) "*Finite Element Analysis of a Threaded Connection Compared to Experimental and Theoretical Research* " Journal of Engineering Technology Vol.14(2) p42-47
- [48] Peter Budgell "*Finite Element Analysis and Optimization Introduction*" Accessed on January 23, 2006. from [http://www3.sympatico.ca/peter\\_budgell/FEA\\_mtro.html](http://www3.sympatico.ca/peter_budgell/FEA_mtro.html)
- [49.] Fagan, M J. (1992). "*Finite Element Analysis*" 1st ed Chapter 1., Pearson Prentice Hall
- [50.] Murata, H , et al (2002) "*Dynamic Viscoelasticity of Soft Liners and Masticatory Function* " Journal Dental Research Vol 81(2)· p123-128
- [51] Dr Karen Gordon "*Biomaterials*" Accessed on January 24, 2006 from [http://www.soe.uoguelph.ca/webfiles/kgordon/Academic%20Courses/Bone\\_for\\_Bio materials.htm](http://www.soe.uoguelph.ca/webfiles/kgordon/Academic%20Courses/Bone_for_Bio materials.htm)
- [52.] Koca, O L., et al. (January 2005) "*Three-dimensional finite-element analysis of functional stresses in different bone locations produced by implants placed in the maxillary posterior region of the sinus floor* " The Journal of Prosthetic Dentistry Vol 93(1) p38-44.



- [53.] Polgar, K., et al. (1999). "*finite element analysis of screw-type dental implants.*" Acta Technica Academy.Science Hungary. Vol.108(3-4): p1997-99.
- [54.] Cibirka, R.M., et al. (March 2001). "*Examination of the implant-abutment interface after fatigue testing.*" The Journal of Prosthetic Dentistry. Vol.85(3): p268-275.
- [55.] Gratton, D., et al. (January 2001). "*Micromotion and dynamic fatigue properties of the dental implant-abutment interface.*" The Journal of Prosthetic Dentistry. Vol.85(1): p47-52.
- [56.] Jorneus, L., et al. (1992). "*Loads and designs of screw joints for single crowns supported by osseointegrated implants.*" Journal of international oral maxillofacial implants. Vol.7(3): p353-359.
- [57.] Heckmann, S.M., et al. (December 2001). "*Overdenture attachment selection and the loading of implant and denture-bearing area. Part I: In vivo verification of stereolithographic model.*" Clinical Oral Implants Research. Vol.12(6): p617-623.
- [58.] Don Shaffer "*ansys.net*" Accessed on January 30, 2006. from <http://ansys.net/ansys/?mycat=search&mytopicid=359>
- [59.] Shigley, J.E. (1986). "*Mechanical Engineering Design*".1st metric ed: p291-309, McGraw Hill.
- [60.] "*Fundamental FEA Concepts and Applications*" Accessed on May28, 2006. from [http://www.ansys.com/customer\\_stories/downloads/guide\\_fea-concepts.pdf](http://www.ansys.com/customer_stories/downloads/guide_fea-concepts.pdf)
- [61.] "*Finite-Element Simulations of Earthquakes--Discretization*" Accessed on June 28, 2006. from [http://pasadena.wr.usgs.gov/office/baagaard/research/papers/thesis/methods\\_discrete.html](http://pasadena.wr.usgs.gov/office/baagaard/research/papers/thesis/methods_discrete.html)
- [62.] Benzley, S., et al. (1995). "*A Comparison of All Hexagonal and All Tetrahedral Finite Element Meshes for Elastic and Elasto-plastic Analysis*" 4th International Meshing Roundtable. pp179-191
- [63.] "*Lifecore Biomedical*" Accessed on May 29, 2006. from <http://www.lifecore.com/default.asp>
- [64.] Ansys "*Défining Pretension in a Joint Fastener*" Accessed on June 9, 2006. from [http://www1.ansys.com/customer/content/documentation/80/ansys/Hlp\\_G\\_BAS2\\_9.html](http://www1.ansys.com/customer/content/documentation/80/ansys/Hlp_G_BAS2_9.html)
- [65.] Lassila, L.V., et al. ( March 2004). "*Mechanical properties of denture base resin crosslinked with hyberbranched polymer*" IADR/AADR/CADR 82nd General Session. in Hawaii Convention Center 325-B Honolulu, HI. USA.:

- [66] webopedia "*computer and Internet technology definitions* " Accessed on July 10, 2006 from [http://www.webopedia.com/TERM/C/CAD\\_CAM.html](http://www.webopedia.com/TERM/C/CAD_CAM.html)
- [67.] Priest, G (2005). "*Virtual-Designed and Computer-Milled Implant Abutments* " American Association of Oral and Maxillofacial Surgeons Vol. 63(9, Supplement 1). p22-32.
- [68 ] GMIT Costello, G.F. "*CNC Machining*" Accessed on July 13, 2006 from <http://webmanager.gmit.ie/webmanager/users/G82Q20RF8P2IV1Q/CNCMachining.doc>
- [69.] Winson, W.S L , et al (2002 ) "*Effects of interface factors on the handgrip and pinchgrip force exertion capabilities, muscular contraction speed and endurance*" City University of Hong Kong Hong Kong (M Eng )
- [70 ] University of New South Wales "*Stress distribution around bolt hole in double lap joint system*" Accessed on July 25,2006 from [http://www.library.unsw.edu.au/~thesis/adt-ADFA/uploads/approved/adt-ADFA20050819\\_111957/public/05chapter4.pdf](http://www.library.unsw.edu.au/~thesis/adt-ADFA/uploads/approved/adt-ADFA20050819_111957/public/05chapter4.pdf)
- [71.] Wieland, M (1999) "*Experimental determination of the surface composition and topography of medical implant surfaces and their influence on osteoblastic cell surface interactions* "Zurich (Ph D )
- [72 ] efunda "*Titanium Mechanical Properties*" Accessed on September 13 2006 from [http://www.efunda.com/materials/common\\_matl/Common\\_Matl.cfm?MatlPhase=Solid&MatlProp=Mechanical](http://www.efunda.com/materials/common_matl/Common_Matl.cfm?MatlPhase=Solid&MatlProp=Mechanical)
- [73 ] Quality Digest Manganelli, M "*Measuring the Real World with High-Performance Scanning Systems*" Accessed on September 21,2006 from <http://www.qualitydigest.com/sept00/html/scanning.html>
- [74.] ThomasNet Randlett, E. "*Metrology Integration Software facilitates off-line programming* " Accessed on September 22, 2006. from <http://news.thomasnet.com/fullstory/13067>
- [75.] Ninian Peckitt Peckitt, N "*ComputerGen Implants Ltd*" Accessed on November 6, 2006, from <http://www.maxfac.com>

## Appendix

- Appendix A. Helical Path GUI Method
- Appendix B. Hexagonal Abutment Part Drawing.
- Appendix C. Round Abutment Part Drawing.
- Appendix D. Final Prosthetic Design
- Appendix E. CMM Report
- Appendix F. Animation CD.

### Helical Path GUI Method

The following GUI method was developed for a particular helical path needed in this thesis, with a 0.6mm pitch 3mm diameter and growing in the positive Y direction, but by changing the keypoints it could be also be used for any diameter, pitch and direction

#### 1 Create 3 keypoints

- 1 The first keypoint is (X, 0) (Y, 0) (Z, 0)
- 2 The second keypoint is (X, 0.3) (Y, 0) (Z, 3.0)
- 3 The third keypoint is (X, 0.6) (Y, 0) (Z, 0)

[ 0.3 = Half the pitch (mm), 3 = Diameter (mm), 0.6 = Pitch (mm) ]

- 2 Create a line between the first and second keypoints, and the second and third keypoints
3. Display the workplane and align it with the first line, with a ratio of 0.5
- 4 Offset the workplane 90° in the X direction.
- 5 Divide the first line into two lines
6. Check the keypoint distance between the first keypoint and the centre of the first line (Make a note of this distance).

7. Create a circular area by dimensions using the distance noted from 6 above as the radius of the circle.
8. Repeat 3-7 for the second line as seen in Figure A.1.



Figure A.1 Helix construction areas.

9. Delete the areas only and the original construction lines and associated keypoints.
10. Copy the left two lines of the bottom circle, and the right two lines of the top circle 4mm in the positive X direction.
11. Delete the original left two lines of the bottom circle, and the right two lines of the top circle. This leaves a left and right hand helix, as seen in Figure A.2.



Figure A.2. Left and right hand helix.

12. Copy all the lines in the positive Y direction 0.6mm, ten times, as seen in Figure A.3.
13. Merge all the keypoints to a 0.0000001 range of coincidence.

14. Add the lines together for each helix.

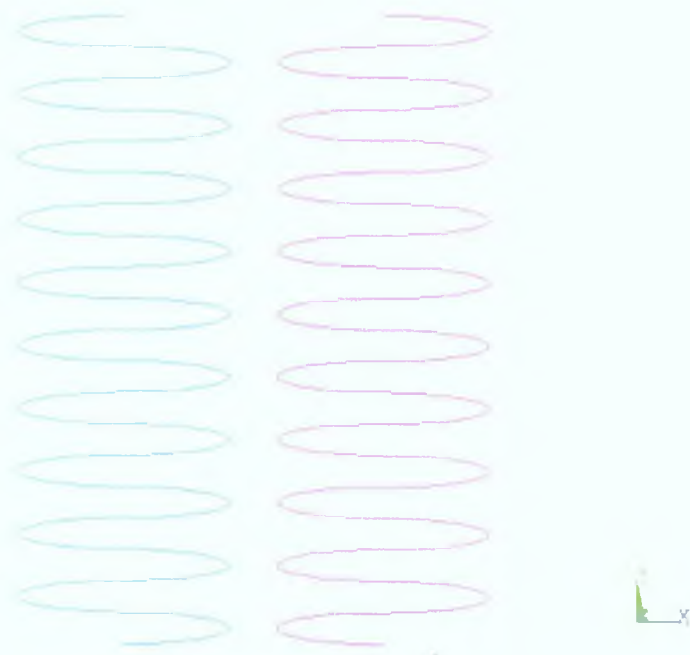
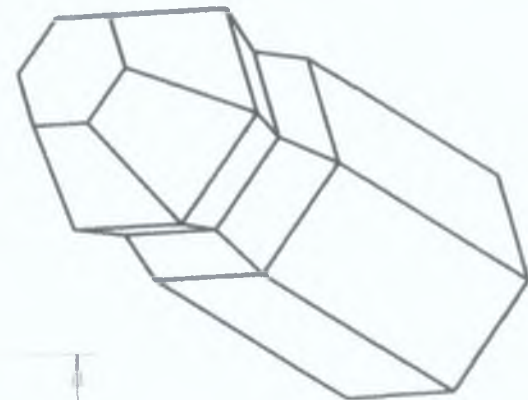
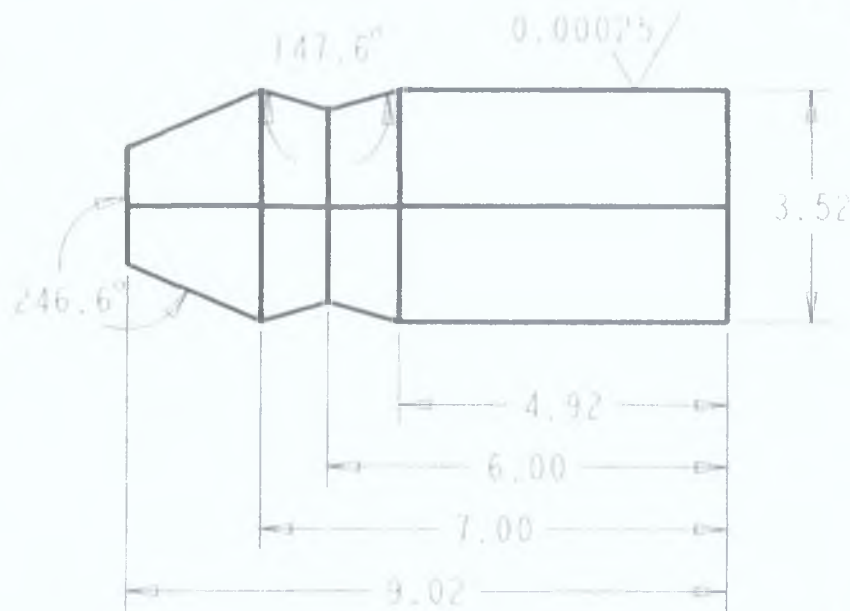
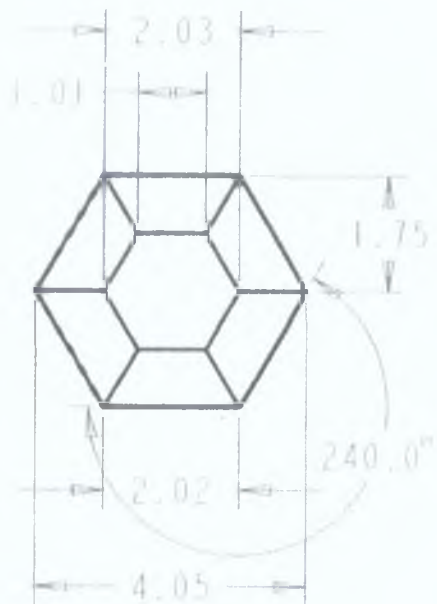


Figure A.3. Left and right hand helix with ten revolutions.



MATERIAL  
Titanium  
Ti6Al4V

STUDENT NAME  
Paul McGarry

DATE  
28-Oct-06

DESCRIPTION  
Titanium Abutment Design

MASS  
kg

STUDENT NUMBER  
G00058640

APP. BY

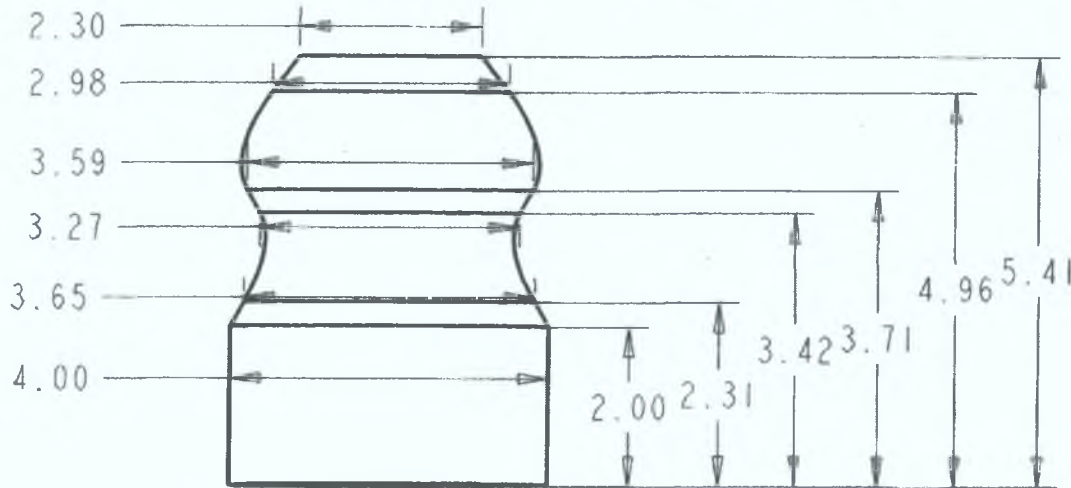
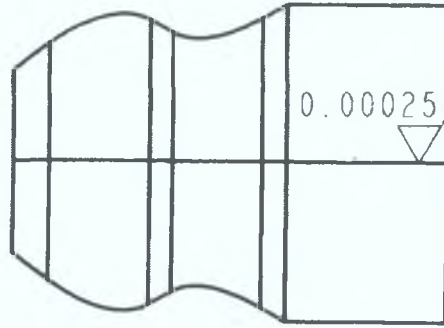
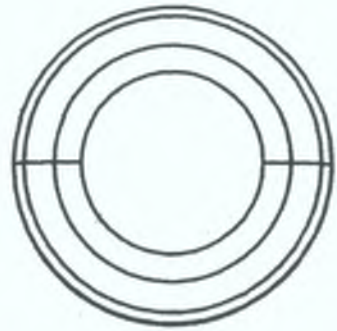
DRAWING No.  
DRW0001

THIS DESIGN IS PROTECTED BY COPYRIGHT.  
ANY REPRODUCTION WITHOUT PERMISSION IS STRICTLY  
PROHIBITED


MODEL NAME  
Hexagonal Abutment

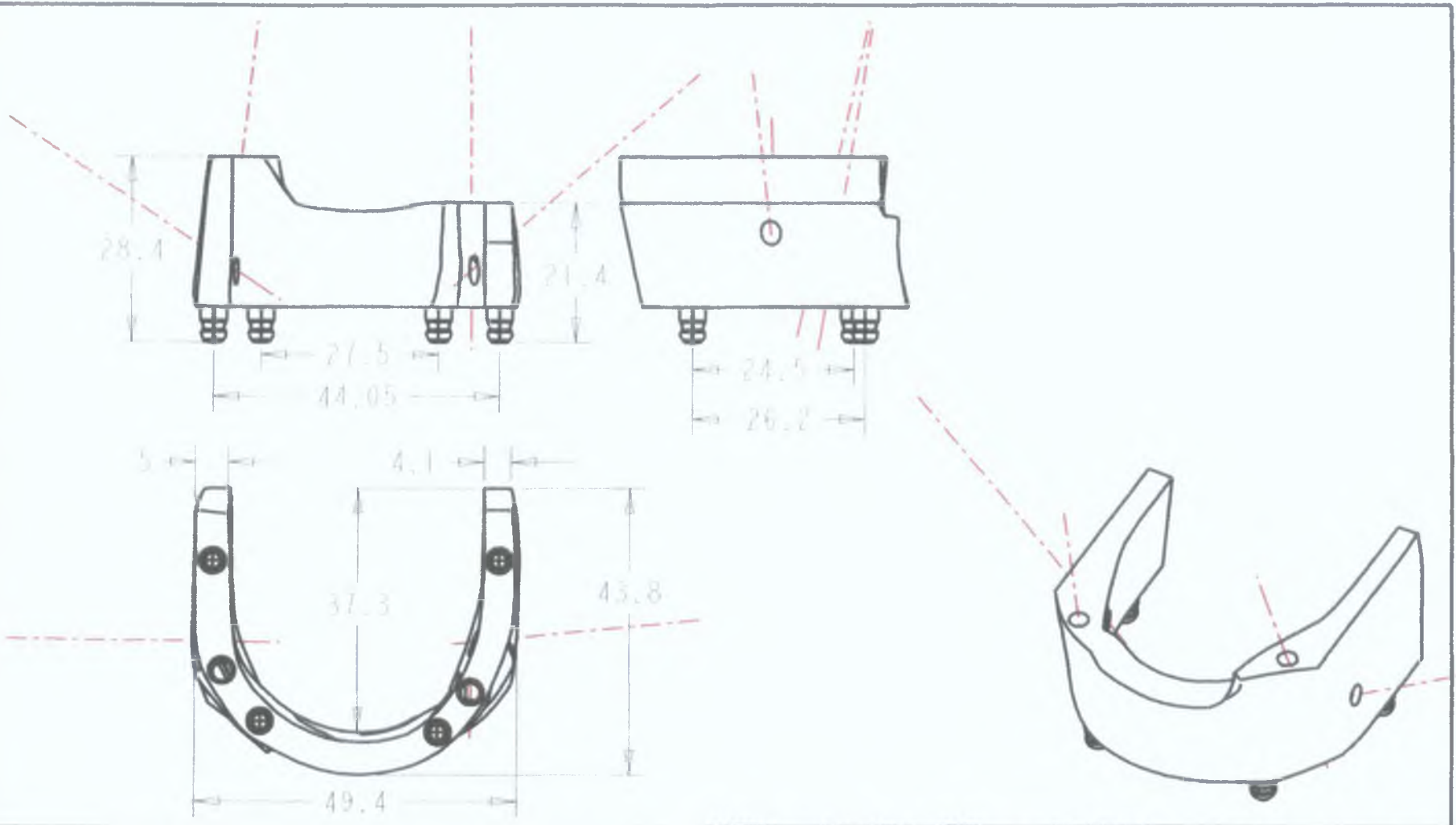
REV  
1





GALWAY INSTITUTE OF TECHNOLOGY

 THIRD ANGLE	MATERIAL Titanium Ti6Al4V	STUDENT NAME Paul McGarry	DATE 08-Feb-06	DESCRIPTION Titanium Abutment
	MASS kg	STUDENT NUMBER G00058640	APP. BY	DRAWING No. DRW0002
THIS DESIGN IS PROTECTED BY COPYRIGHT. ANY REPRODUCTION WITHOUT PERMISSION IS STRICTLY PROHIBITED				MODEL NAME Round Abutment
				REV 1



MATERIAL Titanium Ti6Al4V	STUDENT NAME Paul McGarry	DATE 08-Feb-06
MASS kg	STUDENT NUMBER C00058640	APP. BY

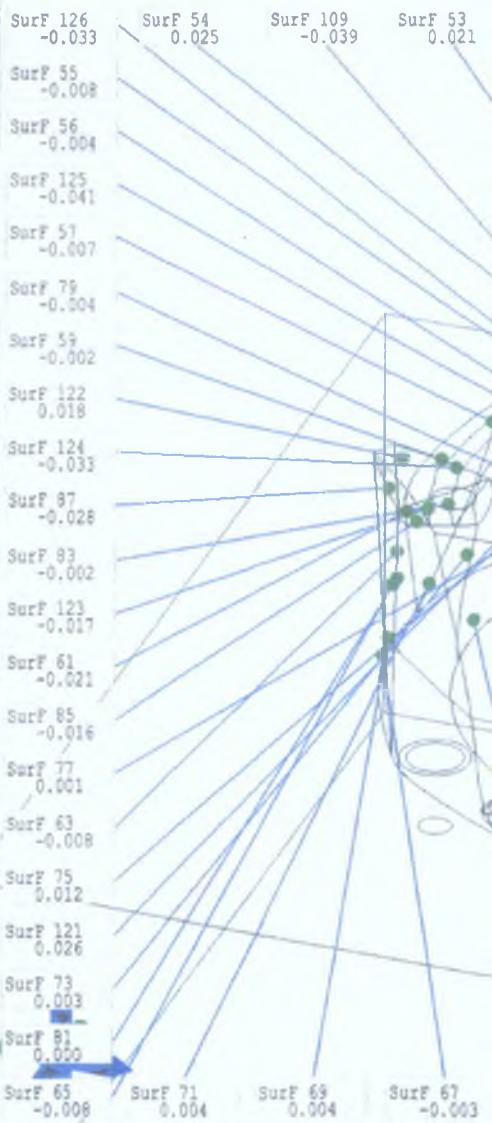
DESCRIPTION <b>Titanium Prosthesis</b>
DRAWING No. <b>DRW0003</b>

GALWAY INSTITUTE OF TECHNOLOGY

THIS DESIGN IS PROTECTED BY COPYRIGHT.  
ANY REPRODUCTION WITHOUT PERMISSION IS STRICTLY  
PROHIBITED

MODEL NAME <b>Proposed Prosthesis</b>	REV
--	-----

132



-0.025	0.025
-0.050	0.050
-0.075	0.075

130 [mm]	
Best fit	
Shift	Rot.
-0.005	-0.004
0.042	-0.003
0.003	-0.024

Srf.	Max.
	Mean
	Min.



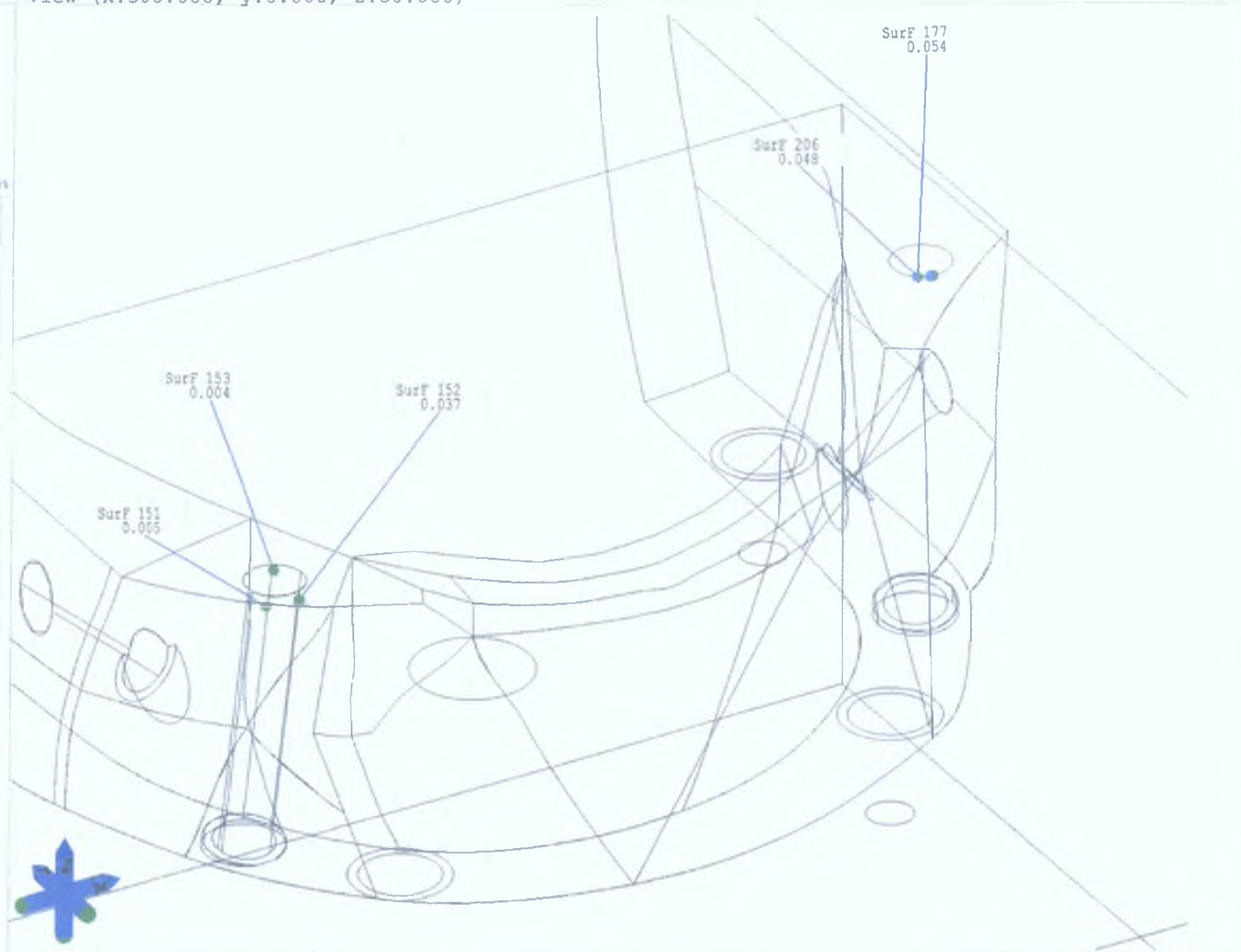
0001

0.031 (118)  
-0.011  
-0.048 (26)

Part CMM/AGIE  
Oper. Admin  
Date 29/08/2006 13:14  
D-No 01  
Comm. mouth peice 2  
Comm. Sean Dolan







-0.025    0.025  
 -0.050    0.050  
 -0.075    0.075

138 [mm]	Srf.	Max.	0.054 (177)
Best fit		Mean	-0.006
Shift	Rot.	Min.	-0.086 (161)
-0.004	-0.011		
0.058	0.004		
0.023	-0.033		

Part CMM/AGIE  
 Oper. Admin  
 Date 29/08/2006 14:02  
 D-No 02  
 Comm. mouth peice 2  
 Comm. Sean Dolan



CMM/AGIE



Operator	Admin	Date	29/08/2006 14:23
Sean Dolan	mouth peice		

Part CMM/AGIE  
Model filename Mouth-Picce.igs

Tolerances            0.100 mm    -0.100 mm  
Sheet thickness       0.000 mm  
Probe Radius          0.995 mm

Meas. mode surface  
Max. deviation        0.054 mm (177)  
Mean deviation       -0.020 mm  
Min. deviation       -0.086 mm (161)

Best fit  
Shift (X, Y, Z)       -0.004 mm    0.058 mm    0.023 mm  
Rot. (X, Y, Z)       -0.011 °     0.004 °     -0.033 °

No. Mode	Meas. Point Surf. Point	Deviation (X, Y, Z)	Total Deviation	
1	110.124	88.228	-2.517	
SurF	110.151	88.229	-2.513	
	-0.028	-0.001	-0.004	-0.028    ---*+---
2	110.218	85.456	-2.509	
SurF	110.251	85.456	-2.505	
	-0.033	-0.001	-0.005	-0.033    ---**+---
3	110.227	82.228	-2.506	
SurF	110.260	82.228	-2.501	
	-0.033	0.000	-0.005	-0.033    ---**+---
4	110.204	79.356	-2.505	
SurF	110.235	79.356	-2.500	
	-0.032	0.000	-0.004	-0.032    ---**+---
5	110.186	75.247	-2.501	
SurF	110.222	75.247	-2.496	
	-0.037	0.000	-0.005	-0.037    ---**+---
6	110.174	71.281	-2.497	
SurF	110.213	71.281	-2.492	
	-0.039	0.000	-0.005	-0.039    ---**+---
7	110.162	67.536	-2.494	
SurF	110.203	67.536	-2.489	



## CMM/AGIE

Operator		Admin		Date		
				29/08/2006 14:23		
		-0.041	0.000	-0.005	-0.041	---**+---
8	110.150	64.615		-2.487		
SurF	110.191	64.615		-2.482		
		-0.041	0.000	-0.005	-0.041	---**+---
9	110.124	61.773		-2.473		
SurF	110.167	61.773		-2.468		
		-0.043	0.000	-0.005	-0.043	---**+---
10	110.090	59.276		-2.450		
SurF	110.132	59.275		-2.446		
		-0.043	0.001	-0.004	-0.043	---**+---
11	110.555	61.429		-7.057		
SurF	110.592	61.427		-7.054		
		-0.036	0.002	-0.003	-0.036	---**+---
12	110.657	64.246		-7.078		
SurF	110.691	64.245		-7.074		
		-0.035	0.001	-0.004	-0.035	---**+---
13	110.687	66.466		-7.083		
SurF	110.723	66.465		-7.079		
		-0.036	0.000	-0.004	-0.036	---**+---
14	110.703	69.045		-7.083		
SurF	110.735	69.045		-7.080		
		-0.032	0.000	-0.003	-0.032	---**+---
15	110.706	71.873		-7.080		
SurF	110.736	71.873		-7.077		
		-0.030	0.000	-0.003	-0.030	---*+---
16	110.706	75.141		-7.077		
SurF	110.734	75.141		-7.074		
		-0.028	0.000	-0.003	-0.028	---*+---
17	110.710	78.864		-7.074		
SurF	110.733	78.864		-7.072		
		-0.023	0.000	-0.002	-0.023	---*+---
18	110.716	84.917		-7.065		
SurF	110.741	84.917		-7.063		
		-0.025	0.000	-0.002	-0.025	---*+---
19	110.574	89.136		-7.065		
SurF	110.599	89.138		-7.063		
		-0.024	-0.001	-0.002	-0.025	---*+---
20	111.272	86.235		-15.153		
SurF	111.316	86.237		-15.150		
		-0.043	-0.002	-0.003	-0.044	---**+---
21	111.357	82.908		-15.160		
SurF	111.404	82.908		-15.156		
		-0.047	-0.001	-0.004	-0.047	---**+---
22	111.397	80.069		-15.166		
SurF	111.440	80.070		-15.162		

## CMM/AGIE

Operator	Admin			Date	
				29/08/2006 14:23	
	-0.043	-0.001	-0.004	-0.043	---*+---
23	111.483	74.286	-15.176		
SurF	111.531	74.286	-15.171		
	-0.048	-0.001	-0.005	-0.048	---*+---
24	111.523	71.347	-15.179		
SurF	111.575	71.348	-15.174		
	-0.052	-0.001	-0.005	-0.053	---*+---
25	111.440	64.470	-15.167		
SurF	111.494	64.467	-15.162		
	-0.054	0.004	-0.005	-0.054	---*+---
26	111.934	64.650	-20.172		
SurF	111.972	64.646	-20.170		
	-0.038	0.004	-0.003	-0.038	---*+---
27	112.071	70.488	-20.193		
SurF	112.108	70.489	-20.189		
	-0.037	-0.001	-0.003	-0.037	---*+---
28	111.950	75.579	-20.187		
SurF	111.981	75.580	-20.185		
	-0.031	-0.001	-0.003	-0.031	---*+---
29	111.839	79.831	-20.180		
SurF	111.866	79.832	-20.178		
	-0.027	-0.001	-0.002	-0.027	---*+---
30	111.720	84.136	-20.173		
SurF	111.747	84.137	-20.171		
	-0.027	-0.001	-0.002	-0.027	---*+---
31	111.610	87.107	-20.174		
SurF	111.636	87.108	-20.172		
	-0.026	-0.001	-0.002	-0.026	---*+---
32	62.636	86.981	-20.134		
SurF	62.619	86.983	-20.133		
	0.017	-0.002	0.000	-0.017	---*+---
33	62.321	83.520	-20.158		
SurF	62.312	83.520	-20.158		
	0.008	0.000	0.000	-0.008	---+---
34	62.229	79.388	-20.146		
SurF	62.230	79.388	-20.146		
	-0.001	0.000	0.000	0.001	---+---
35	62.227	76.077	-20.130		
SurF	62.228	76.077	-20.130		
	-0.001	0.000	0.000	0.001	---+---
36	62.266	72.921	-20.107		
SurF	62.267	72.921	-20.107		
	0.000	0.000	0.000	0.000	---+---
37	62.358	70.756	-20.083		
SurF	62.351	70.756	-20.084		

## CMM/AGIE

Operator	Admin		Date		
				29/08/2006 14:23	
	-0.002	0.006	-0.001	-0.007	—+—
83	82.240	49.209	-15.560		
SurF	82.240	49.205	-15.559		
	0.001	0.003	0.000	-0.004	—+—
84	108.830	57.677	-2.476		
SurF	108.837	57.668	-2.477		
	-0.007	0.009	0.001	-0.011	—*+—
85	106.476	55.770	-2.533		
SurF	106.481	55.764	-2.533		
	-0.005	0.006	0.000	-0.008	—+—
86	104.144	53.717	-2.575		
SurF	104.156	53.704	-2.575		
	-0.012	0.013	0.000	-0.017	—*+—
87	102.656	52.319	-2.587		
SurF	102.670	52.304	-2.586		
	-0.014	0.015	0.000	-0.020	—*+—
88	101.678	51.383	-2.579		
SurF	101.693	51.367	-2.579		
	-0.015	0.016	0.000	-0.022	—*+—
89	106.531	88.984	-2.585		
SurF	106.485	88.984	-2.585		
	0.046	0.000	0.000	-0.046	—**+—
90	106.500	85.790	-2.593		
SurF	106.454	85.791	-2.592		
	0.045	0.000	-0.001	-0.045	—**+—
91	106.450	81.654	-2.603		
SurF	106.409	81.655	-2.601		
	0.041	-0.001	-0.001	-0.041	—**+—
92	106.373	77.929	-2.613		
SurF	106.329	77.931	-2.611		
	0.044	-0.001	-0.002	-0.044	—**+—
93	106.205	74.363	-2.625		
SurF	106.160	74.366	-2.623		
	0.045	-0.003	-0.002	-0.045	—**+—
94	105.895	70.992	-2.650		
SurF	105.852	70.998	-2.646		
	0.043	-0.006	-0.003	-0.044	—**+—
95	104.757	66.882	-2.720		
SurF	104.695	66.909	-2.709		
	0.063	-0.027	-0.010	-0.069	—***+—
96	103.256	63.666	-2.701		
SurF	103.237	63.675	-2.699		
	0.019	-0.009	-0.003	-0.021	—*+—
97	101.302	59.987	-2.851		
SurF	101.277	60.013	-2.840		

3D-TOL-WZ v1.5.R1

**CMM/AGIE**

Operator	Admin			Date	29/08/2006 14:23	
	0.025	-0.027	-0.011	-0.038	---**+---	
98	106.582	87.759	-8.828			
SurF	106.520	87.759	-8.829			
	0.062	0.000	0.001	-0.062	---***+---	
99	106.612	84.257	-8.807			
SurF	106.552	84.257	-8.809			
	0.060	0.001	0.002	-0.060	---***+---	
100	106.628	81.431	-8.792			
SurF	106.573	81.430	-8.795			
	0.054	0.000	0.002	-0.054	---***+---	
101	106.618	77.542	-8.771			
SurF	106.556	77.543	-8.775			
	0.062	-0.001	0.004	-0.062	---***+---	
102	106.517	74.051	-8.751			
SurF	106.450	74.055	-8.757			
	0.067	-0.003	0.006	-0.067	---***+---	
103	93.868	55.279	-8.679			
SurF	93.868	55.286	-8.680			
	0.000	-0.006	0.001	-0.007	---+---	
104	90.880	54.225	-9.072			
SurF	90.847	54.296	-9.053			
	0.033	-0.072	-0.019	-0.081	---****+---	
105	86.247	53.705	-10.571			
SurF	86.247	53.711	-10.571			
	0.000	-0.006	0.000	-0.006	---+---	
106	82.127	54.162	-10.593			
SurF	82.141	54.219	-10.592			
	-0.014	-0.056	-0.001	-0.058	---***+---	
107	78.804	55.532	-10.574			
SurF	78.834	55.591	-10.574			
	-0.030	-0.059	0.000	-0.066	---***+---	
108	75.953	56.780	-10.584			
SurF	75.973	56.840	-10.583			
	-0.020	-0.060	-0.001	-0.064	---***+---	
109	72.786	59.686	-10.566			
SurF	72.812	59.697	-10.567			
	-0.026	-0.012	0.000	-0.029	---*+---	
110	71.210	63.398	-10.508			
SurF	71.238	63.409	-10.510			
	-0.028	-0.011	0.002	-0.030	---*+---	
111	67.845	74.328	-10.519			
SurF	67.894	74.336	-10.522			
	-0.049	-0.008	0.003	-0.050	---**+---	
112	67.518	78.561	-10.550			
SurF	67.567	78.563	-10.551			

**CMM/AGIE**

Operator	Admin			Date	29/08/2006 14:23	
	-0.049	-0.002	0.001	-0.049	--**+---	
113	67.441	83.787	-10.565			
SurF	67.485	83.787	-10.565			
	-0.044	0.000	0.001	-0.044	--**+---	
114	67.444	87.659	-10.573			
SurF	67.491	87.659	-10.573			
	-0.048	0.000	0.000	-0.048	--**+---	
115	67.443	89.222	-10.577			
SurF	67.492	89.222	-10.578			
	-0.048	0.000	0.000	-0.048	--**+---	
116	65.800	90.836	-8.595			
SurF	65.800	90.876	-8.604			
	0.000	-0.041	0.008	-0.041	--**+---	
117	108.472	90.991	-2.776			
SurF	108.473	91.013	-2.776			
	0.000	-0.021	0.000	-0.021	--*+---	
118	108.415	88.325	-0.973			
SurF	108.415	88.325	-1.000			
	0.000	0.000	0.027	0.027	--+*---	
119	108.433	81.517	-0.982			
SurF	108.433	81.518	-1.000			
	0.000	0.000	0.018	0.018	--+*---	
120	108.460	70.710	-0.977			
SurF	108.460	70.710	-1.002			
	0.000	0.000	0.025	0.025	--+*---	
121	108.476	62.939	-0.975			
SurF	108.476	62.939	-1.000			
	0.000	0.000	0.025	0.025	--+*---	
122	100.934	52.757	-0.977			
SurF	100.934	52.757	-0.997			
	0.000	0.000	0.020	0.020	--+*---	
123	92.979	51.659	-9.611			
SurF	92.979	51.654	-9.597			
	0.000	0.005	-0.014	-0.014	--*+---	
124	86.798	51.500	-9.730			
SurF	86.798	51.494	-9.701			
	0.000	0.006	-0.030	-0.030	--*+---	
125	78.856	53.260	-8.996			
SurF	78.859	53.250	-8.961			
	-0.003	0.010	-0.035	-0.037	--**+---	
126	73.641	52.942	-8.066			
SurF	73.642	52.943	-8.037			
	-0.001	-0.001	-0.028	-0.028	--*+---	
127	66.815	63.463	-8.034			
SurF	66.815	63.463	-8.017			

**CMM/AGIE**

Operator	Admin		Date 29/08/2006 14:23		
	0.000	0.000	-0.017	-0.017	---*+---
128	65.741	76.708	-8.016		
SurF	65.741	76.708	-8.001		
	0.000	0.000	-0.015	-0.015	---*+---
129	65.710	88.772	-8.009		
SurF	65.710	88.772	-8.000		
	0.000	0.000	-0.009	-0.009	---+---
130	65.727	82.225	-8.010		
SurF	65.727	82.225	-8.000		
	0.000	0.000	-0.010	-0.010	---+---
151	68.528	56.258	-8.648		
SurF	68.525	56.254	-8.648		
	0.003	0.003	0.001	0.005	---+---
152	70.143	55.982	-8.625		
SurF	70.146	55.945	-8.629		
	-0.004	0.037	0.004	0.037	---+***---
153	70.304	58.620	-8.375		
SurF	70.306	58.624	-8.374		
	-0.002	-0.004	-0.001	0.004	---+---
154	70.238	55.909	-8.673		
SurF	70.205	55.977	-8.661		
	0.033	-0.068	-0.012	-0.077	-.****+---
161	104.713	56.347	-1.015		
SurF	104.729	56.430	-1.002		
	-0.016	-0.083	-0.014	-0.086	-.****+---
168	104.838	56.379	-1.006		
SurF	104.844	56.409	-1.002		
	-0.006	-0.030	-0.005	-0.031	---**+---
177	104.171	56.737	-0.990		
SurF	104.160	56.686	-1.002		
	0.011	0.051	0.013	0.054	---+***---
206	104.176	56.727	-0.993		
SurF	104.167	56.681	-1.002		
	0.010	0.046	0.009	0.048	---+***---



## CMM/AGIE

Operator	Admin			Date	29/08/2006 14:23	
	0.008	0.000	0.000	-0.008	—+—	
38	62.721	67.407	-20.006			
SurF	62.712	67.405	-20.007			
	0.010	0.002	0.001	-0.010	—+—	
39	62.963	88.247	-14.898			
SurF	62.951	88.248	-14.898			
	0.012	-0.001	-0.001	-0.012	—*+—	
40	62.690	83.618	-14.936			
SurF	62.681	83.618	-14.936			
	0.009	0.000	-0.001	-0.009	—+—	
41	62.603	79.661	-14.940			
SurF	62.593	79.661	-14.939			
	0.010	0.000	-0.001	-0.011	—*+—	
42	62.553	75.819	-14.939			
SurF	62.542	75.819	-14.938			
	0.011	0.000	-0.001	-0.011	—*+—	
43	62.527	72.207	-14.932			
SurF	62.518	72.207	-14.931			
	0.009	0.000	-0.001	-0.009	—+—	
44	62.567	68.774	-14.913			
SurF	62.557	68.774	-14.912			
	0.010	0.000	-0.001	-0.010	—+—	
45	62.706	65.964	-14.870			
SurF	62.699	65.963	-14.870			
	0.007	0.001	0.000	-0.007	—+—	
46	63.208	63.919	-9.687			
SurF	63.203	63.919	-9.687			
	0.005	0.000	-0.001	-0.005	—+—	
47	63.167	68.066	-9.713			
SurF	63.162	68.066	-9.713			
	0.004	0.000	-0.001	-0.005	—+—	
48	63.177	74.904	-9.710			
SurF	63.171	74.904	-9.710			
	0.006	0.000	-0.001	-0.006	—+—	
49	63.197	79.111	-9.701			
SurF	63.189	79.111	-9.700			
	0.007	0.000	-0.001	-0.007	—+—	
50	63.229	83.997	-9.683			
SurF	63.220	83.997	-9.682			
	0.009	0.000	-0.001	-0.009	—+—	
51	63.299	89.247	-9.639			
SurF	63.295	89.247	-9.639			
	0.004	0.000	0.000	-0.004	—+—	
52	63.526	61.127	-9.466			
SurF	63.535	61.133	-9.465			

## CMM/AGIE

Operator	Admin			Date	29/08/2006 14:23	
	-0.009	-0.006	-0.001	0.011	---+*---	
53	65.474	58.326	-9.481			
SurF	65.482	58.332	-9.480			
	-0.008	-0.007	-0.001	0.011	---+*---	
54	69.060	54.846	-9.461			
SurF	69.070	54.859	-9.460			
	-0.010	-0.014	-0.002	0.017	---+*---	
55	72.535	52.733	-9.569			
SurF	72.528	52.720	-9.569			
	0.006	0.013	0.000	-0.014	---*+---	
56	75.142	51.570	-9.570			
SurF	75.138	51.561	-9.570			
	0.004	0.009	0.000	-0.010	---+---	
57	77.475	50.726	-11.268			
SurF	77.471	50.714	-11.269			
	0.004	0.011	0.001	-0.012	---*+---	
58	80.205	49.889	-11.284			
SurF	80.202	49.878	-11.285			
	0.003	0.011	0.001	-0.012	---*+---	
59	83.407	49.185	-11.312			
SurF	83.407	49.181	-11.312			
	0.001	0.004	0.000	-0.004	---+---	
60	86.197	48.884	-11.304			
SurF	86.197	48.886	-11.304			
	0.000	-0.002	0.000	0.002	---+---	
61	91.244	49.544	-11.212			
SurF	91.250	49.527	-11.214			
	-0.005	0.017	0.002	-0.018	---*+---	
62	93.276	50.240	-11.233			
SurF	93.274	50.245	-11.233			
	0.002	-0.005	-0.001	0.006	---+---	
63	96.266	50.619	-11.462			
SurF	96.267	50.614	-11.462			
	-0.001	0.005	-0.001	-0.005	---+---	
64	100.420	51.231	-3.506			
SurF	100.428	51.245	-3.507			
	-0.008	-0.014	0.001	0.016	---+*---	
65	95.474	50.009	-14.667			
SurF	95.475	50.004	-14.667			
	-0.001	0.004	-0.001	-0.004	---+---	
66	94.837	49.347	-18.596			
SurF	94.840	49.338	-18.595			
	-0.003	0.009	-0.001	-0.010	---+---	
67	93.415	48.538	-21.763			
SurF	93.414	48.539	-21.763			

## CMM/AGIE

Operator	Admin			Date	
				29/08/2006 14:23	
	0 000	-0 001	0 000	0 001	—+—
68	96 669	49.714	-21 720		
SurF	96 669	49 715	-21.720		
	0 000	-0.001	0 000	0 001	—+—
69	90 887	47.996	-21 806		
SurF	90.886	48 002	-21 807		
	0 001	-0 006	0 001	0 006	—+—
70	88 278	47.755	-21 877		
SurF	88 278	47 762	-21 879		
	0 000	-0 007	0.002	0 007	—+—
71	82.688	48 010	-21.871		
SurF	82 688	48.014	-21 872		
	0 000	-0 004	0 001	0 004	—+—
72	80 493	48 460	-21 839		
SurF	80 493	48 461	-21 840		
	0 000	-0 001	0.000	0 001	—+—
73	78 197	49 131	-21 827		
SurF	78.197	49.132	-21.827		
	0.000	-0 001	0 000	0 001	—+—
74	76.172	49 944	-21 790		
SurF	76 172	49 944	-21 790		
	0 000	0 000	0 000	0 000	—+—
75	73.603	51.449	-21.719		
SurF	73 608	51 455	-21 720		
	-0 004	-0 006	0 001	0 008	—+—
76	72 321	52 460	-21 668		
SurF	72 320	52.459	-21.668		
	0 001	0 001	0 000	-0 001	—+—
77	71 138	53 479	-21.640		
SurF	71 135	53 475	-21 640		
	0 003	0.004	0.000	-0.005	—+—
78	72 895	52 500	-15 476		
SurF	72 890	52 491	-15 476		
	0.005	0 009	0 000	-0 010	—+—
79	76 354	51 006	-15 550		
SurF	76 351	50 999	-15.549		
	0 003	0 007	-0 001	-0 008	—+—
80	86 704	48 860	-15 489		
SurF	86 704	48 860	-15.489		
	0 000	0 001	0 000	-0 001	—+—
81	92.904	49 412	-15 649		
SurF	92 903	49 414	-15 649		
	0.000	-0 002	0 000	0 002	—+—
82	95 717	49 969	-15 555		
SurF	95 718	49.962	-15 554		